DISSERTATION FOR THE DEGREE OF DOCTOR OF PHILOSOPHY (PHD)

Integration Events in the Life Cycle of HIV-2, and its susceptibility to Lenacapavir and Integrase Strand Transfer Inhibitors

by Kiarie Irene Wanjiru

UNIVERSITY OF DEBRECEN
DOCTORAL SCHOOL OF MOLECULAR CELLULAR AND IMMUNE BIOLOGY

DEBRECEN, 2026

DISSERTATION FOR THE DEGREE OF DOCTOR OF PHILOSOPHY (PHD)

Integration Events in the Life Cycle of HIV-2, and its susceptibility to Lenacapavir and Integrase Strand Transfer Inhibitors

by Kiarie Irene Wanjiru

Supervisor: Mohamed Mahdi, M.D, MPH, Ph.D

UNIVERSITY OF DEBRECEN
DOCTORAL SCHOOL OF MOLECULAR CELLULAR AND IMMUNE BIOLOGY

DEBRECEN, 2026

TABLE OF CONTENTS

1. LIST OF ABBREVIATIONS

APOBEC3G	mRNA Apolipoprotein editing enzyme catalytic polypeptide-like 3G
CA	Capsid protein
CA-NTD	Capsid amino terminal domain
CAP-1	Adenylyl cyclase-associated protein 1
cART	Combined antiretroviral therapy
CASP3	Caspase 3
CCD	Catalytic core domain
CCR	C-C motif chemokine receptor
CD	Cluster of differentiation
CMV	Cytomegalovirus
CORO7-PAM16	Coronin7 presequence translocase associated motor 16
CPSF6	Cleavage & polyadenylation specificity factor 6
CRF	Combining recombination Forms
CTD	Carboxyl terminal domain
CUL4	Cullin 4
CXCR	CXC chemokine receptor 4
DCAF1	DDB1 & CUL4 Associated Factor 1
DDB1	Damage specific DNA binding protein 1
DEGs	Differentially Expressed Genes
DEPDC1	DEP domain containing 1
dGTPs	Deoxyguanosine triphosphate differentiation 3
DMEM	Dulbecco modified eagle medium
DNA	Deoxyribonucleic acid
dNTPs	Deoxyribonucleotide triphosphates
EDTA	Ethylene diamine tetra acetic acid
ELISA	Enzyme linked immunosorbent assay

ENV	Envelope
FAK	Focal adhesion kinase
FBS	Fetal Bovine Serum
FDA	Food & Drug administration
FDR	False discovery rate
G1, G2, S	Gap-1, Gap-2, Synthesis phase
GFP	Green fluorescent protein
GO	Gene ontology
GPR15 G	Protein coupled receptor 15
H3K36me3	Histone H3 lysine 36 trimethylation
HAART	Highly active antiretroviral therapy
HHCC	Histidine Cysteine
HHDGF	Hepatoma Derived Growth Factor
HIV- 1/2	Human Immunodeficiency virus type 1or 2
HIVA	HIV associated nephropathy
HIV-D	Dual infection with HIV-1 and HIV-2
HLA-DR	Human Leucocyte Antigen DR-isotype
HRP-2	Hepatoma-derived growth factor related protein 2
HSP40	Heat shock protein 40
HTLV I, II, III	Human T-cell leukemia virus I, II, III
HUSH	Human Silencing Hub
IBD	Integrase binding domain
IFNA	Interferons alpha
IL	Interleukin 1
IN	Integrase
INSTIs	Integrase Strand Transfer Inhibitors
IRF5	Interferon regulatory factor 5

LEDGF/p75	Lens epithelium derived growth factor splice variant 75
LEN	Lenacapavir
LTR	Long terminal repeat
MA	Matrix protein
MDMs	Monocyte Derived Macrophages
MHCI	Major Histocompatibility complex class I
mRNA	messenger ribonucleic acid
MTCT	Mother to child transmission
mTOR	Mechanistic Target of Rapamycin
MYD88	Myeloid differentiation 88
NC	Nucleocapsid
Nef	Negative effector
NF-κB	Nuclear factor kappa B
NNRTI	Non-nucleoside reverse transcriptase Inhibitor
NOP58	NOP58 ribonucleoprotein
NRTI	Nucleoside reverse transcriptase Inhibitor
NSP 13	Non-structural protein 13
NTD	Amino terminal domain
Nup153	Nucleoporin 153
OIS	Opportunistic infections
PBS	Phosphate-buffered saline
PCDHGC4	Protocadherin Gamma subfamily C
PCDHs	Protocadherins
PCR	Polymerase Chain Reaction
PEI	Polyethylenimine
PFV	Prototype Foamy Virus
PI	Protease Inhibitor

PI3K/AKT	Phosphoinositide 3-kinase/ Protein kinase B
PIC	Pre-Integration Complex
PLWHIV	People living with HIV virus
PMA	Phorbol 12-myristate 13-acetate
PPDE	Posterior probabilities of gene differential expression
PR	Protease
PSIP1	PC4 & SRSF1 interacting protein 1
P-TEFb	Positive transcriptional elongation factor beta
PYK2	Proline-rich tyrosine kinase 2
Rbx1	Ring box protein1
RdRp	RNA dependent RNA polymerase
REV	RNA-splicing regulator protein
RIN	RNA integrity number
RNA	Ribonucleic acid
RNAP II	RNA polymerase II
RPMI	Roswell Park Memorial Institute
RRE	Rev Response element
RT	Reverse transcriptase
SAMHD1	Sterile alpha motif and HD domain-containing protein 1
SARS-CoV-2	Severe acute respiratory syndrome coronavirus 2
SDS	Sodium dodecyl sulfate
SEC	Super elongation complex
SiRNA	silencing Ribonucleic acid
SIV	Simian immunodeficiency virus
SIV/sm	Simian immunodeficiency virus of Sooty mangabeys species
SKOR2	SKI family transcriptional co-repressor 2
SMAD	Suppressor of mothers against decapentaplegic

snRNP	Small nuclear ribonucleic proteins
SNX14	Sorting nexin 14
SU	Surface Protein
TAR	Tat-responsive region
TAT	Transcriptional trans-activator
TCR-CD3	T cell receptor in association with the CD3
TGF-β	Transforming growth factor β
TGF-βR1	Transforming growth factor-β receptor 1
TM	Transmembrane
TNF	Tumor Necrosis Factor
TRIM5	Tripartite motif protein 5
U2AF	U2 small nuclear RNA auxiliary factor 1
U2AF1L5	U2 small nuclear RNA auxiliary factor 1 like 5
Vif	Viral infectivity factor
Vpr	Viral protein r
Vpu	Viral protein u
Vpx	Viral protein x
WHO	World Health Organization
Wnt/β	Wingless integration site and beta pathway

2. INTRODUCTION

Acquired Immunodeficiency Syndrome (AIDS) is a condition that gradually weakens the immune system by depleting CD4 T lymphocytes, leading to immunosuppression and a heightened risk of opportunistic infections (Fauci, 1988). AIDS is caused by two distinct types of human immunodeficiency viruses (HIV), namely, HIV type 1 (HIV-1) and HIV type 2 (HIV-2) (Weiss, 1993). HIV-1 is the predominant and most widely studied virus worldwide, infecting over 39 million people as of 2023. HIV-2 on the other hand is less common, with data about its prevalence remaining widely unavailable (Gottlieb et al., 2018; Ceccarelli et al., 2021). Reports from over a decade ago estimate its prevalence at approximately 2 million infections worldwide, a figure which is likely underestimated (Carvalho et al., 2012).

First identified in 1986 among West African patients, HIV-2 is endemic to the region (Clavel et al., 1986), with documented cases elsewhere in Asia, South America, Europe and the United States (Marquart et al., 1988; Reeves et al., 2021; de Mendoza et al., 2017). This dispersion is likely due to migration and trade connections established during colonial times, particularly from Portuguese and French influences (Faria et al., 2012). In Europe, notably high prevalences are reported in France, Portugal, and Spain (Carvalho et al., 2012).

Despite their common lineage, HIV-2 shares an estimated 60% nucleotide sequence identity with HIV-1, although several genetic and clinical differences are evident between the two viruses (Bock & Markovitz, 2001). HIV-2 is less virulent, with lower transmission rate, a long asymptomatic period, and a slow progression to AIDS (Marlink et al., 1994). After infection with HIV-2, an initial spurt in viral replication is followed by a long latency period; a characteristic feature of this virus (Campbell-Yesufu & Gandhi, 2011). Although the precise mechanisms behind this long latency period is still unknown, distinct regulatory characteristics of HIV-2 long terminal repeats (LTR) may contribute to this phenomenon (Marchant et al., 2006). In addition, HIV-2 genome expresses viral protein x (Vpx) which neutralizes host defences, enhancing its infectivity, particularly in myeloid-lineage cells such as dendritic cells and macrophages (Fujita et al., 2010).

A critical event in the retroviruses' replication cycle is the viral DNA insertion into the host genome, a process driven by integrase enzyme in coordination with host cellular factors (Delelis et al., 2008). In HIV-1, this step is made efficient by Lens Epithelium-Derived Growth Factor p75 (LEDGF/p75), a host transcription cofactor which anchors integrase to actively transcribed chromatin through its PWWP (Pro-Trp-Trp-Pro) domain, while engaging

the enzyme through its integrase-binding domain (IBD) (Poeschla, 2008a). This targeted integration enhances viral gene expression and replication efficiency (Ciuffi et al., 2005). HIV-1 has demonstrated its preference for integration into active genes, maintaining robust replication and a lowered tendency for latency (Schroder et al., 2002). Only a few studies have reported integration sites of HIV-2 with varying results. An in vitro study analysing 202 HIV-2 insertion sites found that 82% were located within RefSeq genes, suggesting a preference for gene-dense and GC-rich regions, similar to HIV-1 (MacNeil et al., 2006). However, in vivo studies suggest that HIV-2 integrates more frequently into heterochromatin, which may contribute to its slower replication and lower pathogenicity (Marchant et al., 2006). In addition, HIV-2 dependency on LEDGF/p75 in integration targeting remains largely unexplored. These important functions make integrase and LEDGF/p75 proteins potential targets for antiviral therapies.

HIV-2 is inherently resistant to a variety of drugs commonly prescribed to HIV-1 infected patients. In particular, HIV-2 exhibits resistance to reverse transcriptase inhibitors of non-nucleoside nature (NNRTIs), the fusion inhibitor enfuvirtide, and the attachment inhibitor fostemsavir, in addition, to a weakened response to many protease inhibitors ((Desbois et al., 2008); Witvrouw et al., 1999). However, it has shown susceptibility to nucleotide reverse transcriptase inhibitors (NRTIs), the capsid inhibitor lenacapavir, and to integrase strand transfer inhibitors (INSTIs) (Cardoso et al., 2021).

INSTIs target the integration process by blocking integrase enzymes' active sites, preventing insertion of viral DNA into the host genome (Craigie, 2012). Currently, five INSTIs have received clinical approval: including first-generation inhibitors (raltegravir and elvitegravir) and second-generation inhibitors (dolutegravir, bictegravir, and cabotegravir) (Choi et al., 2018). While initial studies demonstrated promising activity of INSTIs against selected HIV-2 groups, resistance mutations rapidly emerged, particularly in patients receiving raltegravir and elvitegravir (Anstett et al., 2017). This necessitated the development of second-generation inhibitors, characterized by enhanced pharmacokinetic stability and improved resistance profiles. Dolutegravir has demonstrated superior efficacy against HIV-2 groups harboring resistance mutations to earlier INSTIs, and while remaining effective, some mutations similar to those seen in HIV-1, have been reported (Hare et al., 2011). Bictegravir has also shown potent in vitro activity against HIV-2, although clinical data on its efficacy in INSTIs treatment-naive HIV-2 patients remains sparse (Spagnuolo et al., 2018).

To address drug resistance and improve treatment outcomes, new innovative drugs are continuously being developed. This is demonstrated by the recent approval of cabotegravir, the 5th INSTI, and lenacapavir, which are both long-acting inhibitors given orally or through injection (Link et al., 2020; Pinto et al., 2023). Lenacapavir, a novel capsid inhibitor approved in 2022, offers an innovative approach to HIV therapy, particularly for individuals experiencing multidrug resistance (Prather et al., 2023). Although ongoing trials have confirmed its efficacy in HIV-1 patients, its utility in HIV-2 remains largely unexplored, with limited in vitro and in vivo assessments.

All the approved inhibitors are designed for HIV-1 management. Susceptibility of HIV-2 to these inhibitors remains understudied and standardized treatment guidelines are yet to be established in the case of HIV-2. Most research on the efficacy of antiretroviral drugs on HIV-2 has been confined to in vitro studies or clinical evaluations in patients experiencing failure to combined antiretroviral therapy (cART). Therefore, our primary aim was to evaluate the susceptibility of HIV-2 to lenacapavir and INSTIs through cell culture and in vitro based assays. Additionally, we utilized computational molecular docking to model interaction of HIV-2 integrase with the inhibitors and the capsid with lenacapavir.

Due to the limited number of studies on HIV-2 integration mechanisms and its latency period, with existing research yielding inconclusive results (MacNeil et al., 2006), our research sought to fill this gap by investigating interaction between HIV-2 integrase and LEDGF/p75 and characterized preferred integration sites of HIV-2 within the host genome. Additionally, we explored additional functional roles of Vpx in HIV-2's lifecycle. Our findings advanced the understanding of HIV-2 integration mechanisms, confirmed interaction of HIV-2 integrase with LEDGF/p75 and showed that Vpx protein may be possibly linked to the down regulation of HIV-1 in dual HIV-1 and 2 infections through the down regulation of a splicing factor important for the functioning of HIV-1 tat protein. In addition, lenacapavir and INSTIs showed excellent efficacy against HIV-2, similar to HIV-1.

3. THEORETICAL BACKGROUND

3.1 Origin and Classification of HIV

The initial case of AIDS was reported in 1981 and its causative agent, HIV type 1 was isolated by a team of virologists in 1983 (Gallo et al., 1983; Montagnier et al., 1984). A second virus with similar appearance but a different identity, named HIV-2, was discovered in

1986 in West Africa (Clavel et al., 1986). Although the AIDS causing viruses were identified over four decades ago, these viruses have existed among the simians in the African forests as early as 1900s and evolved from the simian immunodeficiency viruses (SIVs) (Sharp & Hahn, 2011). At least a dozen distinct SIV interspecies transmissions involving sooty mangabeys of *Cercocebus atys* species, gorillas of *Gorilla gorilla* species and chimpanzees of species *Pan troglodytes*, in central Africa have been linked to HIV origin by evolutionary studies (Gao et al., 1992). Nine mangabeys isolates produced nine HIV-2 strains A-I, while four strains of SIVs belonging to chimpanzees and gorilla families gave rise to HIV-1, which in turn diverged to M, O, N, and P groups (Hirsch et al., 1989) **(Figure 1).**

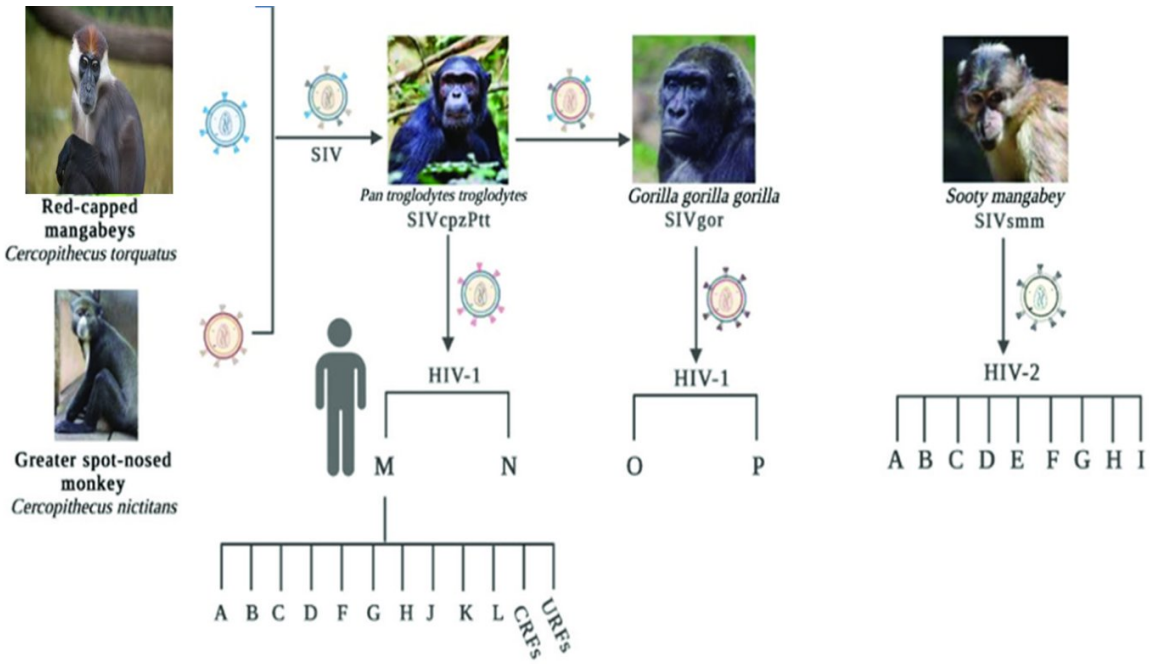

Figure 1: HIV origin and evolution from African primates naturally infected by SIVs. Cross species transmissions resulted in recombinant SIV viruses in chimpanzee and gorilla species giving rise to HIV-1, while HIV-2 originated from sooty mangabeys. Each virus diverged to different groups, subtypes, and unique recombination forms (CRFs/URFs) with different proportions. Subtype C accounts for (46.6%), B (12.1%), A (10.3%), G (4.6%), D (2.7%), F, H, J, K, L (0.9%), CRFs (16.7%) and URFs (6.1%) (Adapted and modified from Dawit Assefa et al., 2022)

This cross-species transmission of the simian retroviruses may have occurred as a result of hunting practices in Cameroon and exposure to contaminated fluids. High sero reactivity to SIV antigens among central African primate bush meat hunters supports this theory of zoonotic transmission (Peeters et al., 2002). According to extensive research, the chimpanzee and gorilla subspecies (*Pan troglodytes troglodytes*) and the subspecies of sooty mangabeys (*Cercocebus atys atys*) are the origins of HIV-1 and HIV-2, respectively (Gao et al., 1992).

Significant recombinations in genetic sequences between viruses resulted in multiple subtypes with different geographic prevalences (Tang et al., 2021).

The envelope (env) gene, specifically the V3 loop, is responsible for majority of the genetic variations observed in HIV and is a key component of tropism (Laakso et al., 2007). Most of infections by HIV-1 globally belong to Group M, which includes up to 158 circulating recombinant forms (CRFs) and groups A-L (Tang et al., 2021). About half of all HIV-1 cases worldwide are caused by subtype C, which is common in Southern Africa where most of HIV-1 infected cases have been reported. Group P and N are found in Cameroon, where there are only a few known isolates, whereas Group O is limited to West Africa and makes up around 1% of all infections (Robertson et al., 1995). Clusters M and N are linked to SIV in chimpanzees, while clusters P and O likely belong to SIV in gorilla populations (Le Hingrat et al., 2020). Only groups A and B have been demonstrated to cause illness out of the nine groups (A–I) that make up HIV-2 viruses (Gao et al., 1992). Group B is found in a few countries, whereas Group A is the most prevalent globally. Groups C-H are less pathogenic, and cause limited infections (Robertson et al., 1995).

3.2 HIV-2 Epidemiology

HIV-2 is known for its lengthy latency period of 15 – 20 years and a slower rate of CD4 decline and development of AIDS, with most patients remaining asymptomatic for long duration. However, if left untreated, it progresses to AIDS similarly to HIV-1. Majority of the infections are found in West Africa, with over 90% of the cases reported in Sierra Leone, Ivory Coast, Guinea-Bissau, Gambia, Cape Verde and Senegal (Hamel et al., 2007).

The spread of HIV-2 to other regions is attributed to the concept of the West African corridor which saw migrations to America, Middle East, Caribbean, Europe, Asia and diverse African regions like Mozambique and Angola (Faria et al., 2012) **(Figure 2).**

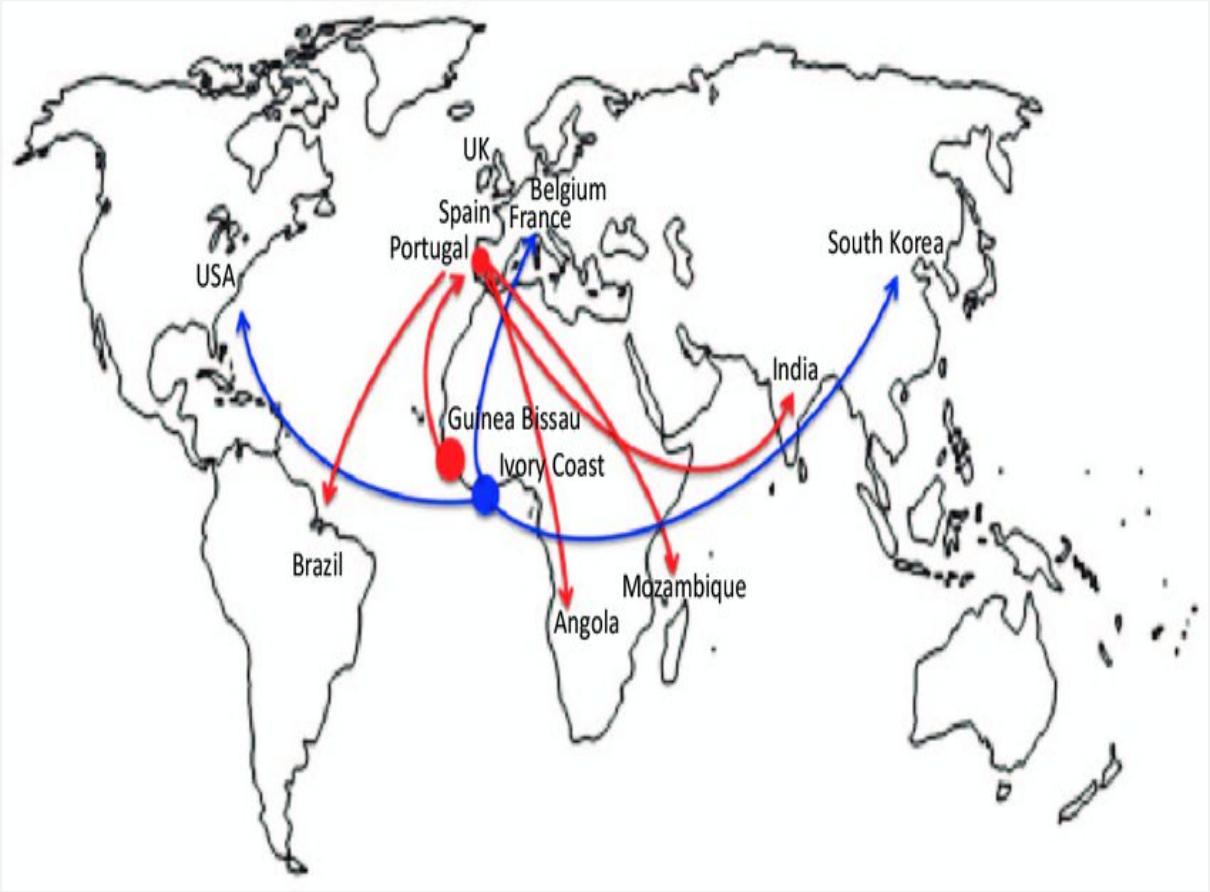

Figure 2: HIV-2 epidemiology and spread pattern. Blue lines represent major spread routes from its origin in Ivory Coast to different continents; Europe, Asia and America. Red lines represent spreading routes related to colonial and trade ties. (Figure adapted from Faria et al., 2013)

A notable number of HIV-2 infections were reported in Spain, Portugal, France, the United Kingdom, Switzerland, and other European countries. In Portugal specifically, HIV-2 infection prevalence is 5%, with descendants of Guinea Bissau accounting for 50% of the approximately 2000 reported cases (Soriano et al., 2000). Among those of sub-Saharan African heritage, the frequency was 2% in France with approximately 1000 cases, and comparable trends are observed in Spain which has reported 424 cases, with 76% of the infections among people of West African descent (de Mendoza et al., 2017). In Switzerland, the prevalence was 0.7% comprising cases of both mono and dual HIV infections(Barin et al., 2007). In Italy, HIV-2 has recently been highlighted as a concern due to continuous human migration from African countries (Ceccarelli et al., 2021). There were one hundred and ninety eight observed cases in the US from 2010 to 2017 comprising of both dual and single infections (Heitzinger et al., 2012).

3.3 HIV Genome

HIV-2 genome is roughly 9,800 nucleotides long compared to that of HIV-1 at approximately 9,200 to 9,600 nucleotides (Hernandez-Vargas & Middleton, 2013). In addition, HIV-2 contains an accessory viral protein x (Vpx) instead of viral protein u (Vpu) which is found in HIV-1 (Fujita et al., 2010). At nucleotide level, HIV-2 shares 60% similarity with HIV-1, including approximately 40% identity in the env gene and 60% identity in structural genes gag and pol (Motomura et al., 2008).

HIV-2 genome comprises of nine genes bordered by long terminal repeats at the 5' and 3' termini of the genome. These genetic elements are organized into three distinct categories: structural genes (gag, pol, env), regulatory genes (tat and rev), and accessory genes (vif, nef, vpr, and vpx) **(Figure 3)**.

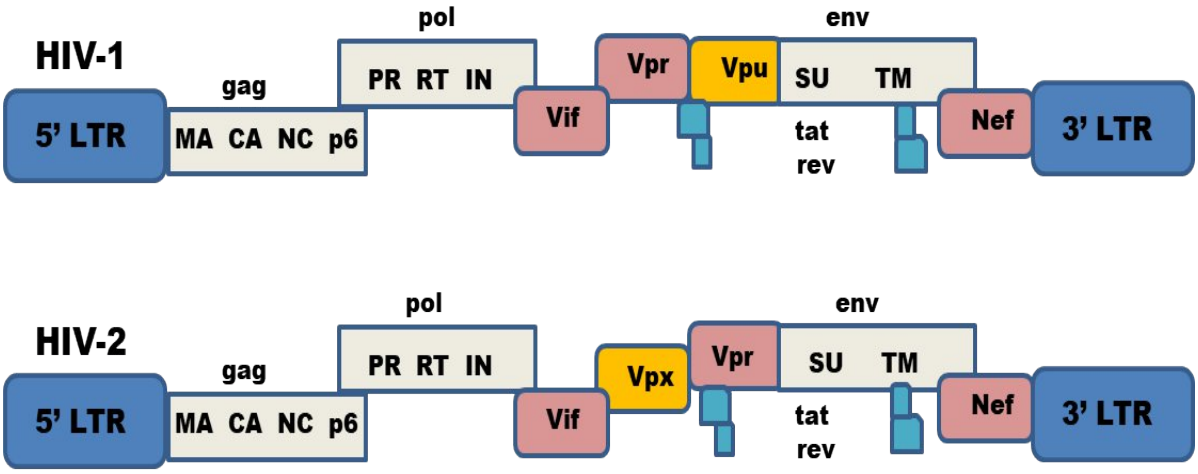

Figure 3: Genomes of HIV -1 and HIV-2 viruses depicting the structural genes; gag, pol, env in grey colour, regulatory genes and LTRs are shown in blue, accessory genes in pink while orange shows the unique genes for each virus**.**

Transcription is initiated by a promoter located at the 5' end of the genome (Guyader et al., 1987). Although similar to HIV-1 in structure and organization, HIV-2 gag protein is larger at 57kDa compared to that of HIV-1 at 55kDa. On the N-terminal domain, gag comprises matrix (MA) p17, capsid (CA) p26, nucleocapsid (NC) p7, and on the Carboxyl terminal, the p6 domain (Talledge et al., 2023). The matrix interconnects the nucleocapsid and the envelope and facilitates the translocation of the gag protein during assembly (Campbell & Hope, 2015a). The capsid functions as a structural shield, safeguarding the viral genome, while the nucleocapsid encapsulates the viral genetic material comprising of two identical single

stranded RNA molecules (Payne, 2017). Additionally, the p6 domain serves as an anchor site for endosomal sorting complexes responsible for protein transport (Görlich et al., 1994).

HIV-2 env codes for the viral envelope, which is composed of a heterodimer transmembrane (TM) protein and surface glycoproteins (SU) (gp36 and gp125 respectively). The surface glycoprotein consists of five variable (V1-V5) and five constant (C1-C5) regions on its binding site. The V3 loop on the SU variable domain binds to the receptors on the CD4 cells similar to HIV-1 (Laakso et al., 2007).

To enhance viral infectivity and replication, the pol gene encodes the following enzymes; protease (PR), reverse transcriptase (RT), integrase (IN) and RNase H (Guyader et al., 1987). HIV-2 protease is a homodimer responsible for the hydrolysis of gag and gag-pol precursor polyproteins, during virion maturation and budding. The proteases of HIV-1 and HIV-2 share 39–48% amino acid sequence identity (Triki et al., 2018).

The reverse transcriptase enzyme utilizes the single-stranded viral RNA as a template to synthesize complementary double-stranded viral DNA, while RNase H facilitates the degradation of RNA strands. Comparative analysis show diminished RT and RNase H activities in HIV-2 in comparison to HIV-1 (Sertznig et al., 2018). Integrase (IN), derived from the gag-pol polyprotein through proteolytic cleavage, integrates the synthesized viral DNA into the host genome(Talledge et al., 2023). Integrase exhibits 40% nucleotide similarity and a 65% amino acid identity between HIV-1 and HIV-2 (Craigie, 2012).

The transactivator protein (Tat) and the RNA- splicing regulator protein (Rev), are regulatory proteins essential for virus replication. HIV Tat protein is an initiator of viral transcription (Ponti et al., 2008). HIV-2 Tat protein is larger, comprising of 130 amino acids, with a molecular weight of 14-16 kDa compared to its HIV-1 counterpart with 86-104 amino acids (Kurnaeva et al., 2021), and a molecular size 9-14 kDa (Bose, 2017). Rev is an RNA-splicing regulator protein transporting viral RNA transcripts from the nucleus to the cytoplasm (Blissenbach et al., 2010).

The HIV-2 genome comprises of four accessory genes, namely viral infectivity factor (Vif), negative factor (Nef), viral protein r (Vpr), and viral protein x (Vpx), which potentiate viral pathogenesis and infectivity (Strebel, 2013). Vif, expressed in the late phase of infection, facilitates reverse transcription and induces proteasomal degradation of the cellular restriction factor APOBEC3G using the ubiquitin ligase E3 complex (Berger et al., 2010). Nef, also

expressed in the late phase, down-regulates the expression of the Major Histocompatibility Complex (MHC) class I and CD4 receptors, enhancing evasion of immune system (Das et al., 2017). Vpr induces G2 cell-cycle arrest, enhancing viral proliferation, and aids in the nuclear transport of the PIC to the nucleus (Fujita et al., 2010). Notably, Vpr and Vpx in HIV-2 share a 22% amino acid sequence identity, and both are incorporated into the viral particles through interaction with p6 region of the gag protein (Belshan & Ratner, 2003). Vpx, exclusive to HIV-2 and its predecessor SIVsmm, is involved in nuclear transport of PIC, and counteracts the antiviral effect of the sterile α motif (SAM) domain and HD domain-containing protein 1 (SAMHD1) immune restriction factor (Laguette et al., 2011).

3.4 Vpx and its functions in the life cycle of HIV-2

Vpx is a small 14-16 kDa accessory protein encoded by HIV-2 and SIVs of sooty mangabeys, rhesus macaques (SIVmac), red-capped mangabeys (SIVrcm), and mandrills (SIVmnd-2) (Reeves & Doms, 2002). Both Vpx and Vpr share structural similarities, including three amphipathic α-helices, despite having only 20–25% sequence similarity (Fujita et al., 2010). Structurally, Vpr/Vpx in HIV-2 have notable distinctions from HIV-1 Vpr, such as an extended N-terminal loop and proline clusters in the C-terminal loop (Belshan & Ratner, 2003). In particular, HIV-2 Vpx contains a longer region between its second and third helices, enriched with glycines, while HIV-1 Vpr has hydrophilic residues and arginines in the corresponding regions. This distinct modular architecture enables its interaction with various host proteins (Hernandez Vargas & Middleton, 2013). Vpx enhances replication of the viruses and modulates host's immune responses, especially in macrophages and dendritic cells. During viral assembly, it is produced as a component of the gag precursor (Pancio & Ratner, 1998).

One of its prominent function is its ability to impede the activity of SAMHD1, a host restriction factor that limits the availability of deoxynucleotide triphosphates (dNTPs) in non-dividing cells (Laguette et al., 2011). As a dNTP triphosphohydrolase, SAMHD1 decreases the availability of dNTPs, thereby impeding viral reverse-transcription. Vpx interacts directly with SAMHD1, facilitating its ubiquitination and subsequent proteasomal degradation. This interaction occurs through the formation of a Vpx-SAMHD1-DCAF1 complex, wherein Vpx acts as a molecular adaptor, promoting the recognition of SAMHD1 by ubiquitin E3 ligase complex (Goldstone et al., 2011). Consequently, the depletion of SAMHD1 enhances the

availability of dNTPs, thereby facilitating efficient HIV-2 replication in dendritic cells and macrophages, which express SAMHD1 in abundance.

In addition, Vpx plays a key role in transporting the viral PIC into the nucleus, where reverse transcription and integration of the viral genome takes place (Singhal et al., 2006). It carries out this function by promoting interaction of the viral integrase with host proteins involved in nuclear transport. Specifically, Vpx enhances PIC's interaction with importin α/β complexes, which mediate translocation of proteins across the nuclear envelope (Gorlich et al., 1994). This interaction not only ensures efficient nuclear localization of the PIC, but also augments the integration in transcriptionally active sites of the host genome, thereby optimizing conditions for viral replication (Singhal et al., 2006).

Vpx significantly influences the early phase of the viral life cycle in SIV and HIV-2. In myeloid cells, Vpx contributes to the persistence of latent viral reservoirs, which are necessary for viral transmission and disease progression (Laguette et al., 2011). Furthermore, Vpx enhances the virus's ability to evade host defences, facilitating chronic infection (Klotman & Chang, 2006).

This characteristic has prompted research into the use of Vpx to improve lentiviral transduction in gene therapy applications particularly by improving gene delivery to non-dividing or slowly dividing cells (Munis, 2020). By degrading SAMHD1, Vpx enhances reverse transcription, increasing lentiviral transduction efficiency, especially in gene therapy targeting immune and hematologic disorders such as hematopoietic stem cells (HSCs), which are essential for treating conditions like severe combined immunodeficiency (SCID) and sickle cell disease (Laguette et al., 2011). In cancer therapy, Vpx enhances macrophage transduction, improving their potential in immune-based treatments by enabling more efficient gene delivery for anti-tumor functions, such as cytokine expression and phagocytic activity. This is particularly beneficial for solid tumors, where macrophages can be genetically engineered to remodel the tumor microenvironment or directly attack cancer cells (McAllery et al., 2016). Vpx can be delivered via virus-like particles (VLPs) or pre-packaged in lentiviral vectors, allowing transient degradation of SAMHD1 and optimizing gene delivery without altering the cell's genetic makeup. The use of Vpx reduces the viral vector dose required, enhancing safety while boosting therapeutic efficiency in both gene therapy and cancer immunotherapy (Munis, 2020).

Moreover, Vpx inhibits NF-κB to counteract transcriptional suppression by promoting transactivation and the degradation of the human silencing hub (HUSH) complex (Chougui et al., 2018). It also facilitates PIC translocation via interaction with heat shock protein 40 (Hsp40) and nucleoporin 153 (Nup153), while suppressing immune activation by interacting with interferon regulatory factor 5 (IRF5) (Buffone et al., 2018). Previous studies suggest that Vpx may reduce infectivity of HIV-1 by inhibiting the reverse transcriptase indirectly (Mahdi et al., 2018).

3.5 HIV-2 Life cycle

HIV-2 replication cycle shares many similarities with HIV-1, although it exhibits unique features that might impact viral replication, contributing to its lower transmissibility, slower disease progression, and different immune control mechanisms (Nyamweya et al., 2013). HIV life cycle is divided into early phase (entry to integration) and late phase (transcription to virion release) (Chougui et al., 2018) **(Figure 4)**.

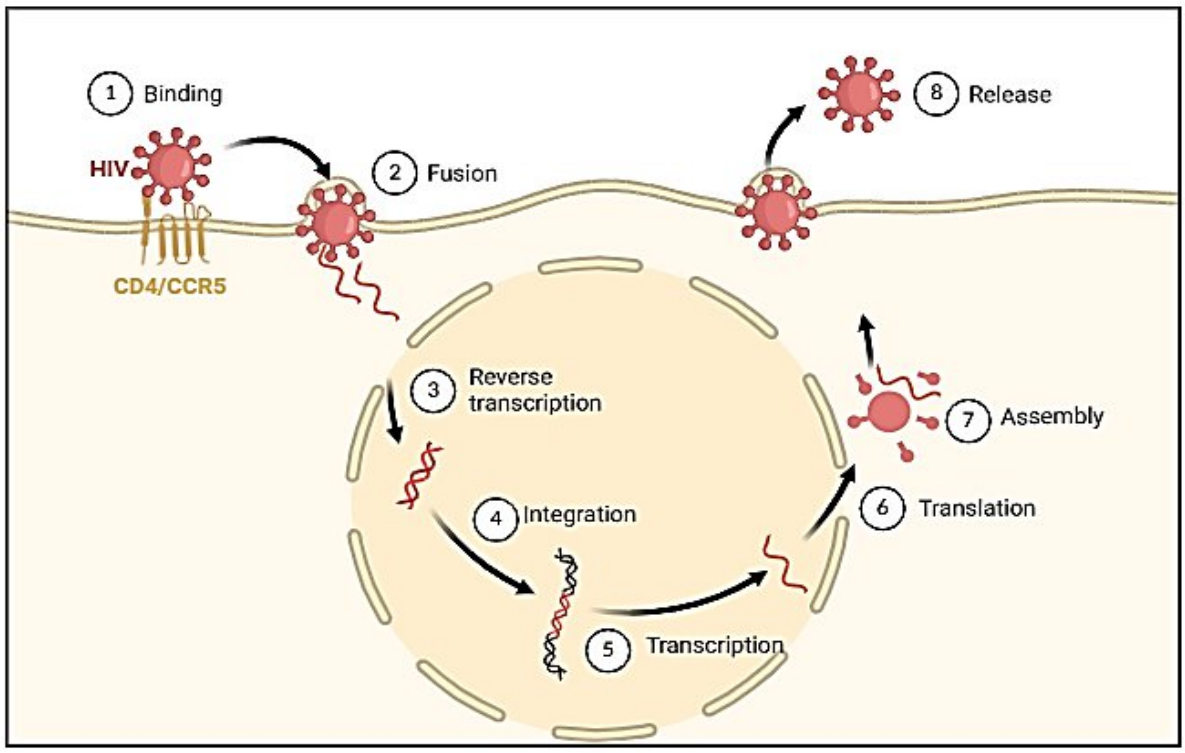

Figure 4: HIV replication cycle (Figure created by BioRender.com). CCR5 is an example of co-receptors utilized by HIV-1. HIV-2 on the other hand can utilize many other co-receptors for entry.

Viral entry is initiated by SU/TM binding to CD4, forming a bridging interaction with co-receptors. The SU gp125 interacts with the cells CD4 receptor, causing conformational

changes that allow the virus to interact with the coreceptors (Reeves & Doms, 2002). Both HIV-1 and HIV-2 target CD4-expressing cells, including CD4+ T lymphocytes**,** macrophages**,** dendritic cells, and microglial cells, with entry mediated by co-receptors such as CCR5 or CXCR4 (Fauci, 1988). While both HIV-1 and HIV-2 utilize CCR5 or CXCR4 co-receptors (Lever, 2021), HIV-2 can utilize a broader range of co-receptors, including CCR1, CCR2, CCR3, CCR5, CXCR4, GPR15, and CXCR6 (Tong & Revill, 2016). Additionally, HIV-2 infects resting CD4+ T cells and myeloid cells more efficiently**,** a property linked to its unique Vpx accessory protein, which is absent in HIV-1 (Laguette et al., 2011).

After fusion, the viral core enclosing the ssRNA genome core enters into the cytoplasm and partial uncoating of the viral core enables the relocation of the PIC into the nucleus through the nuclear pore (Desbois et al., 2008). The enzyme, reverse transcriptase, converts virus RNA genome into a double-strand DNA copy (A. N. Engelman & Cherepanov, 2021). Reverse transcription is a complex process prone to errors (Menéndez-Arias, 2009). HIV-2 RT has lower polymerase activity compared to its HIV-1 counterpart and exhibits reduced RNase H activity (Das et al., 2017).

The integrase enzyme facilitates insertion of proviral DNA into the host genome and host cells' machinery is used to transcribe viral genomic RNA and mRNAs with the help of Tat protein (Chen & Zhou, 1999). This process generates fully spliced, partially spliced, and unspliced mRNAs, encoding different viral proteins. Tat proteins of both viruses function as transcriptional activators of LTRs during replication (Jeeninga et al., 2000).

Rev regulates export of the generated mRNA transcripts from the nucleus into the cytoplasm, ensuring proper viral protein translation and packaging by binding to the Rev Response Element (RRE) segments of viral RNA (Coffin et al., 1997). Viral mRNAs are translated into polyproteins, which are then processed by viral protease to create mature virions after budding(McGraw et al., 2024). During the budding process**,** HIV hijacks the Endosomal Sorting Complex Required for Transport machinery (ESCRT), facilitating membrane scission and viral release (Hurley & Cada, 2018). The release of the viral particles can be inhibited by host viral restriction factor tetherin. HIV-1 uses Vpu to counteract tetherin while HIV-2 relies on its Env protein for partial anti-tetherin activity (Arias et al., 2014).

3.6 Mechanisms of HIV integration

3.6.1 HIV Integrase Enzyme

HIV integrase is a 32kDa protein comprising of three functional domains: the N-terminal, the catalytic core, and the carboxyl DNA binding domains (Jaskolski et al., 2009) **(Figure 5).**

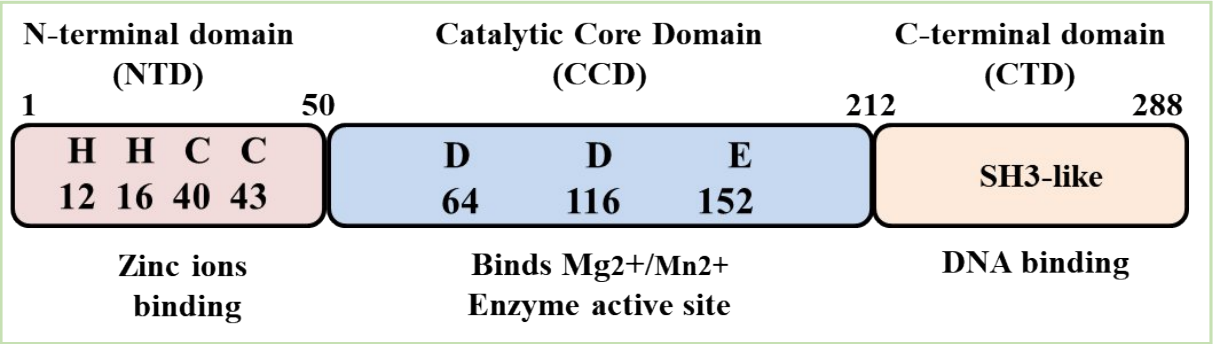

Figure 5: Integrase enzyme. The three domains of HIV integrase and their components; the NTD (purple), CCD (blue), and CTD (pink) are depicted.

With two histidine and two cysteine (HHCC) residues attached to a zinc ion, the amino terminal domain, comprises of amino acid residues 1 - 49 and makes for 20% of the integrase structure (Jóźwik et al., 2020). By stabilising the amino terminus, this zinc binding improves integrase's tetramerization and catalytic activity. According to in vivo research, HHCC mutations obstruct viral replication and integration (Tong & Revill, 2016). The highly conserved active site catalytic core domain, which is made up of half of the integrase polypeptides amino acids from position 50–212, is characterized by the DDE motif (Asp64, Asp116 and Glu152), crucial for enzymatic activity of integrase both in vivo and in vitro. This catalytic triad functions in conjunction with Mg^{2+}/Mn^{2+} ions which are essential for the two step catalytic process (Hare et al., 2012). The carboxyl terminal domain (residues 213-288) is necessary for DNA binding and is the least conserved component of retroviral integrase (Tong & Revill, 2016). It enables protein-protein interactions ensuring stability of the PIC.

3.6.2 Integration of HIV

HIV integration is a process that ensures incorporation of viral genome into the host cell chromatin under the influence of integrase enzyme, establishing a persistent infection (Engelman & Cherepanov, 2012). The process begins after reverse transcription of HIV viral RNA into a complementary DNA copy (Craigie, 2012). Integrase binds to the newly formed double stranded viral DNA on the LTR sequences. The integrase - DNA complex becomes part of the PIC consisting of viral DNA, host proteins and viral proteins; including integrase,

nucleocapsid, matrix, reverse transcriptase and Vpr. This complex also interacts with host factors such as LEDGF/p75 which facilitate chromatin targeting (Kurnaeva et al., 2021).

Enzymatically, IN catalyses two significant sequential processes inside the intasome: the strand transfer and 3′-processing. Initial step involves the 3’ processing where IN removes two GT nucleotides from the conserved CA dinucleotide on the 3’ end, leaving dinucleotide overhang on the 5’ and an exposed 3’ hydroxyl group (Delelis et al., 2008). In the strand transfer, the hydroxyl group attach to the phosphodiester bonds on the opposite strand of the host DNA target, leaving gaps of 4-6 base pairs (Senavirathne et al., 2023). These gaps are filled and conjoined by host repair cellular enzymes: polymerase and ligase enzymes, completing the strand transfer process where viral DNA is embedded in the host DNA (Hare et al., 2012).

The proviral genome is regulated by host and viral transcription factors leading to either active transcription and replication or latency, depending on cellular or environmental conditions (Lever, 2021) **(Figure 6)**.

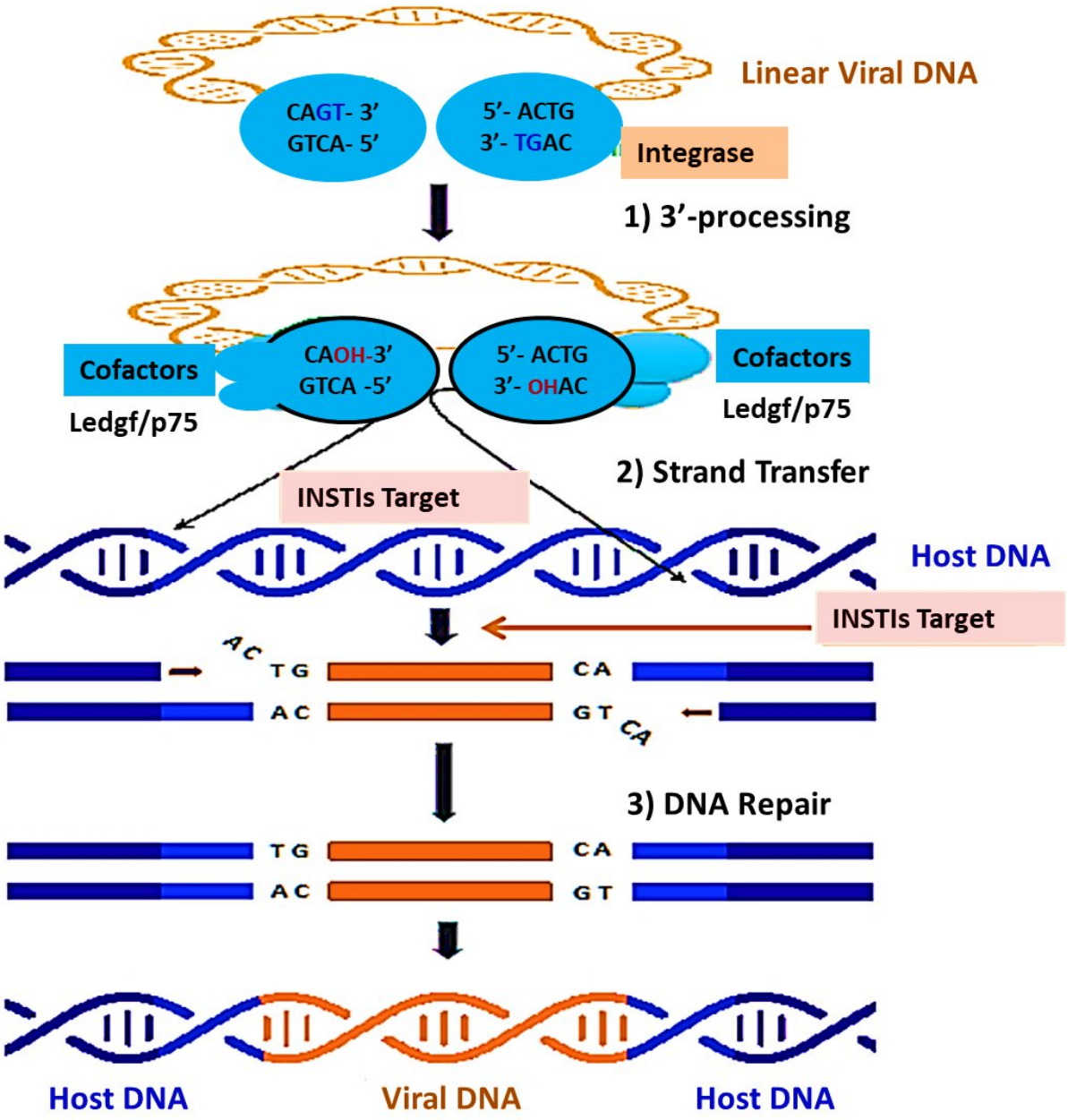

Figure 6: Mechanism of HIV integration starting with 3' processing, strand transfer, insertion and DNA repair. It depicts Viral DNA interaction with integrase enzyme and co factor, LEDGF/p75. Integrase inhibitors (INSTIs) target the strand transfer step (Figure was adapted and modified from Richetta et al., 2022)

The integration process of HIV-1 has been extensively studied to identify virus integration sites, effect of cellular cofactors on integration, and the implications of integration on gene expression (Delelis et al., 2008). Similar studies have been performed for other retroviruses (Desfarges & Ciuffi, 2010), but the mechanisms of viral DNA integration for HIV-2 is less well documented. HIV-2 replication is less frequent in vivo and is also less aggressive compared to HIV-1. It remains to be established whether differences in the integration sites are responsible for the attenuated pathogenicity observed in HIV-2 (Ceccarelli et al., 2021).

An in vitro study on sequences of HIV-2 circle junctions concluded that integrase protein in HIV- 2 cuts the ends of linear DNA unequally leading to removal of two or three bases from the U3 and U5 ends before the integration process (Whitcomb & Hughes, 1991). Another in vitro study found that the nucleotide sequences are mostly similar in both viruses, but they found that HIV-2 contained three base pairs after the 3'CA nucleotide (Hansen & Bushman, 1997).

For retroviruses, actives sites of transcription are favorable targets for integration, although, integration can also occur in non-gene-rich regions within the heterochromatin, leading to varying degrees of expression resulting from chromatin-mediated transcriptional silencing of the integrated provirus (Sunshine et al., 2016). In an in vitro study, selection of the site of integration was dependent on the substrate used and the nucleotide sequence of the target DNA (Dolan et al., 2009) .

In a study by Schroder et al., 2002, unlike HIV-1, HIV-2 integration occurred in opposite direction of the corresponding gene. These events may contribute to HIV-2's prolonged latency (Yeni, 2006). Compared to HIV-1, HIV-2 is more prone to latency and shows a diminished response to activation signals from cells. The long terminal repeats (LTRs) regulate the expression of the virus in response to cellular transcription signals (Jeeninga et al., 2000). Its LTRs differ in composition from HIV-1, and contains fewer and distinct transcription factor binding sites, leading to reduced activation in T cells (Le Hingrat et al., 2020). Additionally, LEDGF/p75 directs lentivirus integration holding integrase and chromatin together during HIV-1 integration (Poeschla, 2008). It is yet to be investigated whether HIV 2 integration site is influenced in a similar fashion by LEDGF/p75 just like in HIV 1.

3.6.3 LEDGF/p75 and its role in integration

LEDGF/p75, a nuclear protein, is involved in regulation of genes, cell survival and disease processes such as cancer, autoimmunity, and HIV integration (Ortiz-Hernandez et al., 2024). It belongs to the family of hepatoma derived growth factor (HDGF)-related proteins, encoded by the PSIP1 (PC4 and SFRS1 interacting protein) gene on chromosome 9p22.2, and functions as a molecular bridge connecting proteins to chromatin (Lampi et al., 2019). This protein has gained significant interest in HIV due to its interaction with integrase, making it a potential target for therapy (Poeschla, 2008).

Structurally, LEDGF/p75 consists of 530 amino acids and features five distinct functional regions within the PWWP domain. This PWWP domain comprises of amino acid residues 1-93 at the N-terminus and interacts with methylated histones to bind chromatin (Ciuffi et al., 2005). The C-terminal domain (residue 347-429) comprises of the integrase-binding domain (IBD) of approximately 80 amino acids. The IBD facilitates interaction between LEDGF/p75 and IN, making it crucial for virus DNA integration into human host chromatin (Lampi et al., 2019). A smaller protein variant, made up of 333 amino acids, LEDGF/p52, lacks the IBD and is thought to be a coordinator between transcription and pre-mRNA splicing. LEDGF/p75 is highly expressed in rapidly dividing tissues, and contributes to genomic stability, DNA repair, and stress response by activating stress-related genes (Maertens et al., 2003)**(Figure 7).**

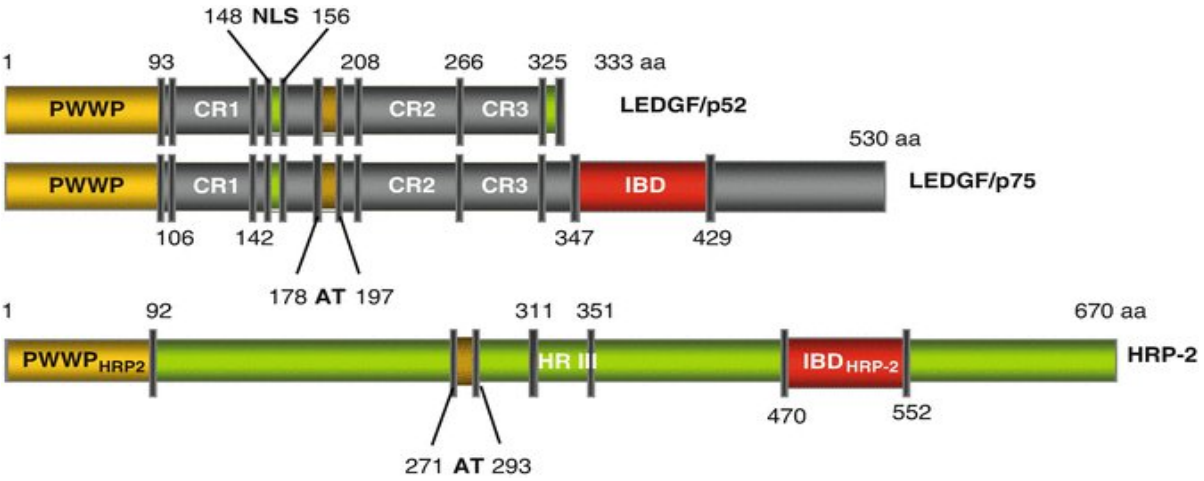

Figure 7: Structural representation of splice variants LEDGF/p75, LEDGF/p52 and HRP-2 based on the amino acid (aa) sequences and highlighting key domains such as the PWWP domain, the nuclear localization signal (NLS), three charged regions (CR1,CR2,CR3), an AT-hook-like motif (AT), homology region III (HR III), and the integrase-binding domain (IBD) (Schrijvers & Debyser, 2018).

The IBD contains an alpha helix that binds to the hydrophobic pockets of the catalytic core domain. This interaction involves LEDGF/p75 residues (Ile365, Asp366 and Phe406) and integrase residues (Trp131, Thr125 and Asn120) enhancing stability of the complex (Schrijvers & Debyser, 2018). This promotes the dimerization of IN, which is necessary for its catalytic function. To enhance integration targeting in gene rich regions, the N-terminal PWWP domain binds to histone H3 lysine 36 trimethylation (H3K36me3); a histone modification factor present in enriched regions of actively transcribed genes (Lampi et al., 2019). This directs HIV to preferentially integrate into gene-dense euchromatic regions

enhancing proviral expression and facilitating stable tethering of PIC to chromatin, thereby increasing the efficiency of integration (Maertens et al., 2003).

Absence of LEDGF/p75 reduces the integration efficiency, and may result in random integration which can lead to suboptimal viral activity (Yoder, 2019). While other proteins such as hepatoma-derived growth factor related protein 2 (HRP-2) may substitute for LEDGF/p75 in some retroviruses, they are less effective in guiding integration towards transcriptionally active sites (Shun et al., 2007). The connection between the LEDGF/p75-IN complex and its role in integration has made it a target for therapeutic development, leading to the creation of inhibitors known as LEDGINs. These inhibitors disrupt the pre-integration complex, reducing viral replication and redirecting the integration to less-active genomic regions (Christ et al., 2012). Unlike conventional antiretroviral drugs, LEDGINs are less prone to resistance since they act on a host protein rather than the virus itself (Christ & Debyser, 2013).

Beyond its role in HIV, LEDGF/p75 is linked to the development of cancer, by promoting proliferation and cell survival, particularly in leukemia and prostate cancer (Ortiz-Hernandez et al., 2024). It is also an auto antigen in diseases like Sjögren's syndrome and systemic lupus erythematosus, suggesting a potential link to the development to autoimmune diseases (Ciuffi et al., 2005). Further research into its functions across different biological and pathological contexts continues to expand its therapeutic relevance.

3.7 HIV-2's Susceptibility to Antiretroviral Therapy

Combined antiretroviral therapy (cART) marked a transformative step in the treatment of HIV, shifting the prognosis from fatal to manageable (Woldegeorgis et al., 2024). cART entails combining agents from various drug classes targeting diverse phases of the virus life cycle, contrasting earlier monotherapies or dual therapies (Yeni, 2006). The goal of cART is to reduce viral load, lower transmission risk, boost immune system and minimize opportunistic infections, thereby, prolonging patient's survival (Reeves et al., 2021).

To date, Food and Drug Administration (FDA) has approved more than thirty antiretroviral drugs targeting different steps in the viral life cycle (Gandhi et al., 2025) . They include CD4 mimics, CCR5 inhibitors, fusion and entry inhibitors, reverse transcriptase inhibitors; further classified into nucleoside analogues (NRTIs) and non-nucleoside analogues (NNRTIs) (Taramasso et al., 2023), protease inhibitors (PIs) (Arts & Hazuda, 2012) and integrase

strand-transfer inhibitors (INSTIs) (Triki et al., 2018). Common drug regimens entail the use of two NRTIs along with one NNRTI, PI or INSTI.

All the approved antiretroviral drugs are designed for HIV-1 management and therapy for HIV-2 lags behind with notable limitations due to the presence of inherent polymorphisms and mutations in NNRTIs (Woldegeorgis et al., 2024) **(Table 1).** With supporting data from a few phenotypic studies, INSTIs have shown efficacy in HIV-2 similar to HIV-1 (Mörner et al., 1999).

Class	Antiretroviral Drugs: HIV-2 Activity	
	Effective	Ineffective
Reverse Transcriptase Nucleoside inhibitors(NRTIs)	*tenofovir, lamivudine, emtricitabine,, islatravir, abacavir*	*didanosine, stavudine, zidovudine*
Reverse Transcriptase non-nucleoside Inhibitors(NNRTIs)	-	*doravirine, nevirapine, rilpivirine, efavirenz, etravirine,*
Inhibitors of Protease	*lopinavir, saquinavir, darunavir*	*nelfinavir atazanavir, indinavir fosamprenavir ,tipranavir*
Inhibitors of Integrase	*Cabotegravir, raltegravir, dolutegravir elvitegravir, bictegravir,*	-
Fusion-entry Inhibitors	*Ibalizumab, maraviroc*	*Fostemsavir, enfuvirtide*
Capsid Inhibitors	*Lenacapavir*	-

Table 1: Approved antiretroviral drugs with activity against HIV-2

3.8 Integrase Strand Transfer Inhibitors (INSTIs)

INSTIs constitute an important class of HIV antiretroviral agents designed to block the integration of the viral DNA into the host cell (Craigie, 2012). Since their introduction, INSTIs have significantly improved HIV treatment by offering potent antiviral effects, favourable tolerability and a high resistance barrier, particularly with second generation agents (Wang et al., 2021). According to guidelines by the European AIDS Clinical Society (EACS), cabotegravir can be administered immediately after primary HIV infection until resistance testing is available, while experienced virologically suppressed individuals can use bictegravir and dolutegravir containing regime (EACS 2025: Summary V12.1).

To date, FDA has approved five INSTIs with the latest inhibitor designed as long acting injectable offering solution to adherence challenge (Messiaen et al., 2013). The first

generation INSTIs include raltegravir (RAL) which was the first INSTI to be licensed over a decade ago (2007) followed by elvitegravir (EVG) (2012). They proved to be effective treatments of HIV but this was short lived as resistant mutations emerged, dampening the notion that they had a low genetic barrier to resistance (Di Perri et al., 2019; Pau & George, 2014).

The second generation INSTIs soon followed and included dolutegravir (DTG, licensed in 2013), bictegravir (BIC, licensed in 2018) and cabotegravir (CAB) which was approved in 2020. Their development was based on a fundamental shift in the central pharmacore from the bicyclic form to the tricyclic ring responsible for the metal ion chelation (Jóźwik et al., 2020), creating additional scaffold with the integrase residues, and increasing their potency in order to combat the rapidly emerging HIV variants These inhibitors increased potency by making broad contact with integrase residues through the enlarged scaffold (Wang et al., 2021) **(Figure 8).**

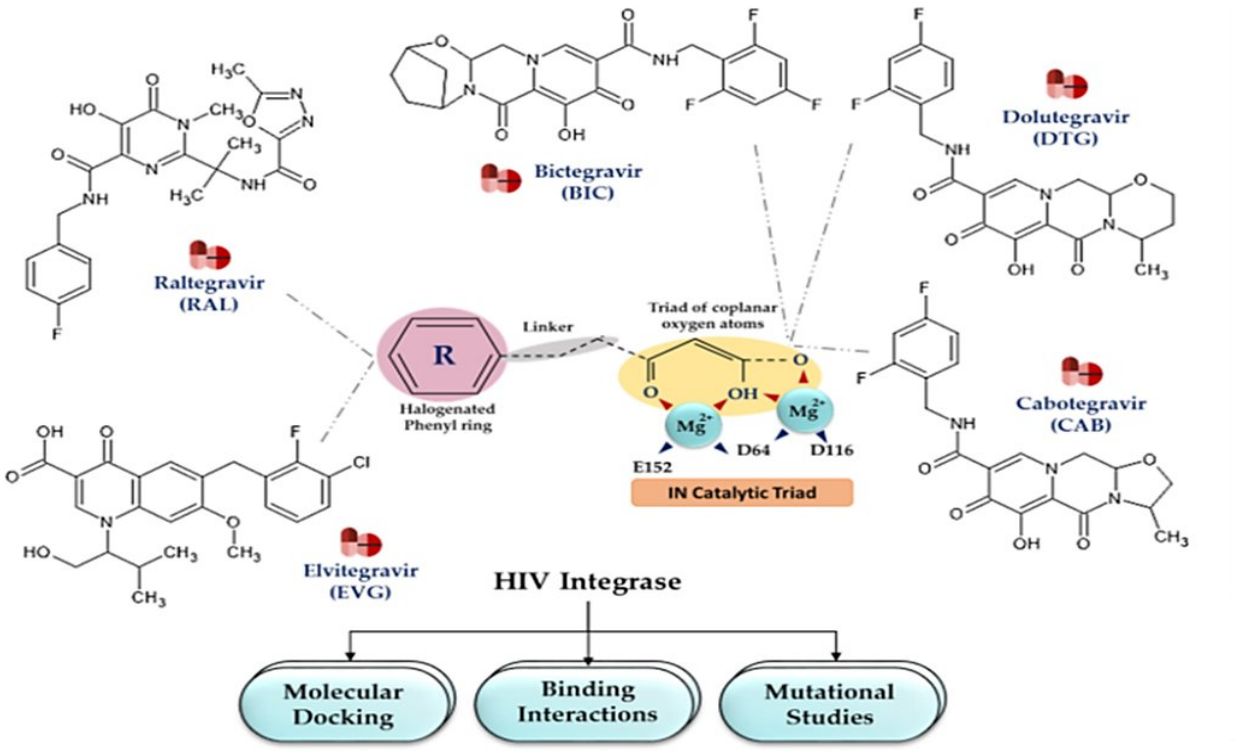

Figure 8: Chemical structures of the INSTIs (Sayyed et al., 2023) highlighting interaction with HIV integrase

3.8.1 INSTIs Mechanism of action

HIV integration is a multistep process involving DNA processing and its incorporation into the host genome. By competitively attaching to their active sites, INSTIs prevent integration and impede the strand transfer phase (Delelis et al., 2008). This is accomplished by either

chelating the divalent cation necessary for the enzymatic activity or by displacing the end of viral DNA 3′region from the catalytic binding site (Anstett et al., 2017). The phenyl ring of INSTIs interacts with residues 145 and 146 of the integrase as well as the viral guanine: cytosine bases. The 3′ processed DNA's terminal adenine is moved out of the IN-DNA complex's active site (Jóźwik et al., 2020). The action of the enzyme depends on the chelation of the Mg^{2+}/Mn^{2+} divalent cations by three coplanar oxygen atoms, which also renders the IN-DNA complex inactive and inserts it into the host's genome (Hare et al., 2011). Since integrase homologue is absent from human cells and given its importance in virus cycle, it has emerged as a promising target for antiretroviral therapy development (Engelman & Cherepanov, 2012).

3.8.2 FDA approved INSTIs

3.8.2.1 Raltegravir

This first INSTI became popular upon approval for its rapid viral suppression and relatively favourable safety profile. It was recommended for use in persons with multidrug-resistant HIV-1, who had previously been exposed to a cocktail of ARVs from the NRTI, NNRTI, and PI classes (Hicks & Gulick, 2009). Later, it was added as a first-line treatment administered with two NRTIs, either once or twice a day for both HIV-1 and HIV-2 patients. When used together with tenofovir disoproxil fumarate (TDF), it demonstrated efficacy in treating naive persons, as well as immunosuppressed individuals (De Clercq, 2009). According to in silico prediction studies, it works by directly interacting with a number of residues on the catalytic region of HIV-1 integrase (Trivedi et al., 2020). However, RAL has a relatively short half-life, necessitating twice daily dosing, impacting adherence and overall treatment effectiveness.

3.8.2.2 Elvitegravir

In a once daily fixed-dose combination, elvitegravir demonstrated efficacy in treating HIV-1 and HIV-2 (Reviriego, 2014). Compared to raltegravir, it was better tolerated and more effective in treating multi-drug resistant strains of moloney leukemia viruses (MLV), HIV and SIV (Trivedi et al., 2020). Elvitegravir hinders the interaction between the IN and DNA, thereby inhibiting integration. This is accomplished by interaction with residues E152 and D64 of the integrase (Shimura & Kodama, 2009).

3.8.2.3 Dolutegravir

Approved in 2013, (Walmsley et al., 2013) dolutegravir inhibits HIV integrase by binding to the enzyme's active site, where it interacts with key residues near the β4-α2 loop and chelates essential magnesium ions, inducing conformational changes that block the strand-transfer step of viral DNA integration (Hare et al., 2011). In contrast to RAL and EVG, DTG's halobenzyl group; a special structural component, increases its reach into the active site and creates a noticeably stronger interaction with the enzyme. This distinctive characteristic enhances DTG's efficacy against strains resistant to EVG and RAL (Le Hingrat et al., 2019).

Dolutegravir showed superior efficacy to its predecessors, forming more stable interactions with the Integrase-DNA complex (Kandel & Walmsley, 2015). Its 14-hour plasma half-life increases its ability to suppress resistant strains, which made it ideal for treatment of naive patients (Aknin et al., 2019). In combination with other drugs, DTG is under trial for use as an injectable antiretroviral therapy (Perazzolo et al., 2023).

3.8.2.4 Bictegravir

In 2018, the FDA authorised the use of bictegravir along with tenofovir and emtricitabine (Spagnuolo et al., 2018) and showed its potent activity against both HIV-1 and HIV-2. Bictegravir has demonstrated greater efficacy than RAL or EVG, in part due to its prolonged dissociation from the integrase–DNA complex (~35 hours), which enhances its antiviral potency and resistance barrier. Additionally, its favorable pharmacokinetic profile, including high bioavailability and sustained plasma concentrations, supports once-daily dosing without a booster. Bictegravir showed little to no cytotoxicity on cells in vitro and a higher barrier to resistance compared to RAL, EVG, and DTG in HIV-1 and HIV-2 (Tsiang et al., 2016; Bártolo et al., 2022).

3.8.2.5 Cabotegravir

The most recent addition to INSTI is cabotegravir, which was approved in 2021 for use as a once-daily oral tablet in conjunction with rilpivirine (Pinto et al., 2023). In patients who have had virological suppression, it is given as a long-acting intramuscular injectable once per month or once every two months (Nachega et al., 2023). An analogue of DTG, cabotegravir has a longer half-life of approximately 40 days when administered intramuscularly (Whitfield et al., 2016). The drug exhibited excellent potency against four HIV-2 isolates with EC_{50} of

0.12 nM. According to a newly released in vitro study, CAB showed efficacy against HIV-2 with a low EC_{50} in a single cycle spreading assay (Fernandez & van Halsema, 2019).

3.8.3 Common treatment - associated resistance mutations

Resistance to INSTIs is primarily caused by mutations in the catalytic core domain of the IN. Primary resistance mutations such as Q148H/R/K, N155H, and Y143C/R; occur near the enzyme's active site, directly interfering with drug binding, thereby reducing INSTI's effectiveness. In people with HIV-2, N155H, Y143 and Q148K/R/H mutations are typically linked to resistance to RAL therapy (Anstett et al., 2017) **(Table 2).**

Category	Mutation	Notes
Primary mutations	Q148H/K/R	Major mutation; causes broad resistance to INSTIs
	N155H	Common pathway; cross-resistance with raltegravir and elvitegravir
	Y143C/R	Specific to raltegravir resistance
	E92Q	Strong impact on elvitegravir and moderate on raltegravir
	R263K	Linked to dolutegravir, bictegravir, and cabotegravir resistance
	S230R	Associated with dolutegravir resistance
	S153Y	Associated with cabotegravir resistance
	H51Y	Associated with cabotegravir resistance
	Q146L	Associated with cabotegravir resistance
Secondary (accessory) mutations	T97A	Accessory; increases resistance, restores viral fitness
	G140A/S/C	Accessory; often co-occurs with Q148 mutations
	L74M	Accessory; enhances resistance with Q148 mutations
	E138A/K	Increases resistance when combined with primary mutations
	L234V	Minor mutation contributing to dolutegravir resistance

Table 2: Major primary and secondary mutations associated with INSTIs

Secondary mutations, such as G140S/A/C, L74M, T97A and E138K/A, amplify the impact of primary mutations, enhancing viral replication and decreasing susceptibility to INSTIs (Mbisa et al., 2020). Cross-resistance is a significant challenge, as certain mutations that confer resistance to one INSTI can also affect the efficacy of others. For instance, the Q148H mutation combined with G140S leads to strong resistance against RAL, EVG, DTG and BIC (Gil et al., 2022). Additionally, mutations such as R263K result in intermediate resistance to multiple INSTIs, complicating treatment choices. In vitro, R263L or M501/R263K mutations diminished BIC's efficiency by 2-3 times, whereas replacement at position Q148 reduced its effectiveness by 63 times (Anstett et al., 2017). However, BIC did not exhibit any resistance to E92Q/T97A and E92A/Q148K, which were seen in RAL and DTG (Bártolo et al., 2022) **(Table 3).**

Drug	Key Mutations	Notes
Bictegravir	E92Q, T97A, Y143C/R, Q148R, N155H; G140A/C/S + Q148H/R/K (+ L74M, T97A, E138A/K)	High genetic barrier to resistance; retains activity against most single mutations
Cabotegravir	R263K, S153Y, S147G, H51Y, Q146L; Q148Q/R, G140G/R, N155N/H, T97T/A, E138E/K, L74I	Moderate genetic barrier to resistance; resistance may cause class-wide cross-resistance
Dolutegravir	R263K, S230R, N155H + E92Q; Q148H + G140S/A/C (+ L74M, E138K/A)	High genetic barrier to resistance; resistance common, occurs with advanced HIV or low drug levels
Elvitegravir	E92Q (most frequent), N155H, Q148H/K/R, T66I	Lower genetic barrier; E92Q alone reduces elvitegravir's susceptibility >20-fold
Raltegravir	N155H + E92Q; Q148H + G140S; Y143R + T97A; G118R, F121Y	Lowest genetic barrier; rapid resistance emergence, significant cross-resistance

Table 3: Drug specific mutations of INSTIs observed in HIV-1 and HIV-2

The genetic barrier to resistance varies across INSTIs, with some drugs requiring multiple mutations while others are compromised by a single mutation (Tang & Shafer, 2012).
DTG and BIC have a high genetic barrier to resistance, maintaining effectiveness unless several mutations accumulate (Zhao et al., 2022). CAB has a moderate barrier while RAL and ELV have a lower barrier, making them more prone to treatment-associated resistance (S. J. Smith et al., 2018). Sub-optimal drug levels, usually as a result of inconsistent adherence or insufficient drug concentrations, can promote the emergence of resistant viral strains (Tam et al., 2008). For example, resistance to DTG is more likely observed in individuals with pre-existing integrase mutations or in cases where serum drug concentrations are insufficient for complete viral suppression (Pena et al., 2018).

Screening of our HIV-2 ROD based CGP sequence for possible polymorphisms, in comparison to deposited sequences in the NCBI database revealed some secondary resistance mutations such as 72I, 74I, 165 I, 201I and 203M which have been reported in HIV-2 ROD and are known to confer resistance to INSTIs in the case of HIV-1.

3.8.4 Molecular docking studies of INSTIs

Molecular docking studies have emerged as critical computational approach in HIV drug discovery, illustrating the mechanisms of interaction between INSTIs and the integrase enzyme, and providing structural basis of drug binding, effects of resistance mutations, and optimization of new inhibitors ((Esposito & Tramontano, 2014). The prototype foamy virus (PFV) intasomes' X-ray crystallographic structures clarified INSTIs' binding to IN; nevertheless, due to the low sequence identity (15% genome) of HIV-1 and PFV, the information acquired was insufficient (Rabe et al., 2021). Later, HIV-1 and SIV red capped mangabeys (SIVrcm) intasomes complexed with DTG and BIC residues were elucidated through Cryo electron microscopy providing more insights into the phenomenon (Cook et al., 2021).

This high-resolution structure revealed that key INSTI binding interactions involve coordination with active site residues such as Asp64, Asp116 and Glu152 (Hare et al., 2012). They demonstrated the ability of INSTIs to chelate metal ions within the active site and form hydrogen bonds with key integrase residues. Docking studies of second-generation INSTIs, such as DTG and BIC, have demonstrated that these inhibitors exhibit stronger binding affinities and enhanced stability, compared to first-generation drugs such as RAL and EVG (Savarino, 2007). The improved potency of these newer drugs has been attributed to their ability to accommodate conformational changes within the integrase enzyme, enabling them to maintain activity against some resistant variants (Tsiang et al., 2016).

Through docking, mutations within the integrase protein, particularly in the catalytic core domain, have been shown to reduce the efficacy of INSTIs by altering the structural conformation of the active site, thereby weakening drug binding (Quashie et al., 2012). Key resistance mutations, such as Q148H/R/K, N155H and Y143C/R, have been extensively studied using molecular docking approaches, revealing significant reductions in binding affinities for several INSTIs (Smith et al., 2009)

For instance, the Q148H mutation, which is commonly associated with high-level resistance to RAL and EVG, disrupts critical hydrogen bonding interactions within the active site, leading to reduced drug binding stability. Docking simulations have further shown that the presence of secondary mutations, such as G140S and E138K, enhances the impact of Q148H by further destabilizing the inhibitor-enzyme complex (Tsiang et al., 2016). Conversely, DTG and BIC exhibit greater resilience to these mutations, as docking studies suggest that their

flexible binding conformations allow them to retain inhibitory activity despite structural alterations in the enzyme (Savarino, 2007).

Although the enzyme binding sites are highly conserved and unique to retroviruses, polymorphisms and point mutations can alter the inhibitor peptide's specificity, lowering its binding affinity (Engelman, 2019). These studies have been done for HIV-1, and given the 60% amino acids sequence differences, it is unclear how certain naturally occurring integrase polymorphisms may impact the structure, function, and binding affinity of INSTIs to HIV-2 integrase (Isaacs et al., 2020).

3.8.5 INSTIs as potential therapeutics for SARS-CoV-2

HIV antiretroviral medications gained attention during the coronavirus epidemic because of their various functions in viral replication. Since there was no known effective treatment for COVID-19, it was necessary to evaluate available antiviral drugs for potential medication repurposing in order to stop the pandemic (Sang et al., 2020). HIV antiviral medications, such as DTG, RAL and some protease inhibitors were among substances tested for use against SARs-CoV-2's polymerase and protease (Indu et al., 2020). Further research was necessary to validate the findings of in silico evaluations that highlighted RAL as a potential therapeutic option based on its strong binding energies to the RNA-dependent polymerase (RdRp) of SARS-CoV-2 (Indu et al., 2020).

Through molecular docking studies, it was hypothesized that integrase inhibitors would interfere with SARS-CoV-2's replication by interfering with essential components such as helicase, non-structural proteins NSP13 and NSP14, and RdRp (Zapata-Cardona et al., 2023). DTG and RAL showed favourable binding affinities in silico through interference at the RNA synthesis stage. Additional simulations against exoribonuclease (nsp14) and helicase (nsp13) revealed that they might also prevent viral RNA from unwinding and proofreading (Ahmed et al., 2020). These interactions were confirmed by molecular dynamic simulations, which revealed stable drug-protein complexes and advantageous binding energies, suggesting that the inhibitors would efficiently suppress SARS-CoV-2 (Mohamed et al., 2023).

DTG, RAL and BIC demonstrated modest antiviral activity in vitro utilising cell lines like Vero E6, HEK 293T and Calu-3, with dose-dependent reduction of viral replication (Dittmar et al., 2021). However, due to potential differences in the replication dynamics between

SARS-CoV-2 and HIV, these medications were not strong enough to completely stop viral reproduction (Zapata-Cardona et al., 2023).

3.9 Capsid Inhibitors

Capsid inhibitors target the viral capsid (Link et al., 2020). Polypeptides, gag & gag/pol, are processed by the viral protease at particular sites during HIV-1 particle formation, resulting in the formation of the mature capsid (Rossi et al., 2021). The capsid plays multiple roles from protection and stabilization of genome, virus uncoating, transport of PIC into the nucleus for integration, immune response and maturation of virions, making it an attractive therapeutic target specifically aiming at the highly conserved N-terminal domain (Campbell & Hope, 2015b).

The exploration of capsid-targeting HIV inhibitors began in 2003, with the identification of Adenylyl cyclase-associated protein 1 (CAP-1), a compound discovered through computational methods aimed at its N-terminal domain. In vitro, it inhibited the assembly of a mature capsid, but the viral core remained intact (Tang et al., 2003). Subsequent scientific advancements included elucidating the crystal structure of the capsid hexamer crystal structure, providing vital insights into molecular underpinnings of capsid assembly. This led to the identification of a new compound (BI-1 & BI-2) that effectively bound to the capsid, though BI-1's limited potency hindered its clinical progression (Lamorte et al., 2013). In 2010, PF-3450074 (PF74) emerged as a promising candidate, targeting a previously unexplored region within the CA amino terminal domain. Having a broad spectrum of inhibition against various HIV isolates with sub-micromolar potency, PF74 disrupted both the early phase; leading to capsid instability, and the late phase by interfering with formation of mature viral cores. Notably, PF74's antiviral effects were influenced by the host factor cyclophilin A, suggesting its mechanism involved disrupting host interactions with the viral capsid (Blair et al., 2010).

The introduction of GS-CA1 in 2017 marked a significant advancement, providing a broad-spectrum effect across all HIV clades. Exhibiting exceptional potency, and favorable pharmacokinetic properties in mononuclear cells, GS-CA1 demonstrated potential for long-acting formulations (Perrier et al., 2017).

In recent years, GS-6207 showcased impressive antiviral potency, with significantly lower EC_{50} values than existing antiretroviral drugs. Its pharmacological profile indicated high

metabolic stability and favorable pharmacokinetics, suggesting viability for once-every-three-month administration in humans (Zheng et al., 2018). Resistance studies revealed specific mutations associated with GS-6207 however it was effective in treatment naïve patients (Marcelin et al., 2020).

3.9.1 Lenacapavir

Lenacapavir, the latest and first FDA-approved HIV capsid inhibitor, administered orally or via subcutaneous injection, exhibits potent efficacy against multidrug-resistant HIV-1 strains (Prather et al., 2023) **(Figure 9).**

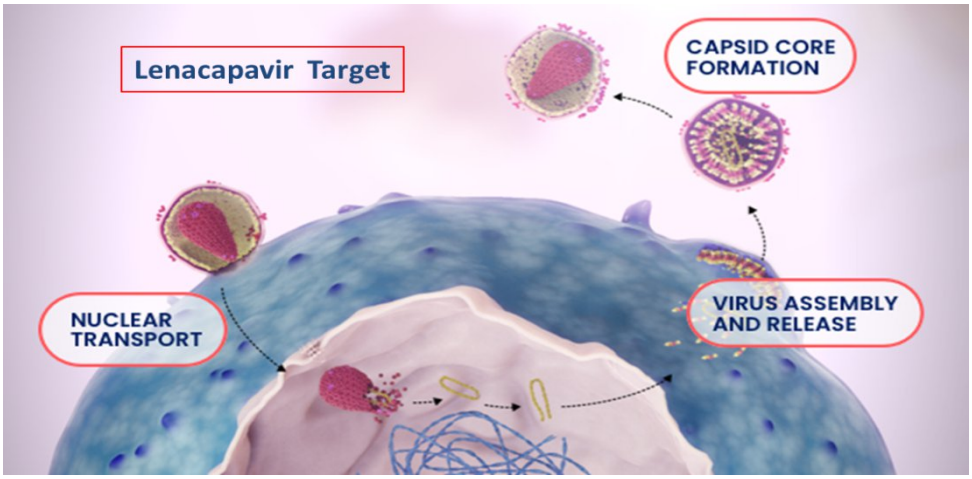

Figure 9: Mechanism of action of lenacapavir **(**Adapted and modified from Segal-Maurer et al., 2022)

It functions by binding to p24 capsid protein subunits, disrupting viral replication in both the early and late stages. Lenacapavir blocks nuclear uptake of proviral DNA by impeding the interaction between nuclear import proteins and the capsid. Moreover, it hampers the efficient functioning of gag/gag-pol polyproteins, preventing capsid core formation, thereby resulting in dysfunctional virion production (Perrier et al., 2017). Furthermore, lenacapavir acts by interfering with essential processes of HIV-1 replication. Specifically, it disrupts interactions between capsid monomers, impeding binding of essential proteins like NUP153 and CPSF6, necessary for entry of capsid into the nuclear and viral genetic integration (Buffone et al., 2018). Lenacapavir's binding mode to the phenylalanine-glycine binding pocket between adjacent capsid monomers prevents efficient nuclear entry of the capsid, thus inhibiting HIV-1 genomic integration (Faysal et al., 2021). Lenacapavir targets the hydrophobic capsid pocket, disrupting gag-pol function and reducing subunit production of the capsid protein.

In low concentrations of picomolar range, it demonstrated broad-spectrum antivirus activity against all HIV-1 clades (Dzinamarira et al., 2023). The efficacy of lenacapavir was shown to be more evident in the early phase, with an EC_{50} of 23-55 pM compared to the late phase with an EC_{50} of 314-439 pM (Link et al., 2020). At higher concentrations (5 nM), formation of two-long terminal repeat (2-LTR) circles was impaired, and overall, there was reduction in HIV-1 DNA levels. Previous studies have shown that at even higher doses (50 nM), lenacapavir also inhibited reverse transcription (Bester et al., 2020). As reported by CAPELLA study and other clinical trials, resistance to lenacapavir was rare in treatment-naive patients, but possible in patients experiencing viral rebound or in case of poor adherence to oral medications. On another note, baseline resistance to major ART classes does not appear to affect lenacapavir's efficacy, making it a valuable option in multidrug-resistant HIV treatment settings (Segal-Maurer et al., 2022).

4. RESEARCH OBJECTIVES

Objective 1: Inhibition profiling of INSTIs and lenacapavir against HIV-2 and investigation of the effects of raltegravir on SARS-CoV-2`s activity

a) Inhibition profiling of INSTIs against HIV-2 *in vitro*
b) Profiling INSTIs inhibitory effects on HIV-2 in cell culture
c) Evaluation of INSTIs against SARS-CoV-2 activity
d) Evaluation of lenacapavir's effects on HIV-2 in cell culture
e) Molecular docking of INSTIs and lenacapavir on HIV-2 integrase and the capsid, respectively

Objective 2: Evaluation of the transcriptomic changes induced by Vpx on gene expression, cytokine profiles and HIV-1 Tat protein

a) Determine the transcriptomic changes induced by Vpx following transfection with wild-type and functionally restricted mutant plasmids
b) Detection of the Vpx effects on the cytokine profile of transfected THP-1 cells
c) Investigation of Vpx's effects on HIV-1 Tat protein
d) Evaluation of effects of Vpx on gene expression following HIV-2 infection or transfection
e) Measurement of Caspase 3 activity

Objective 3: Studies on HIV-2 integration sites and the interaction of LEDGF/p75 with HIV-2 integrase during integration

a) Detection of LEDGF/p75 and integrase expression in Jurkat and HEK293T cell line
b) Evaluation of LEDGF/p75–integrase interaction in Jurkat cells using proximity ligation assay (PLA)
c) Examining the effects of LEDGF/p75 silencing on transduction efficiency and interaction with HIV-2 integrase
d) Analysis of the preferred integration sites of HIV-1 and HIV-2 using genomic sequencing

5. MATERIALS AND METHODS

5.1 Plasmids and inhibitors

Second-generation lentiviral vectors comprising of the packaging, transfer and envelope plasmids were utilized for HIV-1 and HIV-2 pseudovirion production. These included the transfer vector pWOX expressing mCherry (Jochmans et al., 2012), packaging plasmid psPAX2 (which were kind gifts from Dr. D. Trono of the University of Geneva Medical School), and the envelope plasmid pMDG encoding the vesicular stomatitis virus (VSV-G) envelope protein for the production of HIV-1 pseudovirions. For HIV-2, plasmids comprised of HIV-2 CGP (based on the ROD protein containing HIV-2 genes), the transfer plasmid CRU5SINCSW, and the pMDG envelope plasmid (Mahdi et al., 2015). The HIV-2 vectors were generously provided by Joseph P. Dougherty of the Robert Wood Johnson Medical School (NJ, USA). Additionally, CRU5SINCSW (HIV-2's transfer plasmid) was engineered to express the mCherry fluorescent protein under the control of a CMV promoter, inserted between the BamH1 and Nde1 (New England BioLabs, MA, USA) restriction enzyme sites. Verification of cloning and transduction efficiency was conducted using restriction enzyme digestion, PCR, and transduction-based assays. All chemical inhibitors were purchased from MedChem Express (MCE, NJ, USA) and dissolved in DMSO to achieve final concentrations of between 1 nM to 1 μM for INSTIs and 1 pM to 1 nM for lenacapavir.

5.2 Inhibition profiling of INSTIs against HIV-2 in vitro

5.2.1 Cloning, expression and purification of HIV-2 integrase

A HIS- tagged plasmid pQE-60 was constructed (Genscript Biotech Corporation (NJ, USA) containing an 894 bp DNA fragment of the HIV-2 integrase and preceded by six histidine residues at the 5' end of the cloning site. The constructed plasmid was then transformed into competent *Escherichia coli* BL-21(DE3) culture cells expressing pET11a bacteria (Thermo Fisher Scientific, Waltham, MA, USA) and restricted with BamH1 and Nde1 (New England BioLabs, MA, USA) restriction enzymes for confirmation **(Figure 10).**

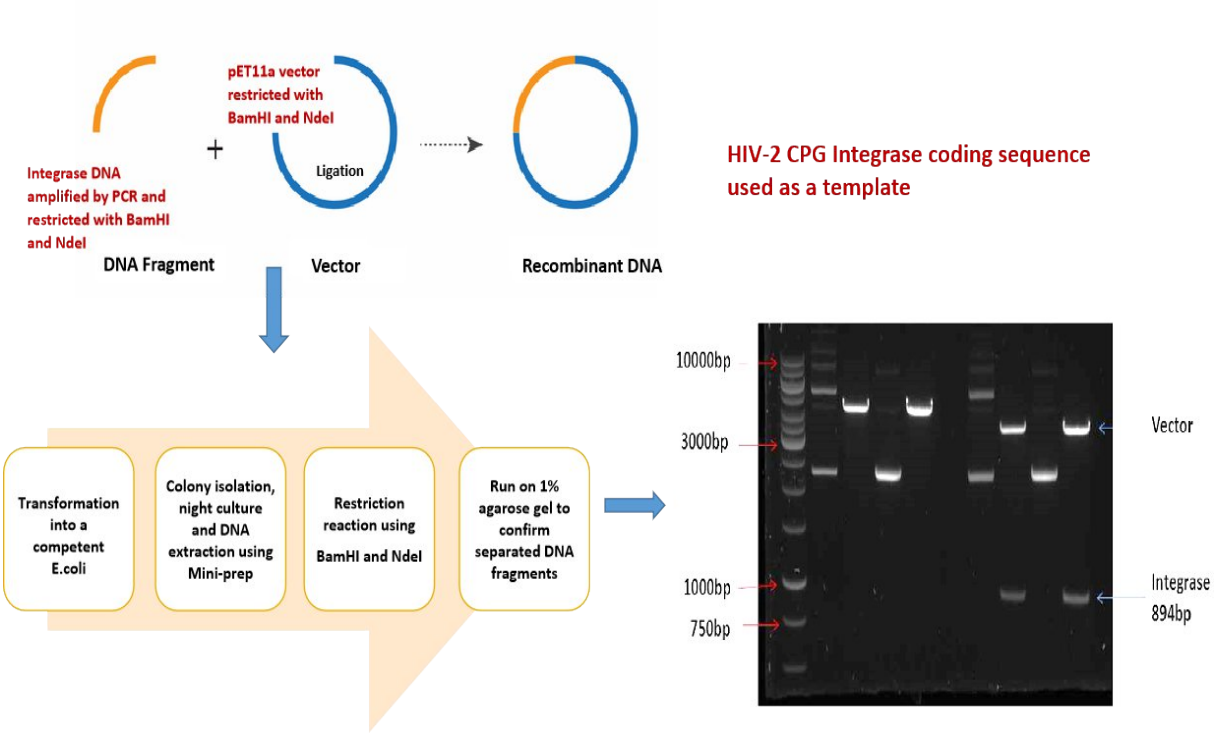

Figure 10: Work flow for cloning of HIV-2 integrase in pET11a vector and confirmation through gel electrophoresis

For protein expression, an overnight culture was prepared containing 60 µl from the bacterial culture and 5 µl ampicillin in 5 ml LB medium, and incubated overnight at 37 °C on a shaker. The pre-culture was transferred into 100 ml LB medium (containing 100 µl Ampicillin), incubated at 37 °C, until the absorbance reached 0.7-0.8 read at a wavelength of 600 nm. Induction of protein expression was performed with 1M isopropyl β-D-1-thiogalactopyr-anoside (IPTG) and growth culture was continued for a further 3h and centrifuged at 6000xg, at 4 °C for 20 minutes. The bacterial pellet was suspended in 8 ml of Buffer A (10 mM imidazole, 50 mM Tris-HCI, 10% glycerol, 20 mM 2- mercaptoethanol, 1 mM PMSF, 0.1 mM EDTA, pH 7.6). Lysis was enhanced by 1 mg/ml of lysozyme followed by culture incubation on ice for 30 minutes. To optimize protein solubilisation, 25 mM CHAPS and 1M Sodium chloride were added. The suspension was subjected to sonication using five 240-W bursts of 20 seconds each, with 1- minute cooling intervals between bursts. It was centrifuged at 20,000xg for 30 minutes. Affinity chromatography was employed for protein purification where 1 ml supernatant was loaded onto His Trap column pre-equilibrated with Buffer B (0.1mM EDTA, 50 mM Tris HCI, 20 mM 2-mercaptoethanol, l mM PMSF, 10% glycerol, 10 mM imidazole, 1M NaCl, 25 mM CHAPS, PH 7.6). Elution was done with 2 ml of Buffer C (20 mM 2-mercaptoethanol, 50 mM Tris-HCI, 0.1 mM EDTA, 10% glycerol, 1 mM PMSF, 25 mM CHAPS, 1M NaCI, 100 mM imidazole, PH 7.6). Eluted samples were collected at

different concentration peaks and run on 16% SDS-PAGE again to identify the purified proteins. Bradford assay determined the protein concentration.

5.2.2 Efficacy of INSTIs against purified HIV-2 integrase

A non-radioactive assay (Xpress Bio, Frederick, MD, USA) was used to quantitatively measure the activity of the purified HIV-2 integrase. Briefly, 100 µl DS oligo was added to HIV-1 LTR U5-coated streptavidin plates and incubated at 37ºC for 30 minutes followed by five times washing using 300 µl wash buffer. Unbound sites were blocked with 200 µl blocking buffer for 30 minutes at 37ºC in a microbiological incubator, followed by washing three times in 200 µl reaction buffer wash. 100 µl of 1:300 dilution of integrase in reaction buffer was added and incubation was done for 30 minutes at 37ºC. Subsequently, 50 µl of INSTI inhibitors (equivalent to 10 µM) diluted in reaction buffer were added and incubated at room temperature for 5 minutes. A uniform concentration of the inhibitors was added at 10 µM each of raltegravir, dolutegravir, bictegravir and cabotegravir (MedChem Express (MCE, NJ, USA). 50 µl of target substrate (TS) oligo was added and incubated for 30 minutes at 37ºC. Five washes with 300 µl wash buffer were followed by addition of 100 µl HRP antibody with incubation for 30 minutes at 37º C. The enzymatic signal was developed by addition of 100 µl/well of TMB substrate. After 10 minutes incubation at room temperature, the assay was terminated using 100 µl stop solution and absorbance measured at 450 nm. The experiment was done in triplicates as per manufacturer's instructions. Controls containing integrase enzyme only without inhibitors were included.

5.3 Inhibition profiling of INSTIs against HIV-2 in cell culture

5.3.1 Assessment of cell viability in the presence of inhibitors

In 96-well plates (Greiner Bio One, catalog no. 655074), 25,000 Jurkat cells (ATCC, Manassas, VA, USA) were cultured in complete RPMI medium (Sigma-Aldrich, St. Louis, MO, USA) (1% L-glutamine, 10% FBS and 1% penicillin-streptomycin) and incubated at 37ºC in 5% CO_2 for 24 hrs. On the subsequent day, cells were treated to a range of serially diluted inhibitor concentrations of between 1 nM to 1 µM for INSTIs and 1 pM to 1 nM for lenacapavir in DMSO (MedChem Express, NJ, USA) and then incubated at 37ºC in 5% CO_2 for two days. Afterward, an MTT assay to evaluate the viability of the treated Jurkat cells was performed following the manufacturer's instructions (Thermo Fisher Scientific, Waltham, MA, USA). Controls included a cell control containing MTT reagent with no inhibitor, and a blank without both inhibitor and MTT.

5.3.2 Production of HIV-1 and HIV-2 pseudoviruses

Pseudotyped virions were generated using human embryonic kidney (HEK-293T) cells (Invitrogen, Carlsbad, USA). Cells were initially cultured in T-75 flask containing 15 ml of complete DMEM (Sigma-Aldrich, St. Louis, MO, USA) supplemented with 1% L-glutamine, 10% fetal bovine serum (FBS), and 1% penicillin-streptomycin and incubated at 37ºC in 5% CO_2. Within 24 hours, the cells reached approximately 70% confluency, equating to 5 to 6×10^6 cells per flask. On the subsequent day, transfection was done utilizing the polyethylenimine (PEI) (Sigma-Aldrich St. Louis, Missouri, USA) method (Mahdi et al., 2018). 10 µg of each plasmid was used. Transfection mixture was added into the cells in 5 ml of 1% DMEM and incubated at 37°C in 5% CO_2 for 5-6 hours. Following this, the media was substituted with 10 ml of complete DMEM. Over the next 24 hours and for the subsequent three days, the viral supernatant was harvested, pooled and filtered using a 0.45 µm polyvinylidene fluoride filter (Merck Millipore, Darmstadt, Germany). To concentrate the pseudovirions, the filtrate was ultracentrifuged at 4°C for 2 hours at 100,000 x g, after which the medium was discarded and the viral pellet suspended in 200 µl of phosphate-buffered saline (PBS), aliquoted and preserved at minus 70°C. To quantify the concentration of pseudovirions, an ELISA-based colorimetric reverse transcriptase assay (Roche Applied Science, Mannheim, Germany) was employed. This assay measured the reverse transcriptase (RT) activity of virions in nanograms per well unit.

5.3.3 Inhibition profiling assays

In 48-well plates (Greiner Bio One, catalog no. 677180), 25,000 Jurkat cells (ATCC, Manassas, VA, USA) were seeded in triplicates in 200 µl of RPMI medium supplemented with 1% L-glutamine and 10% FBS, to reach 50-70% confluency by the following day after incubation at 37°C in 5% CO_2. The cells were then exposed to a series of inhibitor concentrations, ranging from 1 nM to 1 µM of INSTIs (MedChem Express (MCE, NJ, USA) in fresh medium without antibiotics and incubated at 37°C in 5% CO_2 for 3 hours. Subsequently, transduction was performed using 4 ng of RT/well of the pseudotyped HIV-1 or HIV-2 virions in the presence of 8 µg/ml polybrene/well (Sigma-Aldrich St. Louis, Missouri, USA). A cell control containing polybrene without the virus was included. Following 48-hours incubation at 37°C in 5% CO_2, the medium was discarded and the cells were collected in 400 µl in PBS and fluorescence determined by flow cytometry (FACS calibur, BD Biosciences, NJ, USA) **(Figure 11).**

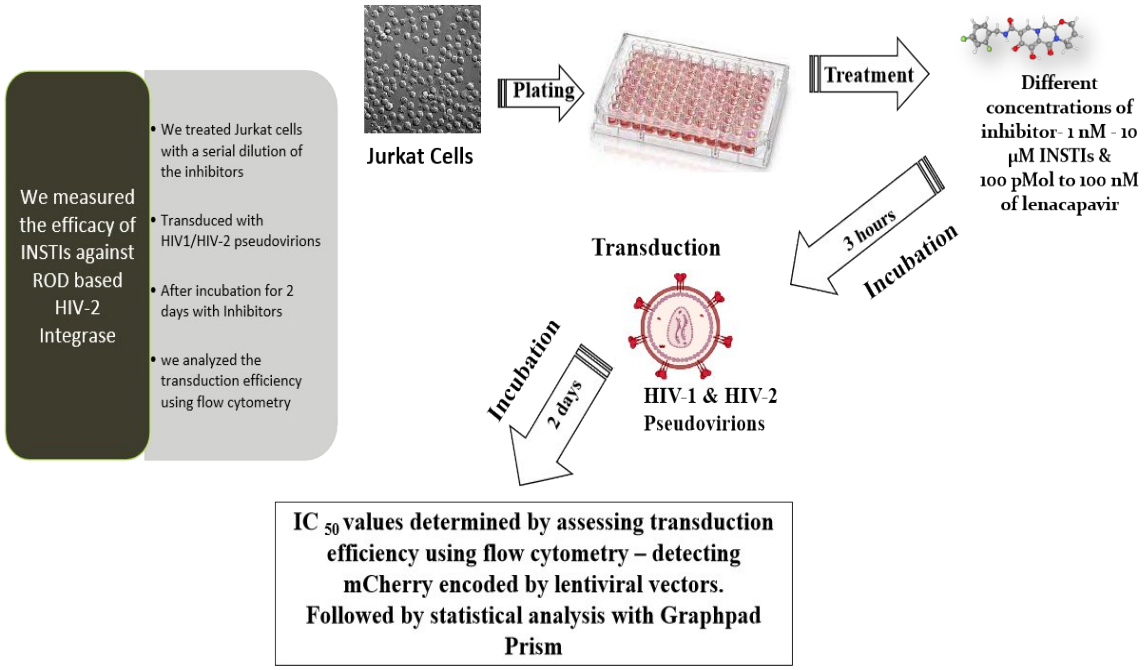

Figure 11: Workflow for inhibition experiment in cell culture

Transduction efficiency was determined based on mCherry fluorescence in 5000 cells per sample using Version 10 of FlowJo Software (Becton, Dickinson and Company; 2019). The 50% inhibitory concentration (IC_{50}) values were calculated by GraphPad Prism version 9.0 (GraphPad Software, Inc. Boston, MA, USA).

5.4 Evaluation of INSTIs against the activity of SARS-CoV-2

In collaboration with our partners from the Laboratory of Virology and Chemotherapy (Rega Institute for Medical Research, Department of Microbiology, Immunology and Transplantation, Belgium), we assessed the potential antiviral activity of INSTIs against SARS-CoV-2 in A549-Dual™ hACE2-TMPRSS2 and VeroE6-GFP cells (provided by M. van Loock, Janssen Pharmaceutical, Beerse, Belgium). 25, 000 VeroE6-GFP cells were cultured in 96-well plates (Greiner Bio One, catalog no. 655090) and pre-treated with raltegravir overnight in the presence of 0.5 µM MDR1-inhibitor CP-100356 (MedChem Express, NJ, USA). The cells were exposed to the SARS-CoV-2 inoculum at a multiplicity of infection (MOI) of 0.001 median tissue culture infectious dose per cell. The GFP fluorescence intensity was quantified on day 4 post-infection, and the percentage of inhibition was determined by subtracting background fluorescence and normalizing to untreated-uninfected control wells. The potential toxicity of compounds was evaluated in treated-uninfected cultures, and the 50% cytotoxic concentration (CC_{50}) was calculated using logarithmic interpolation. The SARS-CoV-2 variants B.1.1.7 and Omicron BA.2 were recovered from

nasopharyngeal swabs of RT-qPCR-confirmed human cases while the SARS-CoV-2 GHB strain was isolated from a nasopharyngeal swab obtained from Wuhan returning patient, and tested in biosafety level 3 and 3+ facilities at the Rega Institute for Medical Research, KU Leuven.

5.5 Evaluation of lenacapavir's effects on HIV-2 in cell culture

5.5.1 Efficacy of lenacapavir against HIV-2 in cell culture

Following a protocol similar to that described in section 4.3.3, 25,000 Jurkat cells (ATCC, Manassas, VA, USA) were seeded in 48-well plates (Greiner Bio One, catalog no. 677180) in triplicates in 200 µl of RPMI (Sigma-Aldrich, St. Louis, MO, USA) medium supplemented with 1% L-glutamine and 10 % FBS and incubated at 37 °C in 5% CO_2 overnight. On the next day, cells were treated with a concentration gradient of lenacapavir ranging from 1 pM to 1 nM (MedChem Express, NJ, USA) in fresh medium without antibiotics followed by incubation at 37 °C in 5% CO_2 for 3 hours. Transduction was subsequently carried out by adding 4 ng of pseudotyped virions per well, along with 8 µg/ml polybrene to enhance viral entry. Controls included cells treated with DMSO without viruses. After 48 hours incubation at 37 °C in 5% CO_2, the cells were collected in 400 µl of PBS and mCherry fluorescence measured using flow cytometry (FACS Calibur, BD Biosciences, NJ, USA).

5.5.2 Production of pseudoviruses in the presence of lenacapavir

Following a similar procedure as described in section 4.3.2, viruses were generated in the presence of varying concentrations of lenacapavir prior to transfection. Initially, on day 1, three million HEK-293T cells were seeded into T-75 flasks containing 10 ml of complete DMEM supplemented with 1% L-glutamine, 1% penicillin-streptomycin and 10 % FBS and incubated at 37 °C in 5% CO_2 overnight. On the subsequent day (day 2), the cells were treated with lenacapavir for a period of 3 hours at concentrations of 1 nM, 10 nM, and 100 nM (MedChem Express, NJ, USA). Following this treatment, the cells were transfected with 10 µg of HIV-1 and HIV-2 vectors in 5 ml of 1% DMEM. After an incubation period of 5 hours at 37 °C in 5% CO_2 overnight, the medium was replaced with fresh complete medium supplemented with the corresponding concentrations of lenacapavir, followed by a two-day incubation period. The supernatant containing virions were harvested and concentrated using Amicon Ultracel 100K (Merck Millipore Ltd Tullagreen, Ireland). An ELISA-based RT assay was then employed to determine the concentration of virions, followed by transduction assays to assess functionality.

5.5.3 Evaluation of lenacapavir's effects on HIV-2 capsid formation

25,000 Jurkat cells (ATCC, Manassas, VA, USA) were plated in a 48-well plate in triplicates in full RPMI (Sigma-Aldrich, St. Louis, MO, USA) medium containing 1% L-glutamine and 10% FBS without antibiotics followed by 24 hours incubation at 37°C in 5% CO_2 overnight. The cells were transduced with 4 ng of RT/well of pseudoviruses produced in the presence of lenacapavir as described in section 4.5.2. 8 µg/ml of polybrene/well was also used to enhance transduction. A control containing cells treated with DMSO only was included. This was then followed by a further incubation at 37°C in 5% CO_2 for 48 hours, after which the cells were collected in 400 µl PBS, and the fluorescence percentage measured using flow cytometry (FACS calibur, BD Biosciences, NJ, USA). Transduction efficiency was determined by FlowJo Software Version 10 (Becton, Dickinson and Company; 2019) and statistical analysis was performed using GraphPad Prism 9.0.

5.6 Molecular docking of INSTIs and lenacapavir

This was conducted by Dr. Gyula Hoffka from the Department of Biochemistry and Molecular Biology, University of Debrecen. We utilized the SIVrcm intasome structure to model the HIV-2 integrase structure, incorporating INSTIs (bictegravir, dolutegravir and cabotegravir) and a DNA substrate. The sequence of SIV DNA was modified to match our HIV-2 sequence, and nucleotide changes were made using UCSF Chimera (Isaacs et al., 2020). Structure minimization was performed using Amber16 force field, incorporating Li/Merz parameters for Mg2+ ions, and TIP3P water solvation model. Bictegravir and cabotegravir structures were geometrically optimized using Gaussian16 and RESP charge calculations. Molecular docking was conducted using PLANTS, targeting subunit A of the integrase active site. The docking centre was defined at the coordinates between the two catalytic Mg2+ ions, with a binding site radius of 12 Å, and the structure that demonstrated lowest energy structure was selected for analysis (Waterhouse et al., 2018). For lenacapavir, a structural model of the HIV-2 capsid protein (p26) was generated using its amino acid sequence and the protein-ligand structures were converted using AutoDock Tools to pdbqt files. Comparative docking was guided by the known binding interface near Asn57 in the HIV-1 capsid protein (p24) structure (PDB ID: 7RHN) as a reference (Pettersen et al., 2004).

5.7 Transcriptomic changes induced by Vpx

5.7.1 Transfection of THP-1 cells

We employed the pcDNA3.1-Vpx-NeGFP plasmid which encodes HIV-2 Vpx conjugated with GFP, obtained from Genscript Biotech Corporation, NJ, USA. The Vpx sequence mirrored that of the HIV-2 ROD-based vector, specifically the HIV-2 CGP (Mahdi et al., 2015). To create a functionally restricted mutant Vpx, K68A and R70A mutations were introduced into the Vpx coding region, generating the pcDNA3.1-MutVpx-NeGFP vector. A mock control, pcDNA3.1-NeGFP lacking Vpx, was used for comparison. Additionally, pcDNA1-Tat encoding HIV-1 Tat was sourced from Addgene, Watertown MA, USA (Plasmid #138478), a gift from Akitsu Hotta (Bolger et al., 2014). For transcriptomic analysis via transfection of THP-1 cells, the THP-1 monocyte cell line (ATCC, Manassas, VA, USA, Number: TIB-202) was cultured in RPMI medium supplemented with 10% FBS and 1% L-glutamine (Thermo Fisher Scientific, MA, USA) without antibiotics. On the day of transfection, cells were seeded into 6-well plates at a density of 5×10^5 cells/well in 500 µl serum and antibiotics-free Opti-MEM (Thermo Fisher Scientific, MA, USA). Transfection was conducted using Lipofectamine LTX reagent (Thermo Fisher Scientific, MA, USA) with 5µg of pcDNA3.1-Vpx-NeGFP, pcDNA3.1-MutVpx-NeGFP, or pcDNA3.1-NeGFP plasmids, following the manufacturer's protocol. Expression of the constructs was assessed using EVOS FLoid cell imaging station (Thermo Fisher Scientific, MA, USA) and flow cytometry to detect positively fluorescing cells. For transcriptomic analysis, RNA isolation was performed 16 hours post-transfection with the aforementioned plasmids using TRIzol Reagent (Thermo Fisher Scientific, MA, USA) according to the manufacturer's instructions. All experiments were conducted in duplicate.

5.7.2 RNA data sequencing and analysis

This was conducted by Balázs Kunkli from the Department of Biochemistry and Molecular Biology; University of Debrecen. RNA samples were prepared for the investigation and sequenced using the Agilent RNA 6000 Nano Kit and 2100 BioAnalyzer (Agilent Technologies, Waldbronn, Germany). Samples chosen for library preparation had an RNA integrity number higher than 7. The Ultra II RNA Sample Prep Kit (New England Biolabs, Ipswich, MA, USA) was used to produce RNA-Seq libraries after oligo-dT magnetic beads were employed to isolate Poly-A RNA, mRNA was eluted and fragmented at 94°C. Random priming reverse transcription was used to create first-strand cDNA, and second-strand synthesis was followed by the production of double-stranded cDNA. Sequencing libraries

were created by PCR enrichment of adapter-ligated fragments. Using the Illumina NextSeq 500 platform (San Diego, USA) single-end 75-cycle sequencing was carried out. FastQC, Bowtie 2, and MultiQC were used for data processing and analysis. Using the EBSeq tool, differential gene expression analysis was carried out to compare gene expression in three different conditions: GFP control, wild-type, and mutant Vpx. The topGO R program was used to perform gene ontology analysis, and genes with significance were filtered using a p-value threshold of less than 0.05. Additionally examined were HIV-1 interaction partners and PubMed metadata pertaining to viral infections. The R tools ggplot2, ggrepel, GOplot, and formattable were used to visualise the data.

5.7.3 Detection of Vpx's effects on the cytokine profile of transfected THP-1 cells

In triplicates, 500,000 THP-1 cells (ATCC, Manassas, VA, USA) were cultured in 6-well plates (Greiner Bio One, catalog no. 657160) containing 500 µl of RPMI medium enriched with L-glutamine (1%) and FBS (10%) (Thermo Fisher Scientific, MA, USA). Following a 3-hour incubation in 5% CO_2 at 37°C, cells were activated with 100 nM phorbol 12-myristate 13-acetate (PMA) (Sigma-Aldrich, St. Louis, MO, USA) for 1 hour. PMA-containing medium was replenished with 500 µl freshly prepared RPMI medium, and the cells were incubated for 24 hours to allow for adherence and differentiation into macrophage-like cells and confirmed via light microscopy.

Subsequently, transfection of the activated cells was performed using 5µg of pcDNA3.1-Vpx-NeGFP or pcDNA3.1-NeGFP (mock) vectors using Lipofectamine LTX Reagent in Opti-MEM (Thermo Fisher Scientific, MA, USA), followed by 5-hour incubation in 5% CO_2 at 37°C and replacement of medium with 1 ml of fresh RPMI medium. Non-transfected cells (lipofectamine-treated only) were also included as controls. The cells were further incubated for 24 hours under the same conditions and centrifuged for 3 minutes at 11,000xg. The supernatant was carefully collected for cytokine analysis. Cytokine levels (IL-1β, TGF-β, IFN-α and IL-6) in the supernatant were quantified by ELISA from BD Biosciences (BD Biosciences, San Diego, CA, USA), and PBL Assay Science (PBL Assay Science, Piscataway, NJ, USA) following manufacturer's protocol. IFN-α quantification was performed using the IFN-α ELISA Kit (TCM) from PBL Assay Science. Statistical comparisons across different conditions were made by comparing cytokine levels across different transfection conditions and analysis was performed using a Kruskal-Wallis test (non-parametric) in version 7.0 of GraphPad Prism software.

5.7.4 Investigation of Vpx's effects on HIV-1 Tat protein

To evaluate the influence of Vpx on HIV-1 Tat expression, western blot assay was conducted. HEK-293T cells (1 x 10^6cells/well) (ATCC, Manassas, VA, USA) were seeded into T-25 flasks containing 5 ml of full DMEM enriched with FBS (10%), penicillin-streptomycin (1%) and L-glutamine (1%) (Sigma-Aldrich, St. Louis, MO, USA) in 5% CO_2 at 37°C, one day prior to transfection. For the initial transfection, 5 µg of pcDNA3.1-Vpx-NeGFP, pcDNA3.1-MutVpx-NeGFP or pcDNA3.1-NeGFP (mock) vectors, were transfected into the cells using PEI as the transfection reagent. Non-transfected, PEI-treated only cells served as native controls. The following day, cells were transfected again with 5 µg of pcDNA1-Tat plasmid encoding HIV-1 Tat (Addgene, Watertown, MA, USA) using PEI. After 24 hours of incubation, the supernatant was discarded, and cells were washed with 1 ml of PBS before gently scraping them from the flask. The cells were then centrifuged, washed with PBS, and the resulting pellet was resuspended in 300 µl of lysis buffer (50 mM Tris-HCl, 25 mM NaCl, 5 mM EDTA, 50 mM NaF and 0.5% NP-40, pH 7.4). The suspension was incubated on ice for 30 minutes with intermittent vortexing. After incubation, the samples were sonicated and centrifuged, and the supernatant was collected. Protein concentration was determined using the Pierce BCA protein assay kit (Thermo Fisher Scientific, MA, USA). Subsequently, 15 µg of protein from each sample was loaded onto an 18% SDS-acrylamide gel for electrophoresis. Proteins were then transferred onto a nitrocellulose membrane (Biorad, Hercules, CA, USA) and probed with Tat antiserum (1:750 dilution) (NIH AIDS Reagent Program, Division of AIDS, NIAID, NIH, Bethesda, MD, USA) and anti-β-actin (Sigma-Aldrich, St. Louis, MO, USA) antibodies as primary antibodies, followed by appropriate secondary antibodies (1:2000) (Sigma-Aldrich, St. Louis, MO, USA). Blots were visualized using Western-bright PICO substrate (Advansta, San Jose, CA, USA) and imaged with an Azure 600 GelDoc system (Dublin, CA, USA).

5.7.5 Effects of Vpx on gene expression following HIV-2 infection or transfection

To investigate Vpx effects on gene expression, a combination of virus infection-based and plasmid-based transfection approaches were employed. For the infection experiments which were conducted by our collaborating partners from the Department of Laboratory Medicine, Lund University, three primary HIV-2 subtype A isolates (1010, 1654, and 1806), obtained from West African individuals, were utilized alongside HIV-1 IIIB and HIV-1 BaL strains as reference controls. Virus stocks were generated by infecting phytohemagglutinin P

(Pharmacia, Uppsala, Sweden) -stimulated peripheral blood mononuclear cells (PBMCs) from healthy donors with the viral isolates. Fresh PBMCs were added weekly, and supernatants were collected on days 7, 14 and 21, and then stored at −80°C. For infection of THP-1 cells, 250,000 cells per well were plated in quadruplicate in 24-well plates with RPMI-1640 medium (Thermo Fisher Scientific) enriched with 10% FBS and 1% L-glutamine (Thermo Fisher Scientific). After 3 hours of incubation, the cells were activated with 100 nM phorbol 12-myristate 13-acetate (PMA) (Thermo Fisher Scientific) for 1 hour, then the medium was replaced, and the cells were incubated at 37°C in 5% CO_2 for 24 hours. Monocyte differentiation into macrophages was confirmed using an optical microscope. Activated cells were transfected with 25 ng of HIV-1 or HIV-2 isolates (capsid equivalent) and incubated for 48 hours under the same condition. Controls included native cells and PMA-stimulated cells. Infection was monitored by reverse transcriptase (RT) activity, measured with a SYBR Green I-based PERT assay.

To assess gene expression changes induced by Vpx on SKOR2, U2AF1 and CASP3 genes, total RNA was extracted from virus infected THP-1 cells using the RNeasy Mini Kit (Qiagen, Hilden, Germany) in accordance with manufacturer's instructions. cDNA synthesis was performed on the extracted RNA using Superscript IV Reverse Transcriptase (Thermo Fisher Scientific Waltham, MA, USA) with an R1 primer and RiboLock RNase inhibitor (Invitrogen, Taastrup, Denmark). The synthesis protocol included initial 5-minute incubation at 23°C, followed by 10 minutes at 55°C, and a final inactivation step at 80°C for 10 minutes. Quantitative real-time PCR was conducted using SYBR Select Master Mix (Thermo Fisher Scientific, Waltham, MA, USA) and gene-specific primers on a CFX96 Touch Real-Time PCR machine (Bio-Rad, Hercules, CA, USA). The results were analysed using the ΔΔCt method, and statistical analysis was performed using the non-parametric Kruskal-Wallis test in GraphPad Prism 7.0 (GraphPad software, LA Jolla, CA, USA).

In parallel, a transfection-based experiment was performed to investigate the effects of Vpx on the expression of SKOR2, U2AF1 and CASP3 genes (Thermo Fisher Scientific, Waltham, MA, USA). 500,000 THP-1 cells were plated in triplicates in six-well plates containing RPMI medium complemented with 1% L-glutamine and 10% FBS. The cells were transfected with 5 µg of pcDNA3.1-Vpx-NeGFP, pcDNA3.1-MutVpx-NeGFP, or pcDNA3.1-NeGFP plasmids using lipofectamine, followed by 16 hours of incubation at 37°C in 5% CO_2. RNA was isolated from the cells using TRIzol Reagent as per the manufacturer's instructions (Thermo

Fisher Scientific, Waltham, MA, USA). Quantitative real-time PCR was performed with 500 ng of RNA using the Cells-to-CT TaqMan RT-qPCR master mix and gene-specific TaqMan assays for SKOR2, U2AF1, CASP3, and GAPDH (Thermo Fisher Scientific, Waltham, MA, USA). The RT-PCR conditions included reverse transcription at 50°C for 5 minutes, RT inactivation at 95°C for 15 seconds, followed by amplification with 40 cycles of 95°C for 15 seconds and 60°C for 1 minute. Data was analysed using the ΔΔCt method, and statistical analysis was performed using the non-parametric t-test in GraphPad Prism 7.0 (GraphPad software, LA Jolla, CA, USA).

5.7.6 Caspase 3 activity measurements

500,000 THP-1 cells/well in triplicates were seeded in a 6-well plate (Greiner Bio One, catalog no. 657160) using antibiotic-free RPMI media supplemented with 1% L-glutamine and 10% FBS (Thermo Fisher Scientific, Waltham, MA, USA) to a final amount of 500 µl/well. The cells were transfected with 5 µg of pcDNA3.1-Vpx-NeGFP, pcDNA3.1-MutVpx-NeGFP, or pcDNA3.1-NeGFP (mock) using lipofectamine LTX reagent (Thermo Fisher Scientific, Waltham, MA, USA). In addition to a native control comprising of lipofectamine LTX-only treated cells, a positive control was included in which the cells were treated with 1 µM of staurosporine (MedChem Express (MCE), Monmouth Junction, NJ, USA) to induce apoptosis. After incubation for 16 hours at 37°C in 5% CO_2, the cells were collected and lysed in a solution that contained 10 mM Tris, 1 mM dithiothreitol, 2 mM EDTA and 1 mM PMSF for 30 minutes on ice at a pH of 7.4. The protein concentration was assessed by BCA after the lysates were centrifuged for 30 minutes at 4 °C at 14,000 rpm. CASP3 activity was evaluated using the MedChem Ac-DEVD-pNA colorimetric substrate (CAS no. 189950-66-1, MedChem Express Monmouth Junction, NJ, USA) (Chopra et al., 2009). To reach a final reaction of 100 µl per well, 40 µg of cell lysate was mixed with 0.2 mM of Ac-DEVD-pNA substrate that had been diluted in the lysis solution in a 96-well plate. The preparation was incubated for one hour at 37 °C. An Agilent BioTek Synergy H1 microplate reader (Agilent Technologies, Santa Clara, CA, USA) was then used to detect absorbance at 405 nm. All the experiments were done in triplicates.

5.8 Experiments on LEDGF/p75 and HIV-2 integrase

5.8.1 Detection of LEDGF/p75 and Integrase expression by Western Blot

500,000 Jurkat cells and HEK-293T cells were plated in triplicates in a six well plate (Greiner Bio One, catalog no. 657160) in complete RPMI and DMEM medium supplemented with

10% FBS, 1% L-glutamine & 1% penicillin-streptomycin ()Thermo Fisher Scientific, Waltham, MA, USA, respectively and incubated at 37°C in 5% CO_2 . The following day, supernatant was discarded and cells were washed with 1 ml PBS, centrifuged for 5 minutes at 870 rpm at room temperature, and the pellet was washed with 5 ml PBS followed by another wash using 1 ml of PBS. The pellet was then re-suspended in 100 µl lysis buffer (150 mM NaCl, 50mM Tris, 0.5% Deoxycholic acid, 0.1% SDS, 0.5% NP-40, 1mM PMSF and 1mM EDTA, pH 8.0).

For integrase detection, 100,000 Jurkat Cells and HEK-293T cells were plated in a 24 well plate (Greiner Bio One, catalog no. 657168) in triplicates in complete RPMI and DMEM medium supplemented with 10% FBS, 1% L-glutamine and 1% penicillin-streptomycin (Thermo Fisher Scientific, Waltham, MA, USA) respectively and incubated at 37°C in 5% CO_2. After 24hr incubation, the cells were transduced with 20 ng of HIV-2 pseudovirions in the presence of 8 µg /ml polybrene. The cells were incubated for 6 hours at 37°C in 5% CO_2 incubator. The supernatant was discarded and cells were washed with 1 ml PBS centrifuged for 5 minutes at 870 rpm at room temperature, and the pellet was washed with 5 ml PBS and washed again with 1 ml of PBS. The pellet was then re-suspended in 100 µl lysis buffer (50 mM Tris buffer, 319 mM potassium chloride, 33 mM magnesium chloride, 11 mM DTT pH 7.8.)

All lysates for LEDGF/p75 and integrase were incubated on ice for 30 minutes and vortexed for 5 seconds every 10 minutes. Following lysis, the samples were sonicated for 2 minutes using a Realsonic sonicator with a break every 20 seconds to prevent overheating. Lysates were then centrifuged at 14,000xg for 30 minutes at 4°C, and the supernatants were collected. Protein concentrations were determined using the Pierce BCA Protein Assay Kit (Thermo Scientific, Waltham, MA, USA).

For immunoblotting, 30 µg of the total protein per sample was resolved on 14% SDS-polyacrylamide gels and transferred onto nitrocellulose membranes (Biorad, Hercules, CA, USA). Detection of LEDGF/p75 was performed using 2 µg/ml anti-PSIP1 monoclonal primary antibody (Sigma-Aldrich, St. Louis, MO, USA), followed by 1:2000 anti-mouse secondary antibody (Sigma-Aldrich, St. Louis, MO, USA). Signal visualization was done using the Western Bright Femto substrate (Advansta, San Jose, CA, USA) and imaged on the Azure 600 Gel Documentation System (Dublin, CA, USA).

For HIV-2 integrase detection, blots were incubated with 1:1000 anti-HIV-2 integrase primary antibody (NIH AIDS Reagent Program), followed by 1:2000 anti-rabbit secondary antibody (Sigma-Aldrich, St. Louis, MO, USA). Detection was carried out using the Western Bright Pico substrate (Advansta) and visualized using the Azure 600 system. B-actin served as the internal loading control, detected with a specific anti-β-actin antibody and its corresponding secondary antibody.

5.8.2 Evaluation of LEDGF/p75-Integrase interaction by Proximity Ligation Assay (PLA)

20,000 Jurkat cells (ATCC, Manassas, VA, USA) were plated in a 96 well plate (Greiner Bio One, catalog no. 677180) in full RPMI medium containing 10% FBS and 1% L-glutamine (Thermo Scientific, Waltham, MA, USA).without antibiotics. They were transduced with HIV-2 pseudoviruses at a MOI of 1 in presence of 8 µg/ml polybrene and centrifuged for 10 minutes. Cells were then incubated at 37°C in 5 % CO_2 for different time points ranging from 0 to 12 hours (0h, 4h, 5h, 6h, 8h, 10h, and 12h). The supernatant was discarded and the cells were washed with 200 µl PBS, centrifuged at 1000 rpm for 5 minutes and re-suspended in 100 µl of 1x PBS. The cells were fixed with 5 % paraformaldehyde (200 µl/well) for 30 minutes and the membrane permeabilized with 0.3 % Triton X-100 (100 µl/well) for 10 minutes at room temperature (Thermo Fisher MA, USA). The duolink PLA protocol was performed according to the manufacturer's recommendations (Duolink ™ PLA Kit (Sigma-Aldrich, St. Louis, MO, USA) using1 µg/ml anti- PSIP1 antibody (Sigma-Aldrich, St. Louis, MO, USA) (Cat no. SAB1404913-100UG) and anti HIV-2 integrase antibody at 1:2000 dilution (NIH AIDS Reagent Program, Division of AIDS, NIAID, NIH, Bethesda, MD, USA) Cat no.12883 Lot 160216). Interaction was detected by fluorescence microscopy using EVOS FLoid Cell Imaging Station (Thermo Scientific, Waltham, MA, USA) at a magnification of x460 and a scale bar of 100 µM. All the experiments were done in triplicates and the control cells were not treated with the antibodies.

5.8.3 Effects of LEDGF/p75 silencing on transduction efficiency and interaction with HIV-2 integrase

100,000 Jurkat cells (ATCC, Manassas, VA, USA) were seeded in triplicates in a 24-well plate (Greiner Bio One, catalog no. 677180) in full RPMI medium containing 10% FBS and 1% L-glutamine without antibiotics. They were transfected with 1.5 µg of PSIP1 siRNA using RNAiMax lipofectamine (Thermo Fisher MA, USA), followed by incubation for 24 hrs at 37^{o}C. After incubation, the cells were collected, centrifuged for 5 minutes at 870 rpm, and

washed with 1ml PBS. The cells were lysed in 100 µl lysis buffer (150 mM NaCl, 50 mM Tris, 0.5% deoxycholic acid, 0.1% sodium dodecylsulfate (SDS) 0.5% NP-40, 1 mM PMSF and 1 mM EDTA pH 8.0) and thereafter incubated for 30 minutes on ice and vortexed for 5 seconds every 10 minutes. After incubation, samples were sonicated (Realsonic sonicator, 2 minutes with a break every 20 seconds) and centrifuged for 30 minutes at 14,000xg at 4^{o}C. Supernatants were transferred into a clean tube and Pierce BCA protein assay kit (Thermo Scientific, Waltham, MA, USA) was used to determine the protein concentration. Proteins were subsequently analysed by western blot to confirm LEDGF/p75 silencing.

For proximity ligation assay, 20,000 of the LEDGF/p75 silenced Jurkat cells were plated in a 96-well plate, and transduced with HIV-2 pseudoviruses at MOI of 1 using polybrene at a concentration of 8 µg/ml. A control of unsilenced cells was added followed by incubation for 6hrs at 37^{o}C. The cells were collected, fixed with 5% paraformaldehyde and permeabilized with 0.3% Triton x100 respectively. Duolink PLA procedure was performed as per manufacturer's instructions (Sigma-Aldrich, St. Louis, MO, USA).

To assess the effects of LEDGF/p75 silencing on the integration, 20,000 of the LEDGF/p75 silenced Jurkat cells were transduced with HIV-2 pseudoviruses at MOI of 1 using polybrene at a concentration of 8 µg/ml followed by incubation for 48hrs at 37^{o}C in 5% CO_2. A control comprising of unsilenced cells was also included. The cells were collected in 400 µl cold sterile PBS and fluorescence was measured by flow cytometry (FACS calibur, BD Biosciences, NJ, USA). Transduction efficiency was determined using Version 10 of FlowJo Software (Becton, Dickinson and Company; 2019).

5.9 Experiments on the integration sites preference of HIV-1 and HIV-2

5.9.1 Detection of HIV-1 and HIV-2 LTR sequences by PCR

To confirm if transduction and integration were successful, the presence of LTRs was confirmed in the isolated DNA obtained from the transduced Jurkat cells before sequencing. Briefly, 35,000 Jurkat cells (ATCC, Manassas, VA, USA) were plated in full RPMI medium (10% FBS and 1% L-glutamine) (Thermo Scientific, Waltham, MA, USA) without antibiotics and transduced with HIV-1 and HIV-2 pseudoviruses at a MOI of 1, in presence of 8 µg/ml polybrene. After 48 hrs incubation at 37°C in 5% CO_2, genomic DNA was extracted from transduced cells and purified using Invitrogen PureLink ™ Genomic DNA Mini Kit (Thermo Fisher Scientific Waltham, MA, USA) as per manufacturer's protocol. 100 µl of DNA was fragmented by sonication for 2 minutes with a short break

after 30 seconds. 100 ng of the fragmented DNA template was amplified by PCR using 10 µl Thermo phusion high fidelity master mix (Thermo Fisher Scientific Waltham, MA, USA), 0.2 µl of HIV-1 and HIV-2 5' forward and reverse primers (shown below). The PCR conditions were: 1 cycle initial denaturation at 98°C for 30 seconds, 35 cycles extension at 72°C for 30 seconds and 1 cycle final extension at 72°C for 10 minutes. Thereafter, 20 µl of the amplified PCR sample was loaded onto agarose gel electrophoresis.

The following primer sequences were used for confirmation of LTRs sequences based on the transfer plasmids sequences **(Figure 12)** for HIV-2 and HIV-1 respectively (Sigma-Aldrich, St. Louis, MO, USA).

CGW LTR Forward: 5'- CCGCTCGAGCGCCACCATGGTGAG-3'
CGW LTR Reverse: 5'- CCGCTCGAGGCCGCTTTACTTGTA-3'

pWOX LTR Forward: 5'- TGGCTAACTAGGGAACCCAC-3'
pWOX LTR Reverse: 5'- CCACACTGACTAAAAGGGTCTG-3'

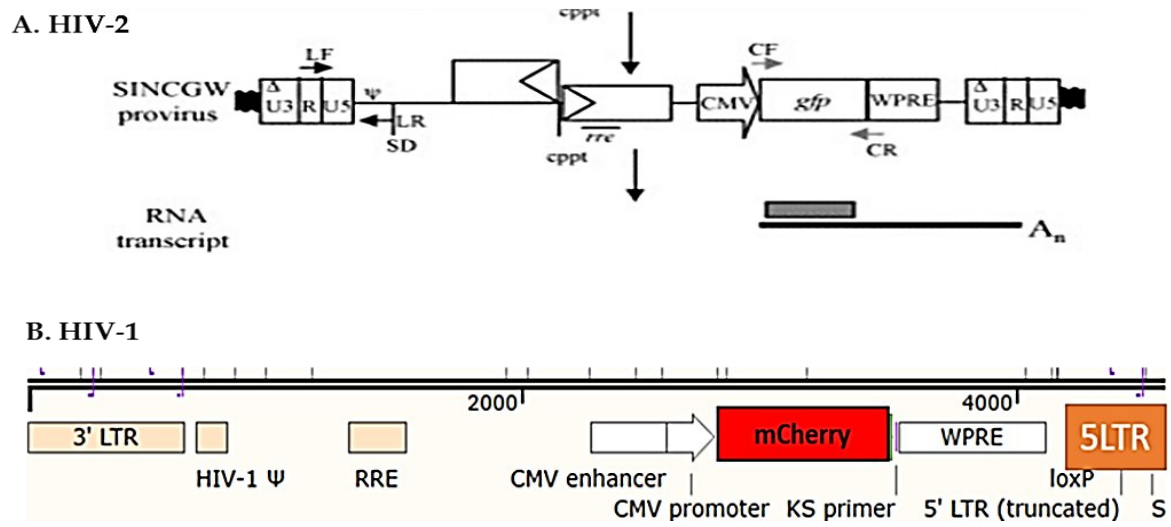

Figure 12: Transfer plasmids showing the LTRs A: HIV-2 CGW plasmid expressing GFP **B.** HIV-1 pWOX plasmid expressing mCherry

5.9.2 Transduction of Jurkat cells with HIV-1 and HIV-2 pseudoviruses

35,000 Jurkat cells (ATCC, Manassas, VA, USA) were plated in a 48-well plate in complete RPMI medium containing 1% L-glutamine, 10% FBS and 1% penicillin-streptomycin (Thermo Fisher Scientific Waltham, MA, USA), antibiotic in triplicates. The cells were immediately transduced with HIV-1 and HIV-2 pseudoviruses at a MOI of 1 in the presence of 8 µg/ml polybrene followed by centrifugation for 10 minutes to enhance viral entry into the

cells. A control containing cells with polybrene only was included. The transduced cells were incubated for 48hrs in 5% CO_2 incubator at 37°C. Cells were collected, centrifuged for 5 minutes at 870 rpm and the pellet was washed with 5 ml, then with 1 ml of PBS. The pellet was then re-suspended in 200 µl PBS.

5.9.3 Genomic DNA extraction from the transduced cell lysates

DNA extraction and purification was carried out using Invitrogen PureLink ™ Genomic DNA Mini Kit (Thermo Fisher Scientific Waltham, MA, USA), as per manufacturer's protocol. Briefly, the cells in 200 µl PBS were transferred into a sterile micro centrifuge tube containing 20 µl Proteinase K. 20 µl RNAse was added to the sample, vortexed briefly and incubated for 2 minutes at room temperature. Then, 200 µl of genomic lysis buffer was added, vortexed to obtain homogenous solution, and incubated at 55^{o}C for 10 minutes for protein digestion. 200 µl of 96% ethanol was added to the lysate and well vortexed for homogeneity and purification. The lysate was loaded onto spin column and centrifuged at 10,000xg for 1 minute at room temperature, washed with 500 µl wash buffer 1 and centrifuged at 10,000xg for 1 minute at room temperature. This was followed by a second wash using 500 µl wash buffer 2 and centrifuged at a maximum speed (17,000xg) for 3 minutes. The DNA was eluted with 25 µl elution buffer into 1.5 ml eppendorf tube after 1 min incubation and centrifugation at 17,000xg for 1 minute. The purified DNA concentration was measured using Nano drop 2000 and stored at -20°C and later sent for genomic analysis.

5.9.4 Genomic sequencing to assay for integration sites

This was performed by Dr. Szilárd Póliska from the Genomic Medicine and Bioinformatics Core Facility at the Department of Biochemistry and Molecular Biology, University of Debrecen. In accordance to manufacturers' guideline, 1 µg of the purified DNA per sample, from 5 replicates each, was used to prepare the library using the NEBNext DNA Library Prep Kit (New England Biolabs, MA, USA). Ultrasound shearing was employed to randomly fragment the genomic DNA to approximately 350 base pairs. The DNA fragments were then end-polished, A-tailed, and ligated using the NEBNext adapter for Illumina sequencing (New England Biolabs, MA, USA). P5 and indexed P7 oligos were then used to further enrich the DNA in PCR. The AMPure XP system (Beckman Coulter, Paris, France) was used to purify the PCR products, and the Agilent 2100 Bioanalyzer (Agilent Technologies, Waldbronn, Germany) was used to assess the size distribution of the resulting libraries and quantify them using real-time PCR. Using multiple lanes per volume to reduce batch impact, the selected libraries were pooled based on their optimal concentration and projected data volume before

being sequenced by Illumina NovaSeq 6000 sequencers (San Diego California, USA) with paired-end reads that were 150 bases long.

5.9.5 Bioinformatic analysis of the sequenced data

With the assistance of Noemi Caballero Sanchez from the Department of Biochemistry and Molecular Biology, University of Debrecen, raw sequencing reads were trimmed using Trimmomatic v0.39 and quality-checked with FastQC. Cleaned reads were aligned to a hybrid reference genome (hg19) and reference genomes of HIV-1 (GenBank: K03455.1) and HIV-2 (GenBank: M15390.1), using BWA-MEM. Viral integration sites were identified using VirusClip, to detect host-virus junctions via soft-clipped reads and filters for high-confidence breakpoints (≥2 supporting reads, consistent orientation). Integration coordinates were annotated against GENCODE v41 using BEDTools and downstream analyses were performed in R v4.3.1 using GenomicRanges. Only autosomal, annotated loci were retained. To assess chromatin context, Jurkat cells ATAC-seq data (SRA: SRR15931092, SRR15931093) were processed using BWA-MEM and MACS2. Signal tracks were generated with DeepTools and normalized around ±2 kb HIV integration windows using EnrichedHeatmap with 50 bp bins. Heatmaps and enrichment profiles were visualized with EnrichedHeatmap and circlize, enabling comparison of HIV-1 and HIV-2 integration preferences in open chromatin regions.

5.10 Statistical Analysis

5.10.1 Inhibition profiling experiments

Quantitative flow cytometry analysis measuring mCherry fluorescence in transduced Jurkat cells was conducted using FlowJo Software version 10, for assessment of transduction efficiency and evaluation of the antiviral activity of integrase strand transfer inhibitors (INSTIs) and lenacapavir. GraphPad Prism version 9.0 was employed to calculate the 50% inhibitory concentration (IC_{50}) values for INSTIs and lenacapavir in both the in vitro integrase activity assays and pseudotyped lentiviral inhibition assays. IC_{50} values were derived using nonlinear regression models (log [inhibitor] vs. normalized response – variable slope). In SARS-CoV-2 cytotoxicity assays, 50% cytotoxic concentration (CC_{50}) values were estimated via logarithmic interpolation. All experiments were performed in biological triplicates. Statistical analyses were conducted in GraphPad Prism version 9.0, and a p-value ≤ 0.05 was considered statistically significant.

5.10.2 Vpx Functional Assays

RNA sequencing and differential gene expression analyses were conducted to assess transcriptomic changes following transfection with wild-type Vpx, mutant Vpx, or GFP-only control vectors. Quality control and alignment of sequencing reads were performed using FastQC**,** Bowtie 2, and MultiQC**.** Differential expression analysis was conducted using EBSeq; with downstream gene ontology (GO) enrichment analysis performed using the topGO package in R, applying a significance threshold of $p < 0.05$. Data visualization was carried out using ggplot2**,** ggrepel**,** GOplot, and formattable packages in R.

Cytokine quantification for IL-1β, TGF-β, IFN-α, and IL-6 was performed using ELISA, and group comparisons were analyzed using the Kruskal–Wallis test in GraphPad Prism version 7.0. For RT-qPCR validation of selected genes (SKOR2, U2AF1, and CASP3), relative gene expression was quantified using the ΔΔCt method. The Kruskal–Wallis test was applied to infection-based datasets, whereas non-parametric unpaired t-tests were used for transfection-based analyses. All experiments were conducted in triplicates, and statistical significance was defined as $p \leq 0.05$.

5.10.3 LEDGF/p75 and Integration Site Analysis

Data analysis in LEDGF/p75-related experiments focused on protein expression, protein–protein interactions, and viral integration efficiency. Western blotting for LEDGF/p75 and HIV-2 integrase expression was evaluated qualitatively based on band intensity, using β-actin as a loading control. Proximity ligation assays (PLA) were quantified by counting fluorescent dots per nucleus as captured in fluorescence microscopy at a scale of 100 μM and a magnification of x460. Comparative analysis of the images at different time points and comparative analysis between silenced and unsilenced conditions were performed using Image J software. Flow cytometry (FACS) was employed to assess transduction efficiency in LEDGF/p75-silenced versus control in Jurkat cells. Data was analyzed in FlowJo v10, with GFP positive cell percentages used as a proxy for transduction success. Statistical significance was set at $p \leq 0.05$. Statistical comparisons (using t-tests) were carried out in GraphPad Prism version 9.0 to assess differences in PLA signal counts or transduction efficiency between experimental groups.

PCR followed by gel electrophoresis was performed to qualitatively confirm the presence of integrated HIV-1 and HIV-2 long terminal repeat (LTR) sequences.

6. RESULTS

6.1 Inhibition profiling of INSTIs in vitro and in cell culture

6.1.1 Efficacy of INSTIs against purified HIV-2 integrase in vitro

The inhibitory effect of INSTIs was evaluated using purified integrase enzymes. While significant inhibition of HIV-1 integrase activity was observed with all the tested INSTIs compared to the control, no appreciable inhibition was detected against HIV-2 integrase although the enzyme demonstrated excellent activity in the controls **(Figure 13)**.

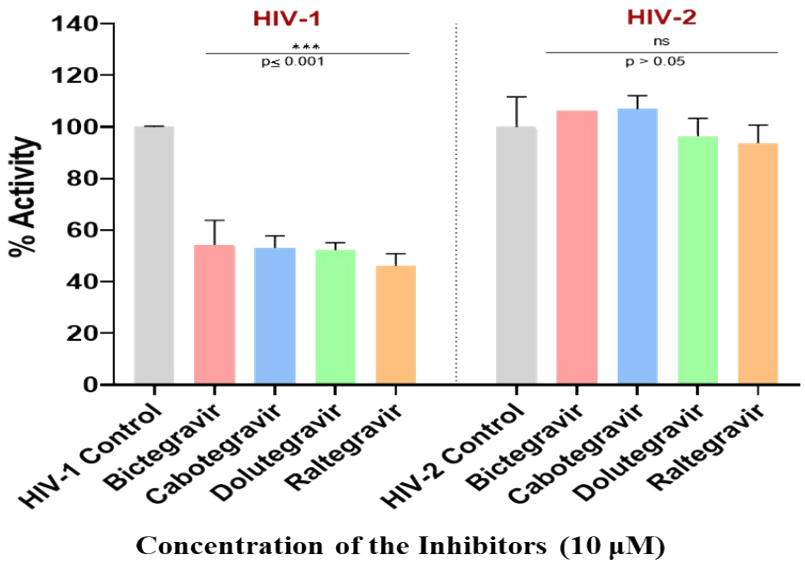

Figure 13: In vitro Inhibition profiling of INSTIs against purified HIV-2 integrase using a quantitative non-radioactive assay. 10 µM of the inhibitors diluted in the assay's reaction buffer was used and the absorbance was measured at 405 nm. The y axis is the percentage activity of the enzyme relative to the control while the x-axis shows the tested inhibitors relative to the controls. The controls contained integrase enzyme without the inhibitors. The experiment was carried out in triplicates and the significance level *** p value ≤ 0.001, ns p > 0.05

It is important to note that the commercial kit used to evaluate the inhibition was designed for HIV-1; however, the manufacturer stated that measurement of HIV-2 integrase activity was also possible.

6.1.2 Efficacy of INSTIs against HIV-2 in cell culture

Subsequent evaluation of antiviral efficacy in cell culture revealed potent inhibition of the HIV-2 ROD strain by all the tested INSTIs. Low nanomolar IC_{50} values were achieved across all the inhibitors with dolutegravir demonstrating the highest potency against HIV-2 (IC_{50} =0.9 (±0.4) nM) **(Table 4 and Figure 14)**.

	IC_{50} (nM)	
INSTI	**HIV-1**	**HIV-2**
Elvitegravir	2.4 (±0.08)	2.1 (±0.1)
Raltegravir	7.2 (±0.1)	2.1 (±0.1)
Dolutegravir	2.2 (±0.07)	0.9 (±0.4)
Bictegravir	1 (±0.3)	1.8 (±0.08)
Cabotegravir	0.4 (±0.3)	2 (±0.1)

Table 4: IC_{50} values of INSTIs against HIV-1 and HIV-2 in cell culture. Data is represented as mean ± standard error (SE) expressed as the logIC_{50} value of the inhibitor. Results were concluded from triplicate measurements.

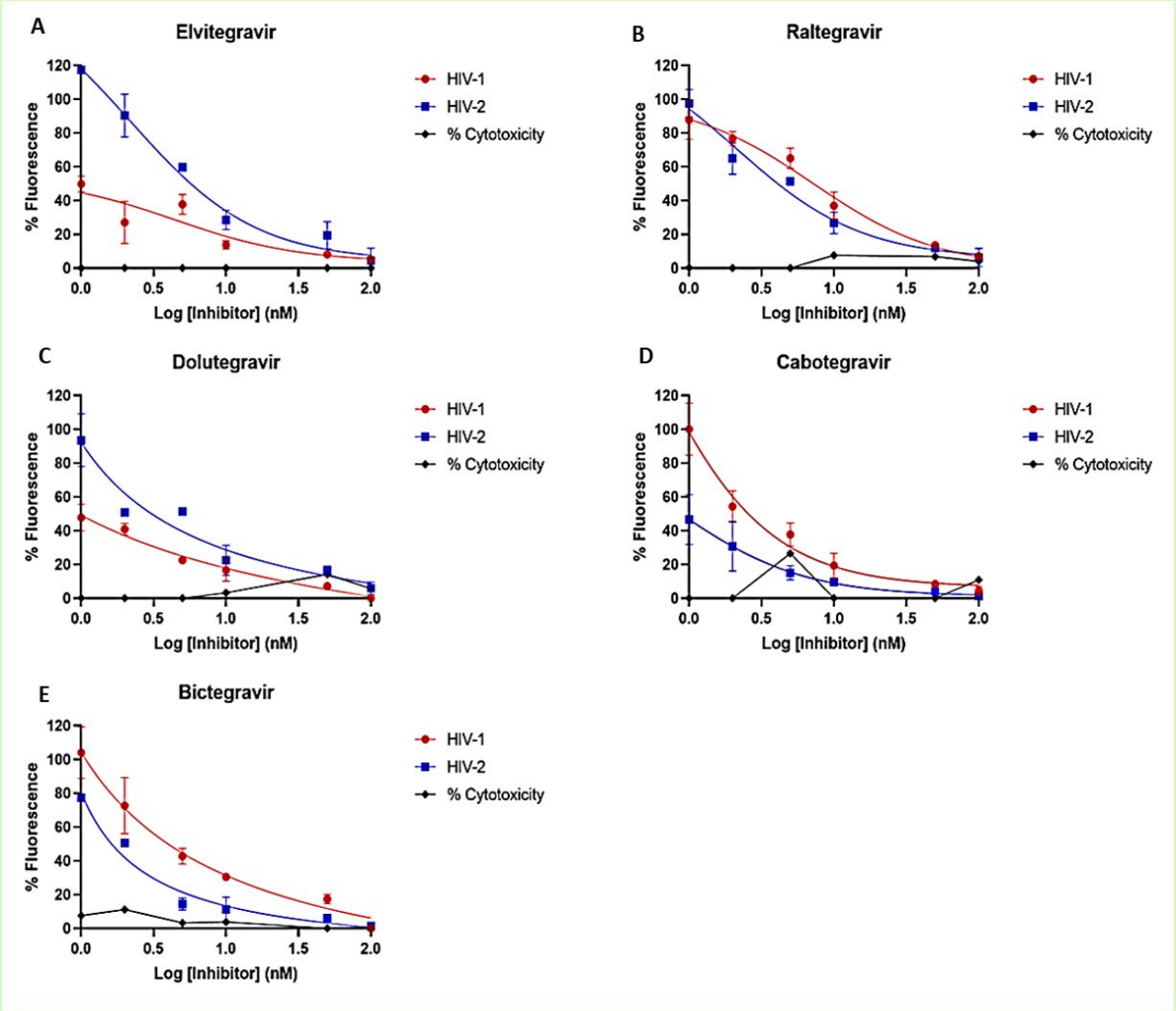

Figure 14: Representation of dose response curves of inhibitors in cell culture using serial dilutions of the INSTIs ranging from 1 nM to 1 µM diluted in DMSO. The y-axis represents the percentage of fluorescence (indicating infectivity) relative to the negative control (cells treated with DMSO in the absence of the inhibitor), while the x-axis shows the logarithmic concentration of the inhibitor. Cytotoxicity percentages are also displayed and can be inferred from the y-axis relative to the control. The data are based on measurements performed in

triplicate using Jurkat cells. There is reduction in fluorescence with increasing concentration of the inhibitors.

6.1.3 Effects of INSTIs on the activity of SARS-CoV-2

Raltegravir did not exhibit noteworthy antiviral activity against the Wuhan-1 (GBH), B.1.1.7 or BA.2 omicron spike variants of SARS-CoV-2, with IC_{50} values exceeding 100 uM, in Vero E6 cells and A549 hACE2-TMPRSS2 cell lines **(Figure 15).** This was also observed in the assessment of dolutegravir and cabotegravir using similar methodology with no significant inhibition.

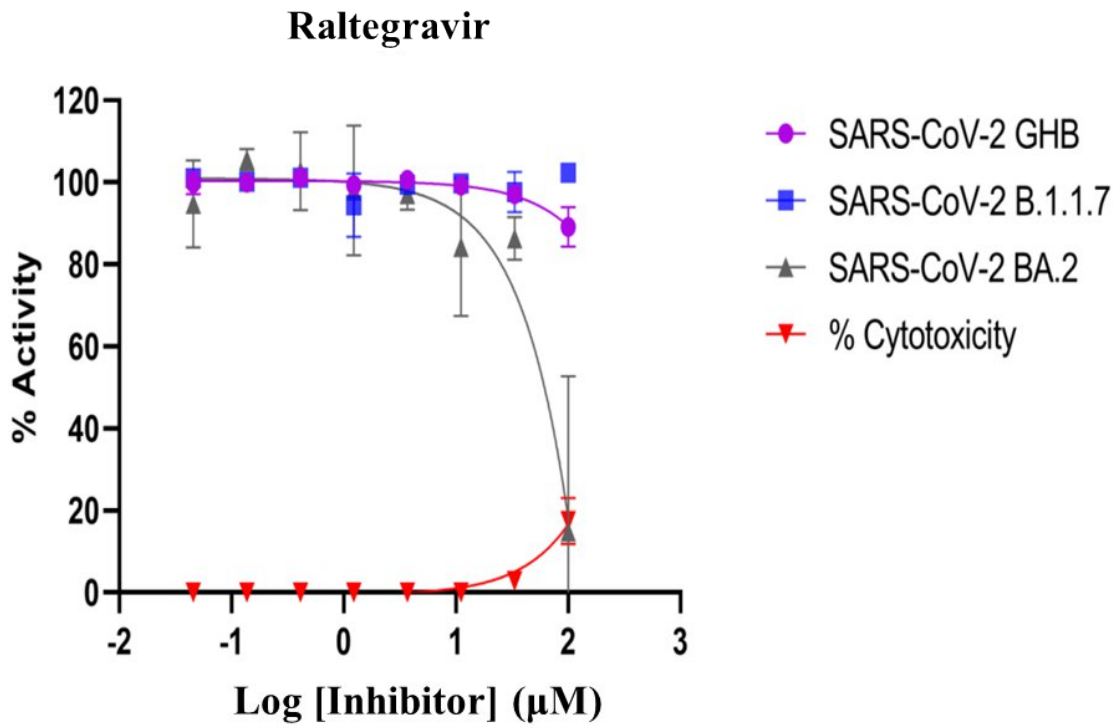

Figure 15: Inhibition profiling of Raltegravir against SARS-CoV-2. Efficacy against the prototypical Wuhan-Hu-1 (GBH) is shown in purple, while that against the B.1.1.7 variant is shown in blue, and omicron BA.2 is shown in grey. Percentage of cytotoxicity is indicated in red. Inhibition profiling was carried out in Vero ™ TMPRSS2 cells using three fold serial dilution of the inhibitor to a final concentration of 0.5 µM. *y* axis indicates percentage of inhibition, and *x* axis is the logarithmic transformation of the inhibitor's concentration. Results represent at least triplicate measurements.

6.1.4 Efficacy of lenacapavir against HIV-2 in cell culture

Lenacapavir exhibited potent antiviral activity against both HIV-1 and HIV-2 in cell culture with IC_{50} values in the low picomolar range. The IC_{50} for HIV-1 was 399.2 (±0.2) pM, while HIV-2 displayed a slightly lower IC_{50} of 206.2 (±0.2) pM, indicating greater susceptibility of

ROD-based HIV-2 to lenacapavir. The dose-response curves demonstrated a concentration-dependent inhibition of viral replication, with near-complete suppression observed at higher concentrations of the inhibitor. Importantly, the cytotoxicity (black curve) remained negligible across the tested concentration range, indicating that the observed inhibitory effects were not attributable to compound toxicity **(Figure 16)**.

A

	IC_{50} (pM)	
CAPSID INHIBITOR	**HIV-1**	**HIV-2**
Lenacapavir	399.3 (±0.2)	206.2 (±0.2)

B

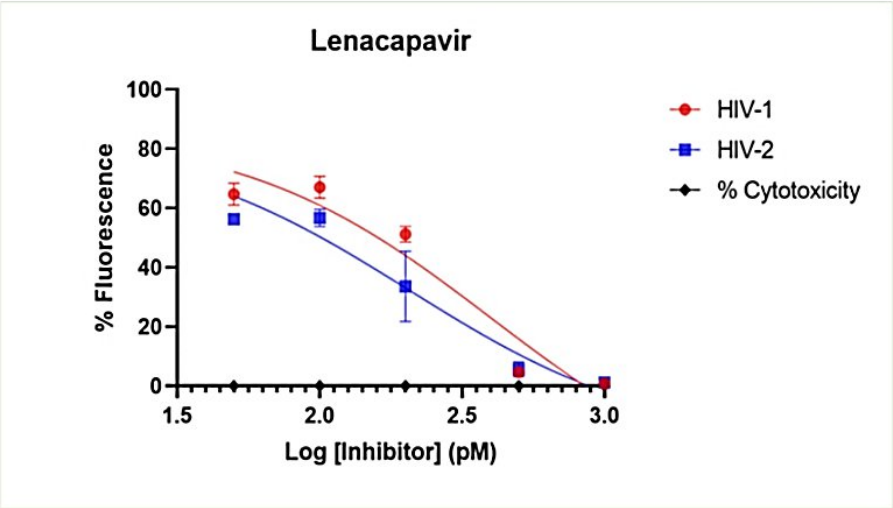

Figure 16: Inhibition profiling of lenacapavir in cell culture using Jurkat cells

A: Picomolar IC_{50} values of lenacapavir against HIV-1 and HIV-2 in cell culture **B:** Dose-response curve of lenacapavir showing percentage fluorescence (x-axis) and the logarithmic transformation of lenacapavir concentration in picomoles (y-axis). The percentage of cytotoxicity is indicated with black dotted line. The inhibitor concentration ranged from 1 pM to 1 nM serially diluted in DMSO. The experiment was carried in triplicates.

6.1.5 Effects of lenacapavir on HIV-2 capsid formation

There was no significant difference in the reverse transcriptase (RT) activity between the HIV-2 pseudoviruses produced in the presence of different concentrations of lenacapavir compared to the control. However, transduction efficiency was significantly reduced when these pseudoviruses were used to transduce cells **(Figure 17)**, suggesting a defective the virion formation in the presence of lenacapavir, despite having normal RT activity.

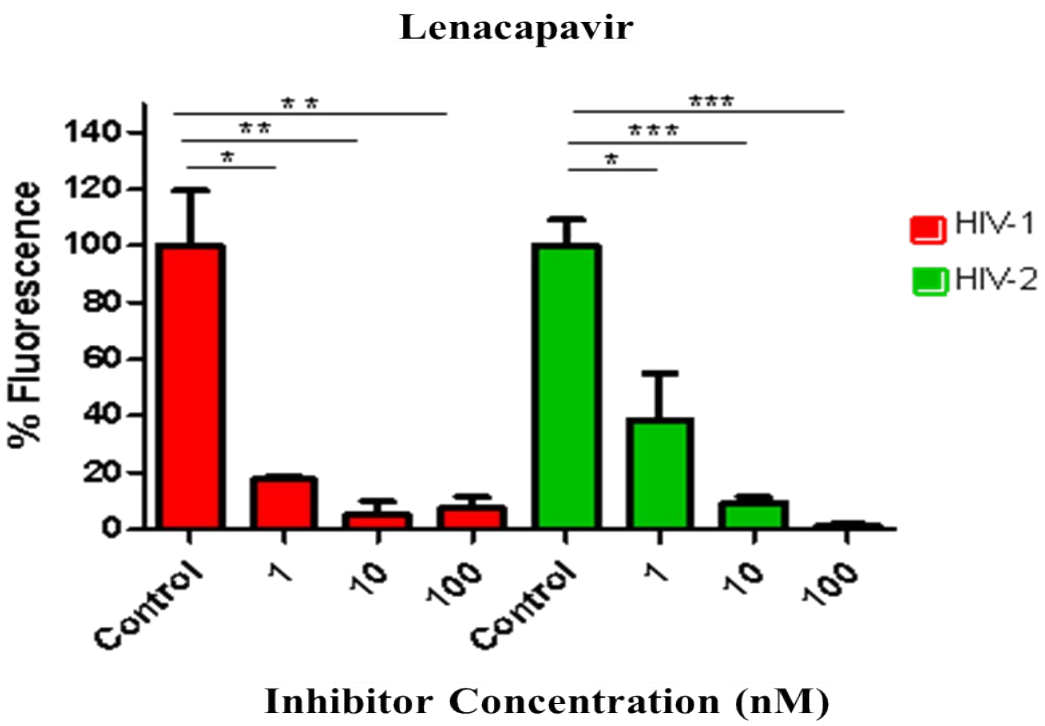

Figure 17: HIV-1 and 2 pseudovirions with aberrant capsids produced in the presence of lenacapavir. Pseudovirions were produced in the presence of 1, 10, and 100 nM of lenacapavir. The y axis indicates percentage of transduction efficiency (percentage of fluorescence), and x axis denotes the concentrations of lenacapavir used to treat the cells. Control cells were only treated with DMSO. Results are concluded from triplicate measurements. * p value ≤ 0.05, ** p value ≤ 0.01, *** p value ≤ 0.001.

6.1.6 Molecular docking analysis of INSTIs and lenacapavir

Molecular docking simulations revealed favourable binding of dolutegravir, bictegravir and cabotegravir within the HIV-2 integrase's active site. The inhibitors engaged DNA substrates and coordinated with the Mg^{2+} ions essential for enzymatic activity **(Figure 18)**.

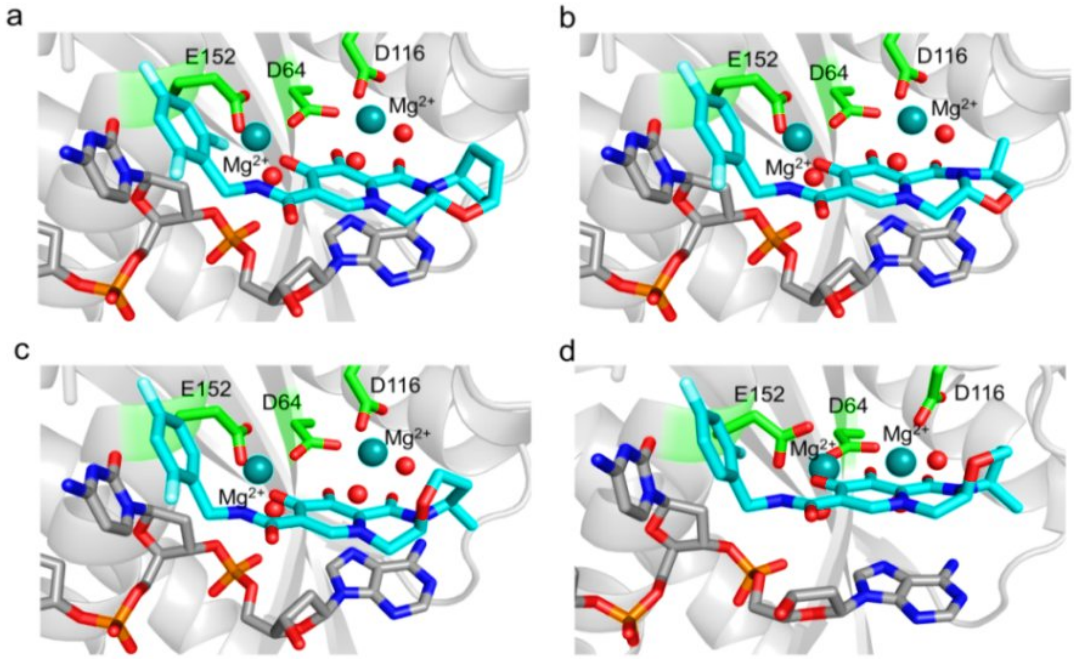

Figure 18: Molecular docking of the INSTIs on HIV-2 integrase active site
Structure of (a) bictegravir, (b) cabotegravir, and (c) dolutegravir inhibitors docked by PLANTS in the active site of HIV-2 integrase. The inhibitor (teal), the DNA substrate (grey), and the Mg2+ coordinating active site residues (green) are represented in stick format, the Mg2+ ions (deep teal), and the coordinated water molecules (red) as spheres. (d) For comparison, the SIV integrase crystal structure (PDB ID: 6RWN (Waterhouse et al., 2018) that binds dolutegravir, applying the same colouring and representation schemes.

Additionally, lenacapavir demonstrated favorable docking to the p26 capsid protein of HIV-2 with binding characteristics comparable to its interaction with the HIV-1 p24 capsid crystal structure **(Figure 19)**.

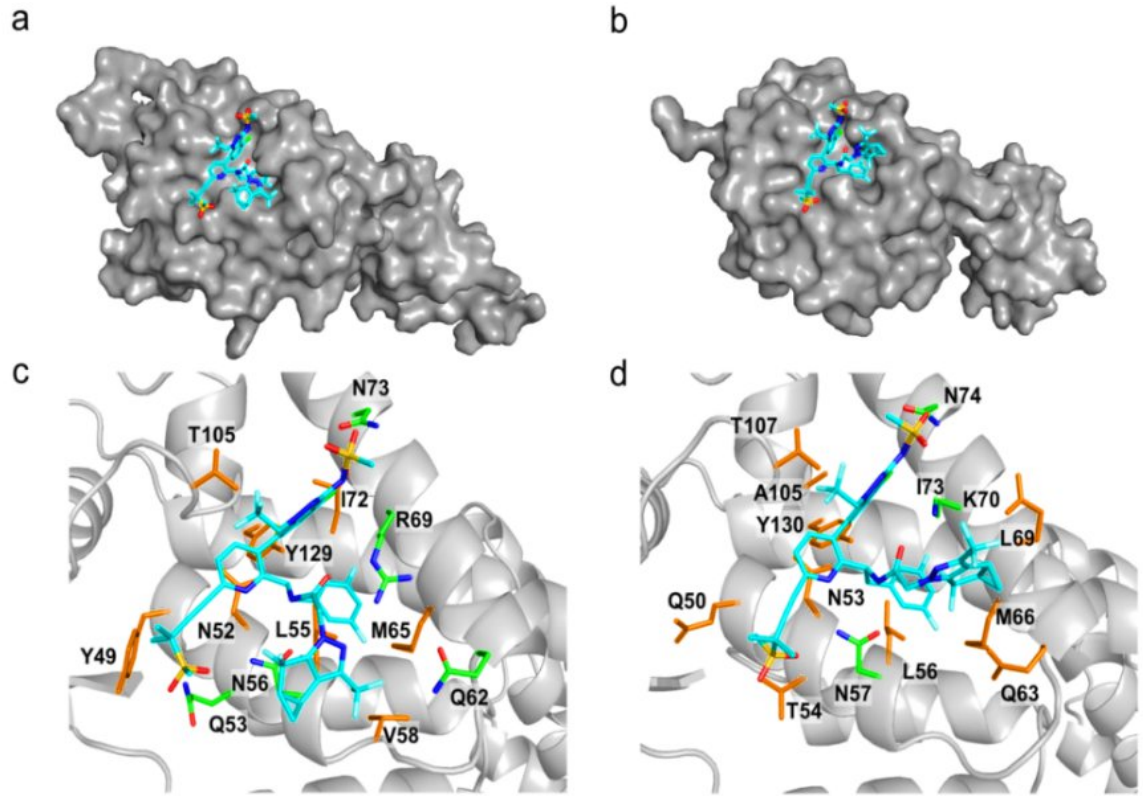

Figure 19:
(a) Lenacapavir in complex with the HIV-2 capsid protein (p26) docked by AutoDock Vina to the AlphaFold model; (b) in complex with the active site of HIV-1 capsid protein (p24), crystal structure (PDB ID: 6V2F). The protein is represented with a grey surface and lenacapavir as blue sticks. Close up of lenacapavir in (c) the HIV-2 model and (d) the HIV-1 crystal structure. The inhibitor (teal) and the interacting capsid residues (hydrogen bond forming—green, a polar interaction forming—brown) are represented as sticks, the rest of the protein as cartoon. The interactions were determined with LigPlot+.

6.2 Transcriptomic changes induced by Vpx

6.2.1 Analysis of gene regulation by Vpx

In this work, we assessed the effects of HIV-2's accessory protein Vpx on the transcriptome of THP-1 cells after transfection with both the wild–type, and functionally restricted Vpx plasmids. Our analysis revealed that hundreds of genes with different functions were either upregulated or downregulated by Vpx. Many genes involved in critical biological processes, such as immune response regulation, cell division, and cell death, were upregulated by wild-type Vpx.

Wild-type Vpx significantly upregulated genes associated with immune modulation, apoptosis, and cellular differentiation, such as RANBP2-like, caspase 3(CASP3), GRIP domain containing 2, U2 small nuclear RNA auxiliary factor 1 like 5 (U2AF1L5), NOP58

ribonucleoprotein, and protocadherin gamma subfamily C (PCDHGC). Conversely, genes such as the U2 small nuclear RNA auxiliary factor 1 (U2AF1), SKI family transcriptional co-repressor 2 (SKOR2), mucin 4 cell surface associated (MUC4), CORO7-PAM16 read-through (CORO7-PAM16) and serpin family A member 1 (SERPINA1) among others, were downregulated **(Figure 20)**.

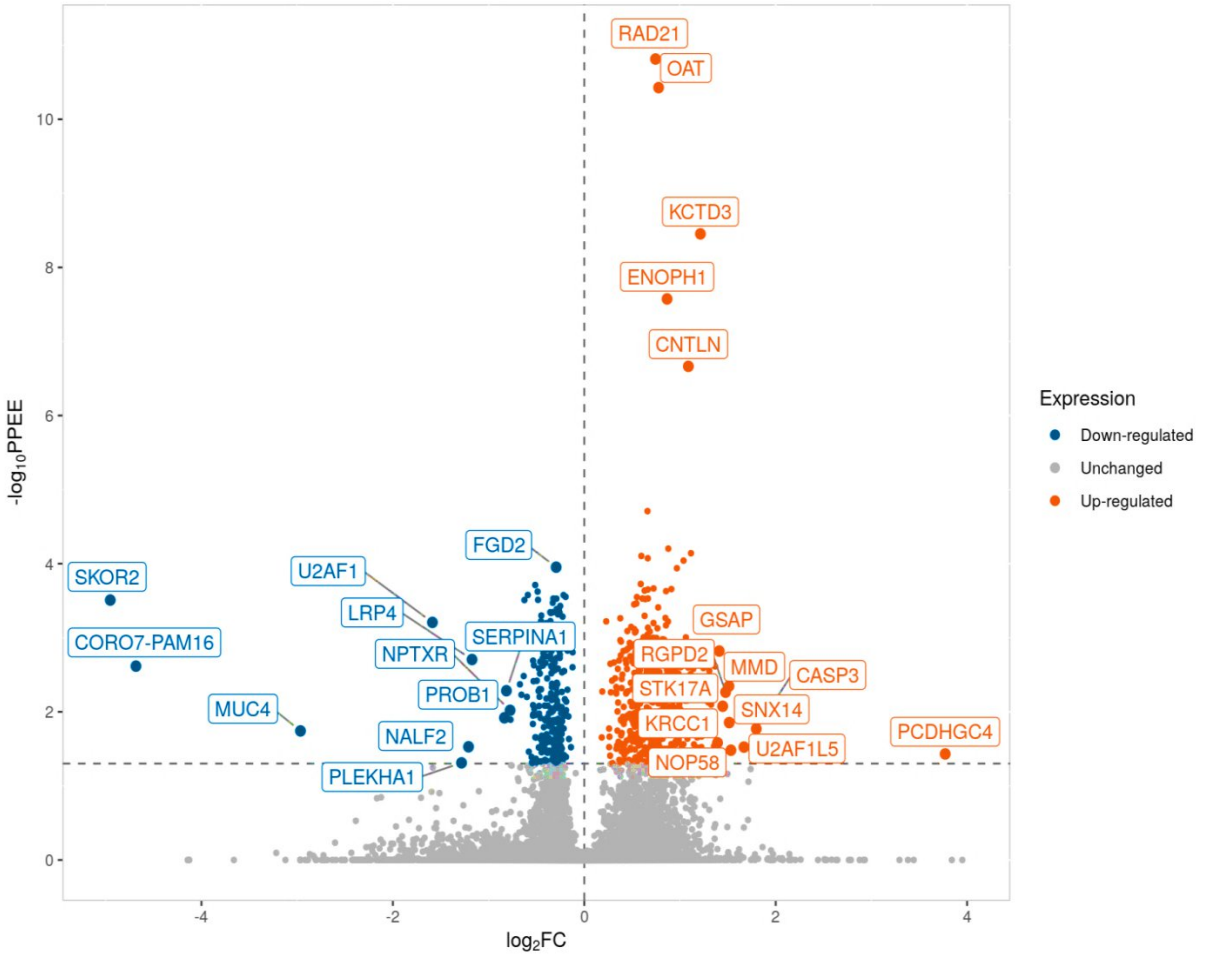

Figure 20: Differential gene expression profile. Volcano plot showing differentially expressed genes in the presence of wild-type Vpx compared to GFP expressing mock control in THP-1 cells. Plotted are the negative base 10 posterior probabilities of genes being equally expressed (-$\log_{10}$PPEE) in the function of log2 transformed fold changes. Probability values were subject to FDR correction at an alpha level of 0.05.

On the other hand, transfection with a construct expressing the functionally impaired K68A-R70A mutant of Vpx led to increased expression of several keratin-related genes (KRT81, KRT5, KRT19, KRT6A), along with MAL, T-cell differentiation protein 2 (MAL2), SERPINB5, MAGEA3, MAGEA6, KLK6, and RHOD. In contrast, a number of genes were found to be downregulated, including EIF3CL, CNR2, SENP8, TOR1AIP2, PARD6G, ZNF490, RSPH3, SLC35E3, PSTPIP2, and SHOX. Similar to what was observed with wild-type Vpx, SKOR2 expression was also reduced.

6.2.2 GO analysis of differentially expressed genes

GO enrichment analysis of genes differentially expressed in response to wild-type Vpx identified 27 molecular functions, 28 cellular component groupings and 72 biological process categories. Biological process (BP) analysis revealed that the impacted genes were primarily associated with the negative regulation of viral processes (GO:0048525), the type I interferon signaling pathway (GO:0060337), spliceosomal snRNP assembly (GO:0000387), regulation of transcription elongation from the RNA polymerase II promoter (GO:0034243), negative regulation of the innate immune response (GO:0045824), positive regulation of interferon-beta production (GO:0032728), and DNA-templated transcription elongation (GO:0006354) **(Figure 21)**.

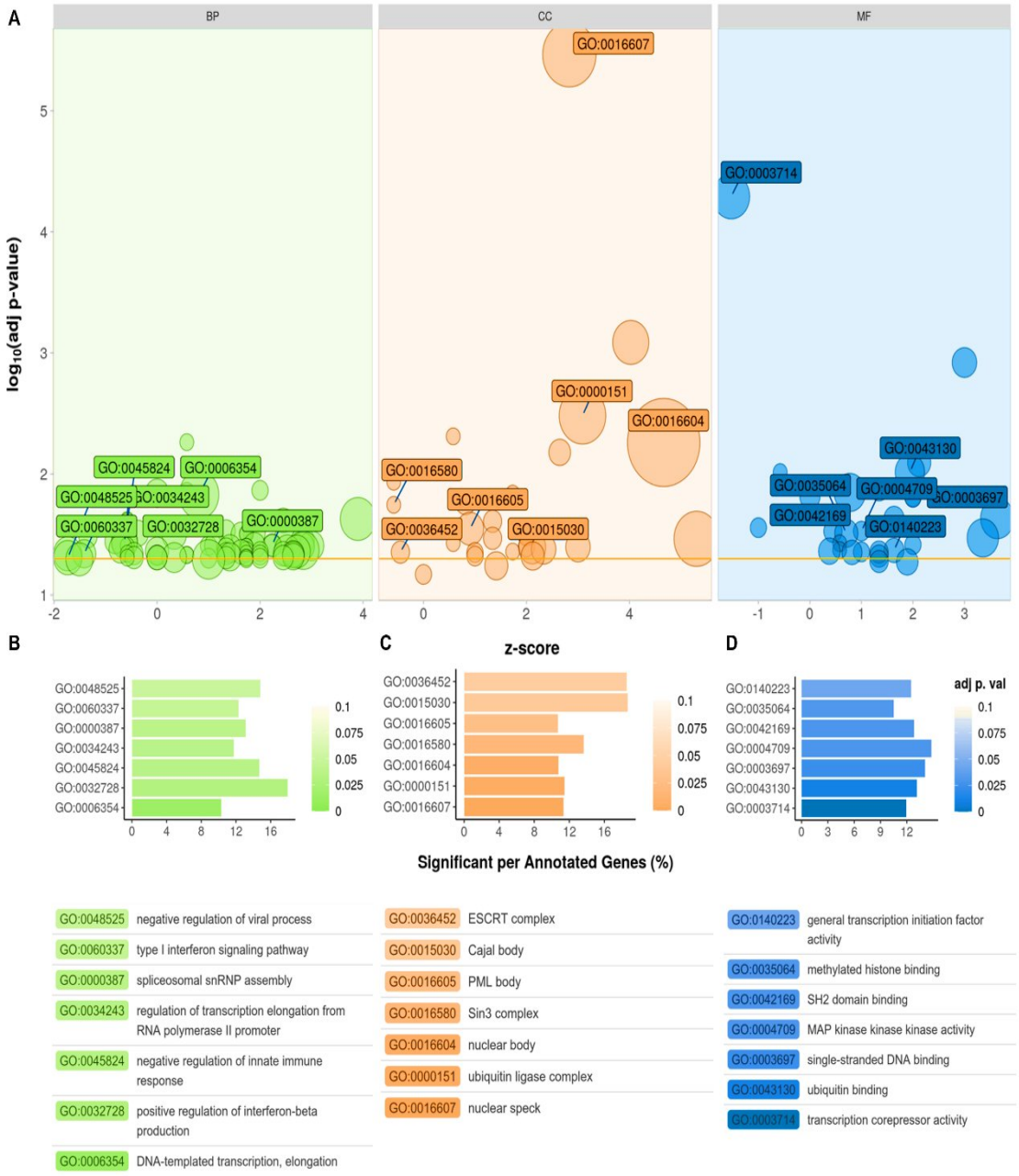

Figure 21: Bubble plots illustrating significantly enriched GO categories of the differentially expressed genes (DEGs) impacted by transfection with wild-type Vpx. A) GO analysis highlights the top seven enriched terms in each category with BP representing Biological Processes; CC is the Cellular Components and MF is the Molecular Functions respectively. Bubble size reflects the number of DEGs associated with each term. The accompanying horizontal bar plots indicate the proportion of DEGs relative to the total number of annotated genes within the top seven terms under B) Biological process C) Cellular component (CC) and D) Molecular function(MF).

Further analysis of the identified pathways that were altered significantly was carried out, with a focus on the link between the top selected GO terms and the DEGs. The analysis showed that the differentially expressed genes (DEGs) were predominantly associated with

processes such as regulation of transcription elongation from the RNA polymerase II promoter (GO:0034243), DNA-templated transcription elongation (GO:0006354), involvement in the ubiquitin ligase complex (GO:0000151), localization to the nuclear speck (GO:0016607), ubiquitin binding (GO:0043130), and negative regulation of the innate immune response (GO:0045824). The connection between the GO terms and DEGs is represented in **Figure 22**.

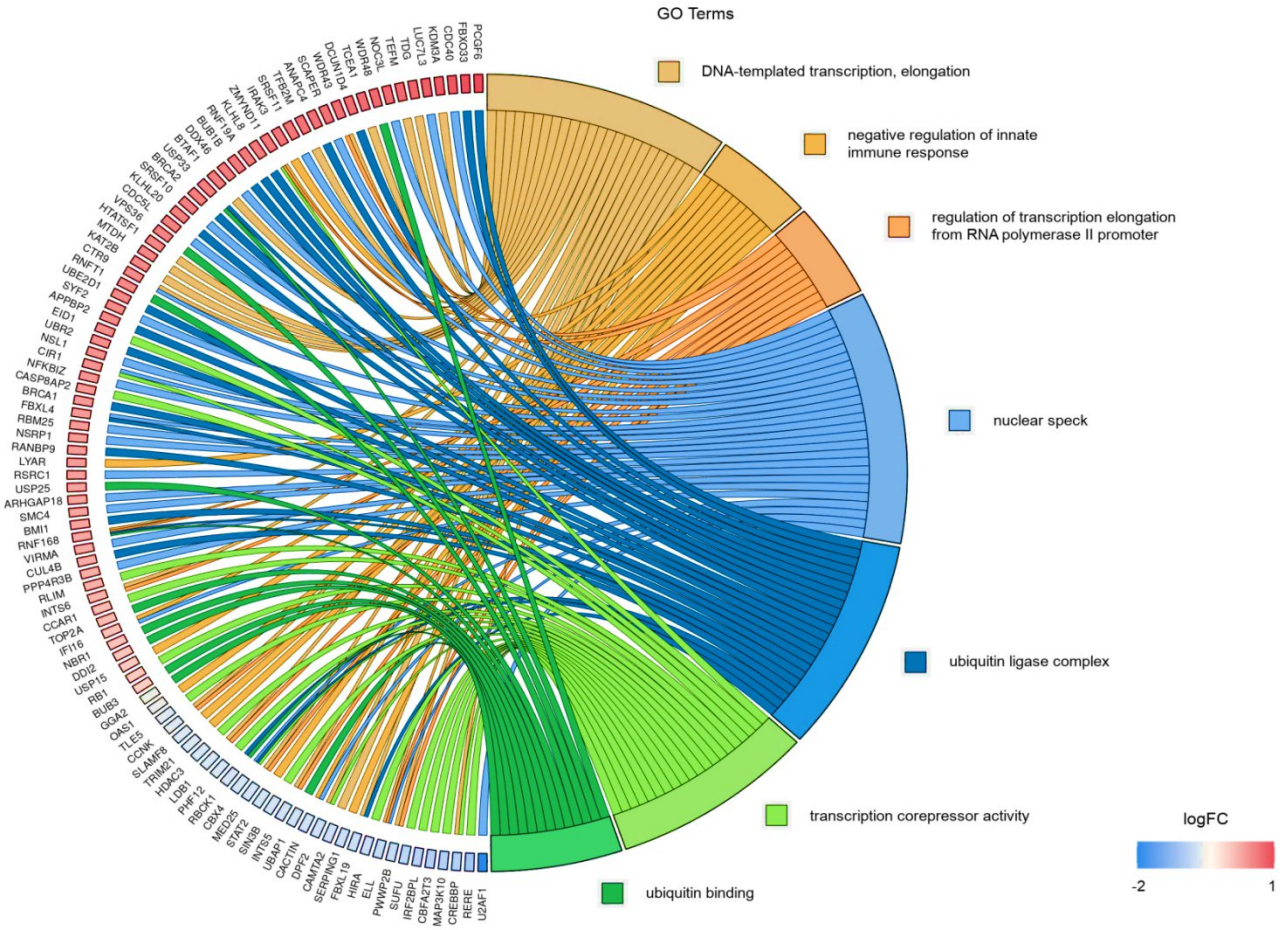

1.36	PCGF6	polycomb group ring finger 6
1.30	FBXO33	F-box protein 33
1.24	CDC40	cell division cycle 40
1.23	KDM3A	lysine demethylase 3A
1.19	LUC7L3	LUC7 like 3 pre-mRNA splicing factor
1.14	TDG	thymine DNA glycosylase
1.10	TEFM	transcription elongation factor, mitochondrial
1.10	NOC3L	NOC3 like DNA replication regulator
1.10	WDR48	WD repeat domain 48
1.09	TCEA1	transcription elongation factor A1
1.07	DCUN1D4	defective in cullin neddylation 1 domain containing 4
1.05	WDR43	WD repeat domain 43
1.04	SCAPER	S-phase cyclin A associated protein in the ER
1.03	ANAPC4	anaphase promoting complex subunit 4
1.02	TFB2M	transcription factor B2, mitochondrial
1.00	SRSF11	serine and arginine rich splicing factor 11
0.98	IRAK3	interleukin 1 receptor associated kinase 3
0.98	ZMYND11	zinc finger MYND-type containing 11
0.96	KLHL8	kelch like family member 8
0.96	RNF19A	ring finger protein 19A, RBR E3 ubiquitin protein ligase
0.96	BUB1B	BUB1 mitotic checkpoint serine/threonine kinase B
0.95	DDX46	DEAD-box helicase 46
0.94	BTAF1	B-TFIID TATA-box binding protein associated factor 1
0.93	USP33	ubiquitin specific peptidase 33
0.93	BRCA2	BRCA2 DNA repair associated
0.92	SRSF10	serine and arginine rich splicing factor 10
0.92	KLHL20	kelch like family member 20
0.91	CDC5L	cell division cycle 5 like
0.90	VPS36	vacuolar protein sorting 36 homolog
0.88	HTATSF1	HIV-1 Tat specific factor 1
0.88	MTDH	metadherin
0.86	KAT2B	lysine acetyltransferase 2B
0.85	CTR9	CTR9 homolog, Paf1/RNA polymerase II complex component
0.85	RNFT1	ring finger protein, transmembrane 1
0.85	UBE2D1	ubiquitin conjugating enzyme E2 D1
0.84	SYF2	SYF2 pre-mRNA splicing factor
0.83	APPBP2	amyloid beta precursor protein binding protein 2
0.82	EID1	EP300 interacting inhibitor of differentiation 1
0.82	UBR2	ubiquitin protein ligase E3 component n-recognin 2
0.81	NSL1	NSL1 component of MIS12 kinetochore complex
0.79	CIR1	corepressor interacting with RBPJ, CIR1
0.77	NFKBIZ	NFKB inhibitor zeta
0.75	CASP8AP2	caspase 8 associated protein 2
0.74	BRCA1	BRCA1 DNA repair associated
0.73	FBXL4	F-box and leucine rich repeat protein 4
0.73	RBM25	RNA binding motif protein 25
0.72	NSRP1	nuclear speckle splicing regulatory protein 1
0.72	RANBP9	RAN binding protein 9
0.72	LYAR	Ly1 antibody reactive
0.69	RSRC1	arginine and serine rich coiled-coil 1
0.66	USP25	ubiquitin specific peptidase 25
0.66	ARHGAP18	Rho GTPase activating protein 18
0.66	SMC4	structural maintenance of chromosomes 4
0.65	BMI1	BMI1 proto-oncogene, polycomb ring finger
0.64	RNF168	ring finger protein 168
0.63	VIRMA	vir like m6A methyltransferase associated
0.61	CUL4B	cullin 4B
0.59	PPP4R3B	protein phosphatase 4 regulatory subunit 3B
0.58	RLIM	ring finger protein, LIM domain interacting
0.53	INTS6	integrator complex subunit 6
0.48	CCAR1	cell division cycle and apoptosis regulator 1
0.48	TOP2A	DNA topoisomerase II alpha
0.44	IFI16	interferon gamma inducible protein 16
0.43	NBR1	NBR1 autophagy cargo receptor
0.41	DDI2	DNA damage inducible 1 homolog 2
0.38	USP15	ubiquitin specific peptidase 15
0.38	RB1	RB transcriptional corepressor 1
0.33	BUB3	BUB3 mitotic checkpoint protein
-0.19	GGA2	golgi associated, gamma adaptin ear containing, ARF binding protein 2
-0.20	OAS1	2'-5'-oligoadenylate synthetase 1
-0.22	TLE5	TLE family member 5, transcriptional modulator
-0.23	CCNK	cyclin K
-0.23	SLAMF8	SLAM family member 8
-0.24	TRIM21	tripartite motif containing 21
-0.25	HDAC3	histone deacetylase 3
-0.25	LDB1	LIM domain binding 1
-0.26	PHF12	PHD finger protein 12
-0.26	RBCK1	RANBP2-type and C3HC4-type zinc finger containing 1
-0.27	CBX4	chromobox 4
-0.28	MED25	mediator complex subunit 25
-0.29	STAT2	signal transducer and activator of transcription 2
-0.29	SIN3B	SIN3 transcription regulator family member B
-0.29	INTS5	integrator complex subunit 5
-0.30	UBAP1	ubiquitin associated protein 1
-0.31	CACTIN	cactin, spliceosome C complex subunit
-0.31	DPF2	double PHD fingers 2
-0.33	CAMTA2	calmodulin binding transcription activator 2
-0.34	SERPING1	serpin family G member 1
-0.34	FBXL19	F-box and leucine rich repeat protein 19
-0.35	HIRA	histone cell cycle regulator
-0.38	ELL	elongation factor for RNA polymerase II
-0.39	PWWP2B	PWWP domain containing 2B
-0.45	SUFU	SUFU negative regulator of hedgehog signaling
-0.48	IRF2BPL	interferon regulatory factor 2 binding protein like
-0.51	CBFA2T3	CBFA2/RUNX1 partner transcriptional co-repressor 3
-0.53	MAP3K10	mitogen-activated protein kinase kinase kinase 10
-0.54	CREBBP	CREB binding protein
-0.67	RERE	arginine-glutamic acid dipeptide repeats
-1.59	U2AF1	U2 small nuclear RNA auxiliary factor 1

Figure 22: Gene association analysis of DEGs. Association between 99 DEGs and the top 7 selected GO terms: (1) DNA-templated transcription elongation; (2) the negative regulation of innate immune response and (3) the regulation of transcription elongation from RNA polymerase II promoter classified under biological processes; (4) nuclear speck and (5) ubiquitin ligase complex belonging to cellular components; (6) transcription co-repressor activity and (7) ubiquitin binding pertaining to molecular functions, along with the corresponding log2FC values of genes are represented in GOChord plot. Genes associated only with nuclear speck or ubiquitin ligase complex in the range of $-0.58 < \log2FC < 0.58$ ($0.58 \approx \log21.5$) were omitted. The color intensities of the rectangles reflect the significance of change in the corresponding gene level relative to the control (color scale: log FC = −2 blue, log FC = 0 white and log FC = 1 red).

6.2.3 Vpx effects on the cytokine profile of THP-1 cells

We analysed the culture medium of transfected cells to assess the secretion of key pro-inflammatory cytokines, including Interleukin-6 (IL-6), Interleukin-1 beta (IL-1β), and Transforming Growth Factor Beta (TGF-β). Our findings demonstrated that transfection with the wild-type HIV-2 Vpx led to a notable increase in the levels of these cytokines, suggesting a pro-inflammatory response. However, this effect did not extend to type I interferons (IFN-α), which are critical antiviral mediators; their expression remained unchanged compared to control cells. These results suggest that while Vpx enhances inflammatory signaling, it may not directly influence the type I interferon response **(Figure 23).**

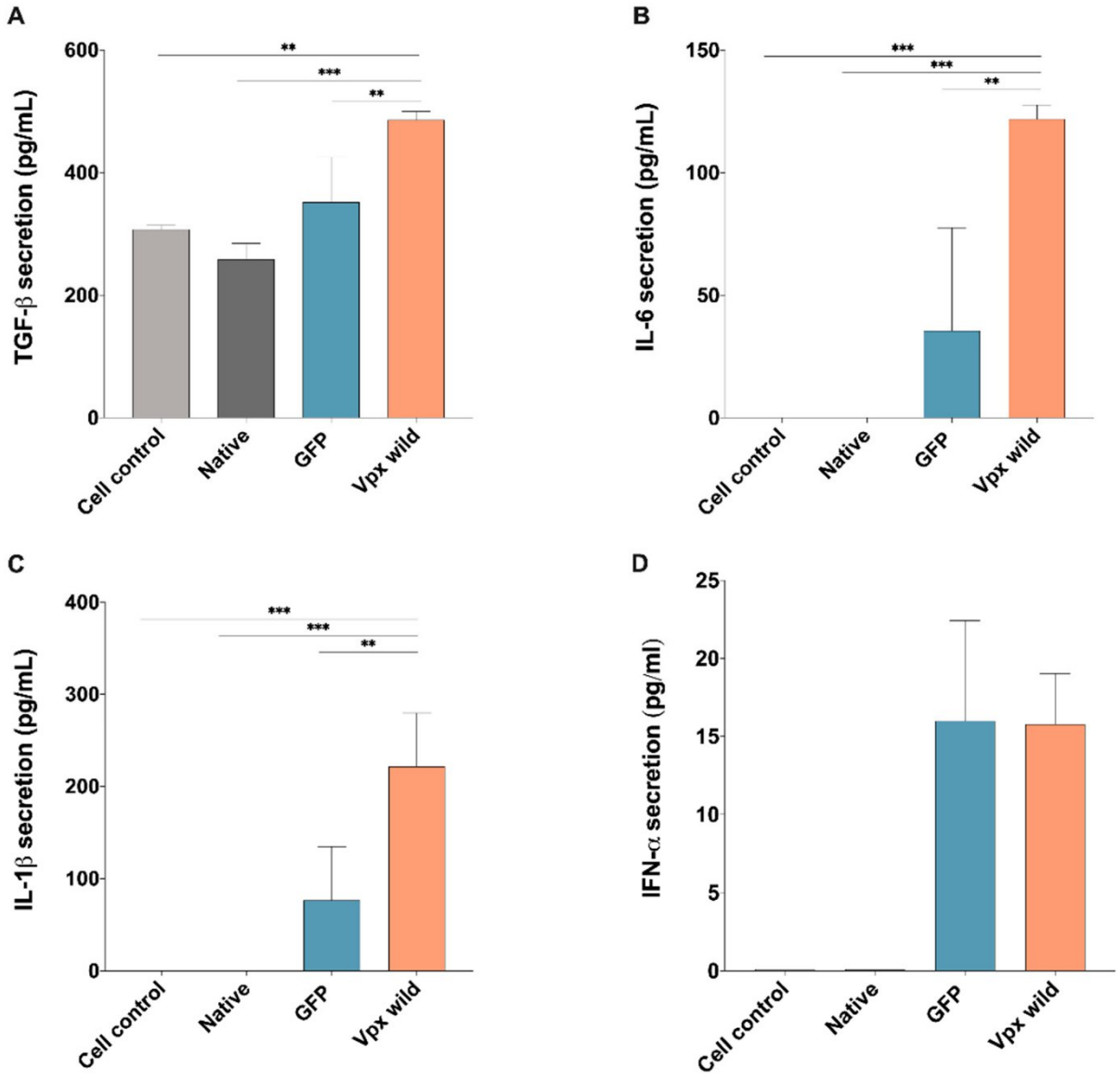

Figure 23: Vpx effects on the cytokine profile 24hrs after THP-1 cells transfection. Secretion of **A:** TGF- β **B:** IL-6 **C:** IL-1 β and **D:** Type I α interferons in the medium of transfected cells. Bars represent the average values obtained from two separate experiments. * depicts statistical significance $p < 0.001$***, $p < 0.01$**. The experiment was carried out in duplicates. Native cells were treated with lipofectamine only.

6.2.4 Effects of Vpx on the expression on HIV-1 Tat

Following co-transfection of HEK-293T cells with plasmids encoding HIV-1 Tat and either wild-type or functionally restricted Vpx, western blot analysis revealed a substantial reduction in HIV-1 Tat expression in cells expressing wild-type Vpx. The mutant Vpx (K68A-R70A) also led to reduced Tat expression compared to the control; however, this effect was considerably less pronounced than that observed with the wild-type Vpx **(Figure 24).**

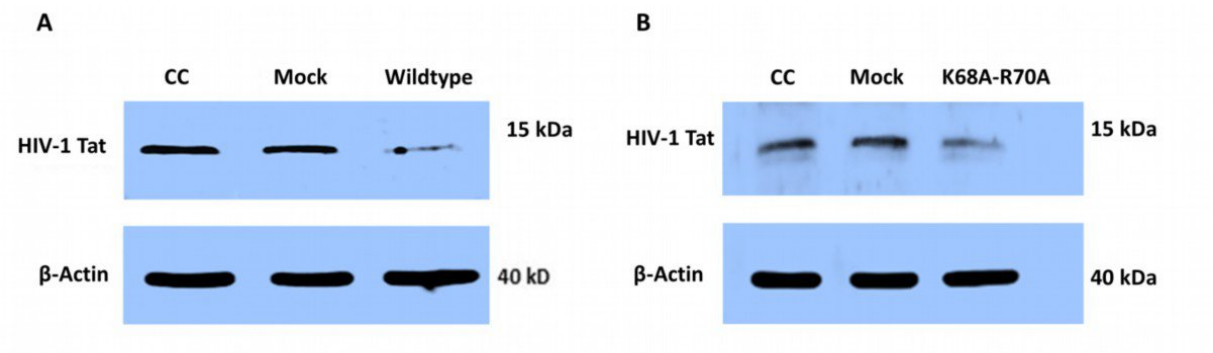

Figure 24: HIV-1 Tat expression measured by Western blot from wild type Vpx transfected cells (A) and mutant K68A-R70A Vpx shown in (B). Controls consisted of cells transfected with pcDNA1-Tat alone (CC) and mock transfected cells with pcDNA3.1-Vpx-NeGFP; β –actin was used for normalization. Results are obtained from a single representative experiment.

6.2.5 Effects of Vpx on the expression of SKOR2, U2AF1 and CASP3 genes

RT-qPCR analysis showed that U2AF1 expression was significantly downregulated in THP-1 cells transfected with either the wild-type Vpx or the functionally restricted mutant plasmids (**** $p<0.0001$). However, SKOR2 and CASP3 expression levels remained largely unchanged under similar conditions. A significant decrease in U2AF1 expression was observed in cells infected with the HIV-2 1806 isolate (*$p < 0.05$), while CASP3 expression was significantly downregulated following infection with the HIV-2 1654 isolate (*$p < 0.05$). In contrast, SKOR2 expression remained unchanged across all HIV-2 primary isolates **(Figure 25)**.

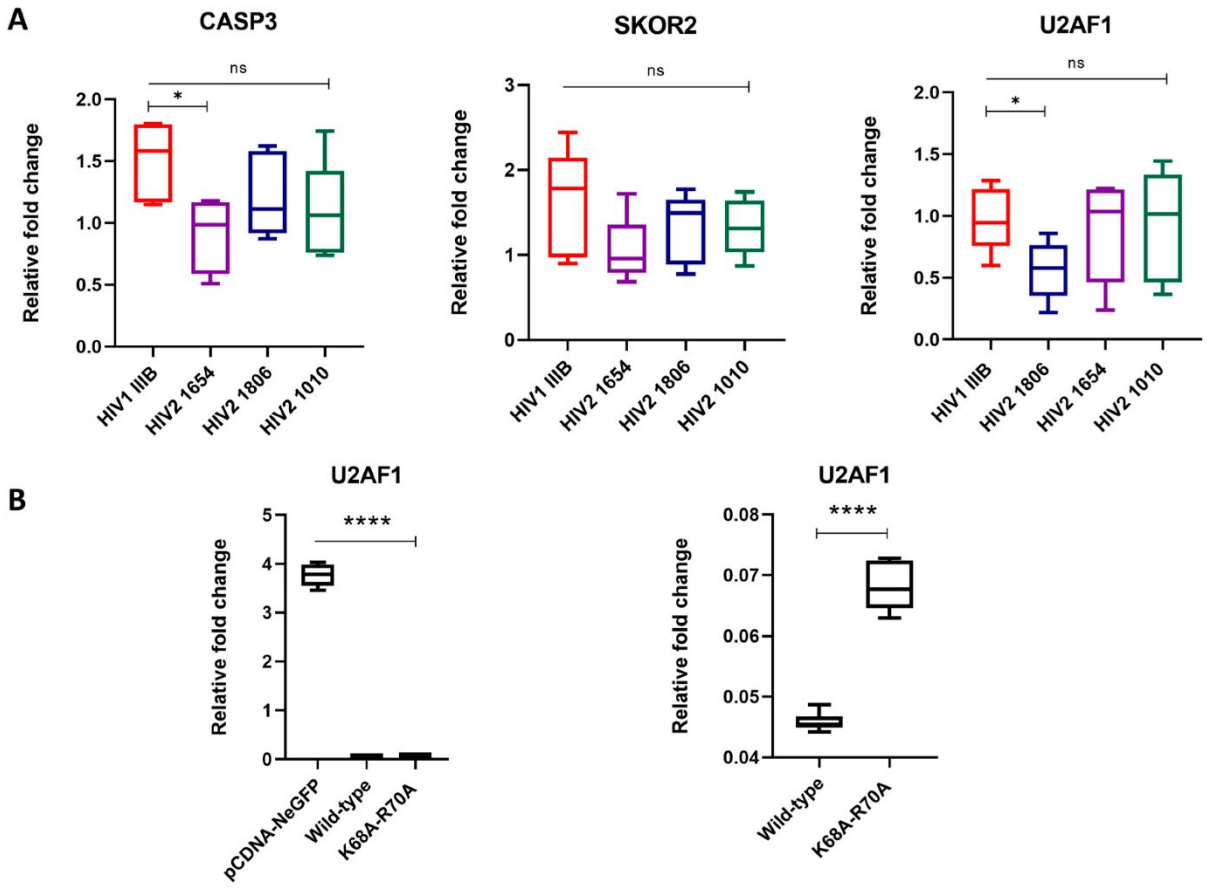

Figure 25: RT-qPCR validation of significantly altered transcripts. Relative fold changes of RT- qPCR Ct values of CASP3, SKOR2 and U2AF1 are shown in **(A):** THP-1 cells infected with HIV-1 and HIV-2 isolates, and **(B):** Wild-type and functionally restricted Vpx-transfected THP-1 cells. PcDNA-NeGFP was used as a mock control. The experiment was carried out in triplicates * $p < 0.05$; **** $p < 0.0001$.

CASP3 was upregulated in our analysis of DEGs of Vpx-transfected cells, however, from RT-qPCR analysis, it was downregulated as a result of infection by HIV-2, and significantly so with variant 1654. To address this discrepancy, we measured CASP3 levels from cell lysates using colorimetric substrate after transfection of THP-1 with Vpx-expressing plasmid. A significant increase in the activity of CASP3 was observed in wild-type Vpx transfected cells while CASP3 activity was comparable to the control after transfection with a functionally restricted Vpx mutant **(Figure 26)**.

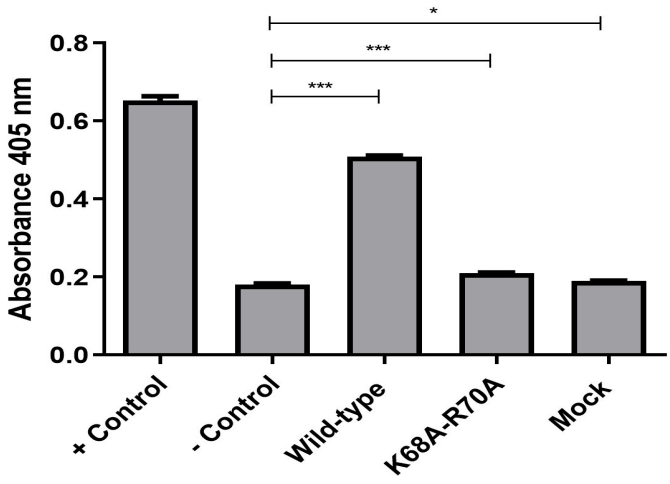

Figure 26: CASP3 enzymatic activity in THP-1 cells transfected with pcDNA3.1-Vpx-NeGFP (wild-type), pcDNA3.1-MutVpx-NeGFP (K68A-R70A mutant) and pcDNA3.1-NeGFP (mock) plasmids. Non-transfected THP-1 cells were used as negative controls (− Control), while cells treated with 1 μM staurosporine were used as positive controls (+ Control). An unpaired t-test was used to calculate statistical significance. * p-value ≤ 0.05; *** p-value ≤ 0.001. The experiment was carried out in triplicates.

6.3 Interaction between LEDGF/p75 and HIV-2 integrase

6.3.1 Detection of LEGDF/p75 and Integrase by western blot

To assess the expression of proteins, western blot analysis was performed. LEDGF/p75 was detected in lysates of HEK-293T and Jurkat cells using an anti-PSIP1 monoclonal antibody, identifying two isoforms of LEDGF: p52 and p75. For the detection of integrase, HEK-293T and Jurkat cells were transduced with HIV-2 pseudoviruses, and a 32 kDa integrase protein band was detected 48 hours post-transduction using an anti-HIV integrase antibody **(Figure 27).**

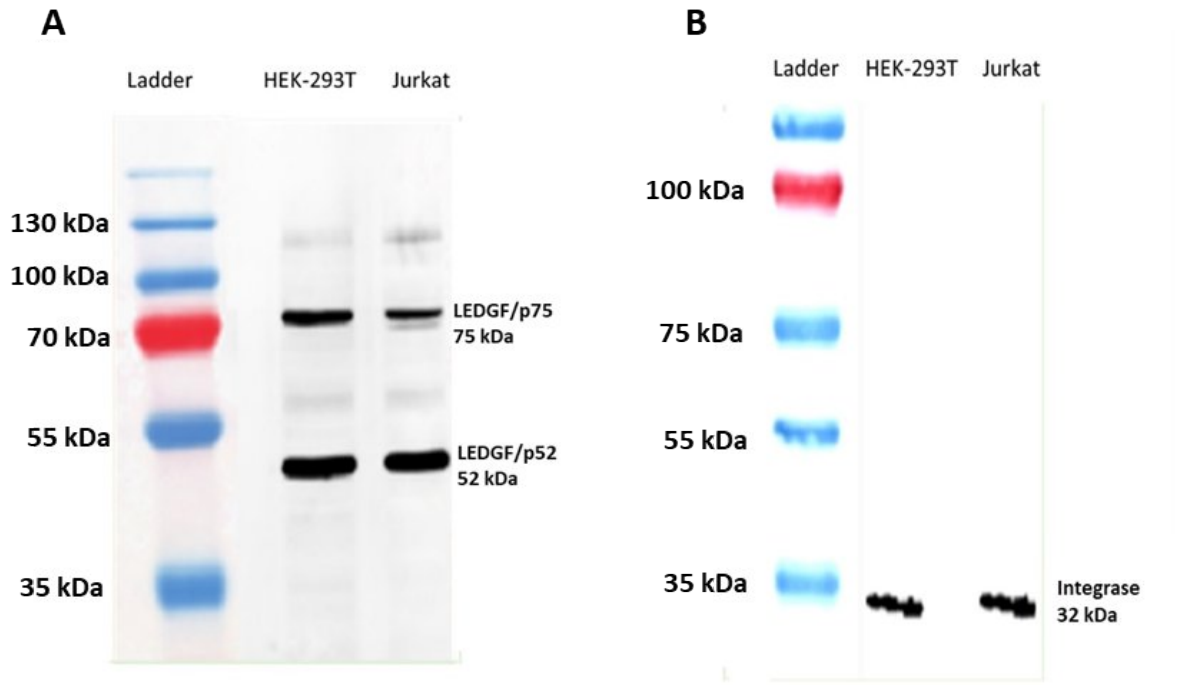

Figure 27: Western blot analysis of cell lysates collected from HEK 293T and Jurkat cells **A:** Detection of LEDGF isoforms (p52 and p75) and **B:** Detection of HIV-2 Integrase protein (32 kDa) following transduction of cells with Jurkat and HEK 293T cells. Results are obtained from a single representative experiment.

6.3.2 Time dependent interaction between LEDGF/p75 and HIV-2 integrase

We detected the interaction signal between LEDGF/p75 and HIV-2 integrase as early as 4hrs post transduction with the peak interaction at 6 hour time-point **(Figure 28)**, hinting to the possibility of utilization of LEDGF/p75 by HIV-2 for integration into the host's genome, as in the case of HIV-1.

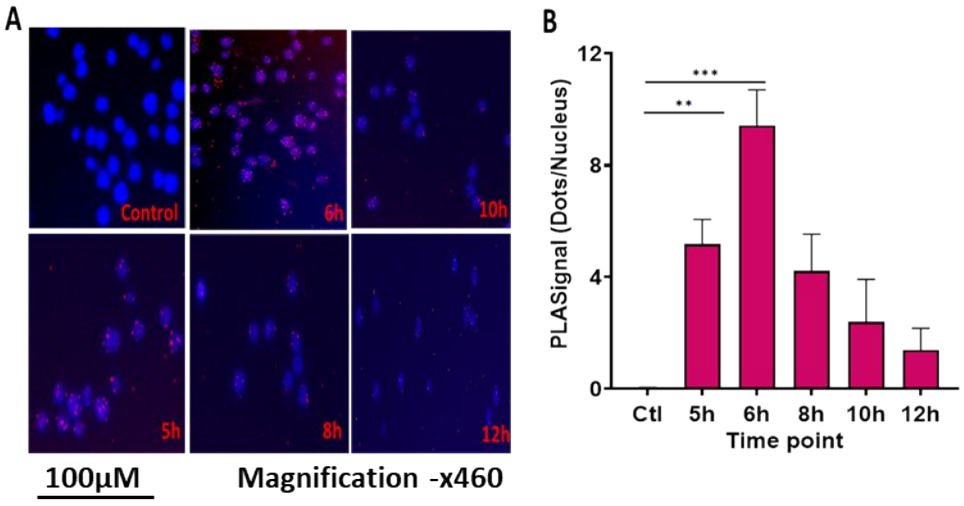

Figure 28: Interaction between LEDGF/p75 and HIV-2 Integrase

A: Representative processed images showing DAPI-stained nucleus (blue) and PLA signals (red dot) implying interaction between the two proteins and **B:** Quantification of PLA signals. The y axis is the mean +/-SEM (dots/nucleus) while x axis shows interaction of the proteins after transduction at different time points. Control included cells not treated with LEDGF/p75 or integrase antibodies.

6.3.3 Effects of LEDGF/p75 silencing on the transduction efficiency and interaction with HIV-2 integrase

To ascertain the optimum time required for silencing using siRNA, we incubated the silenced cells for 1–3 days (24–72h). Western blot analysis confirmed efficient silencing after 24 hours of incubation, which was selected as the optimal time point for further PLA analysis. PLA results demonstrated a clear reduction in the interaction signal between LEDGF/p75 and HIV-2 integrase in silenced cells compared to unsilenced controls at 6 hours post-transduction **(Figure 29).**

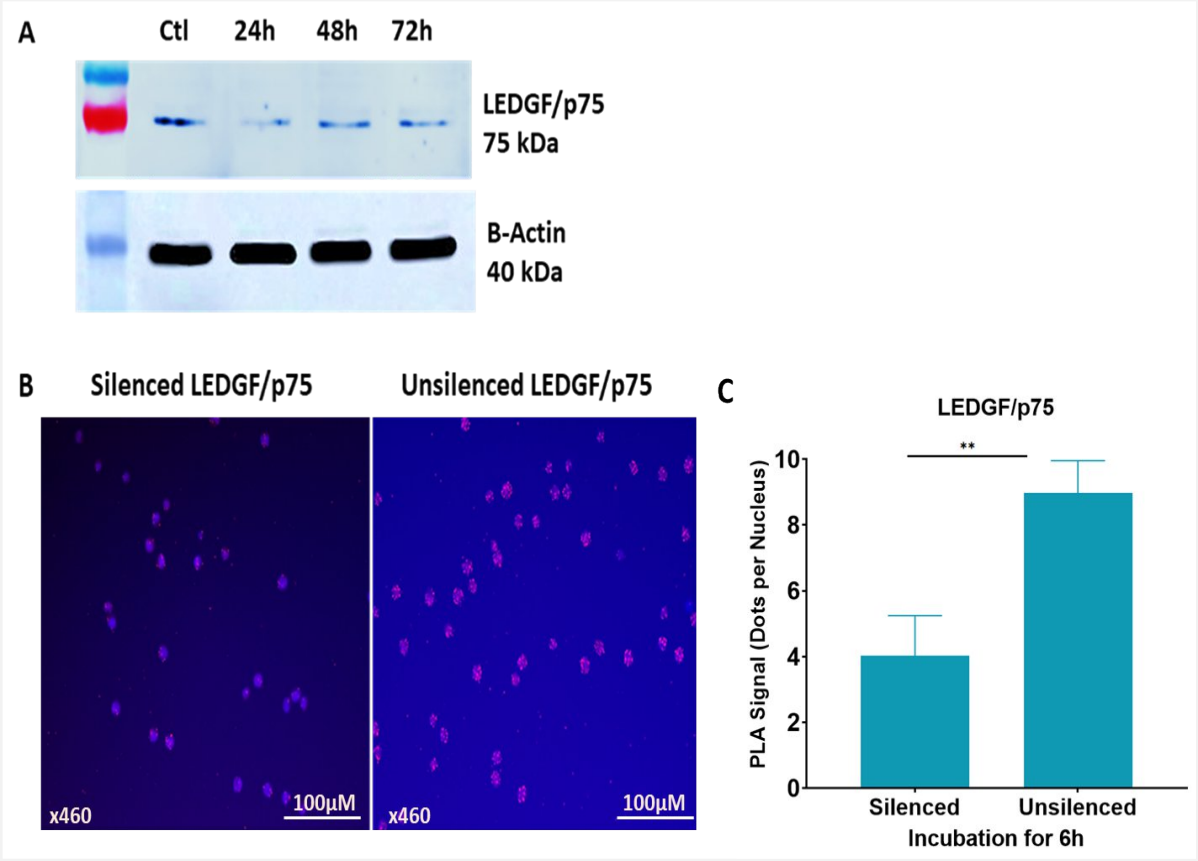

Figure 29: Results of the LEDGF/p75 silencing in Jurkat cells

A: Western blot showing results of silencing following incubation for 1-3 days. Jurkat cells silenced through transfection with 1.5 µg of PSIP1 siRNA in appropriate lipofectamine RNAiMAX as per manufacturers guidelines. β actin was used for normalization. Results are obtained from a single representative experiment.

B: Representative images showing DAPI-stained nucleus (blue) and PLA signals (red dots) as seen under fluorescence microscope showing reduced LEDGF/p75-IN interaction in

silenced versus unsilenced cells after 6hrs incubation. Images acquired at a magnification of x460 and a scale bar 100 μM.
C: A bar chart showing quantification of PLA signals between silenced versus unsilenced cells. The y axis is the mean +/-SEM (dots/nucleus) while x axis shows interaction of the proteins after transduction and incubation for 6 hours. Image is representative of a single measurement ** p value ≤ 0.01

To further investigate the effects of LEDGF/p75 silencing on integration, we transduced the silenced cells with HIV-2 pseudoviruses and measured the transduction efficiency after 48hrs of incubation using flow cytometry. There was no difference in the percentage of fluorescence between the silenced cells and the control **(Figure 30)**.

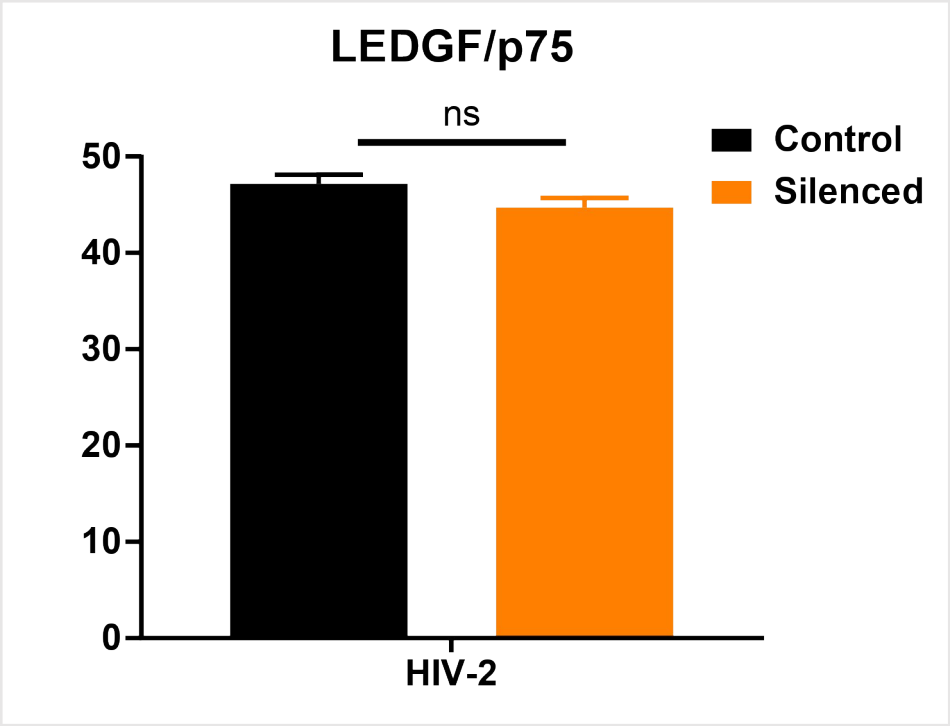

Figure 30: FACs analysis results of LEDGF/p75 silenced Jurkat cells (orange) transduced with HIV-2 pseudovirions relative to the control (black). The control represents unsilenced Jurkat cells transduced with HIV-2 pseudoviruses. Measurements were done in triplicates- ns; p > 0.05

6.4 Confirmation of HIV-1 and HIV-2 LTRs from the transduced cells

Successful viral transduction and integration were confirmed by PCR amplification of the HIV-1 and HIV-2 LTR regions from genomic DNA of transduced cells. Gel electrophoresis revealed bands corresponding to the expected sizes: approximately 640 bp for HIV-1 LTR and 850 bp for HIV-2 LTR **(Figure 31).**

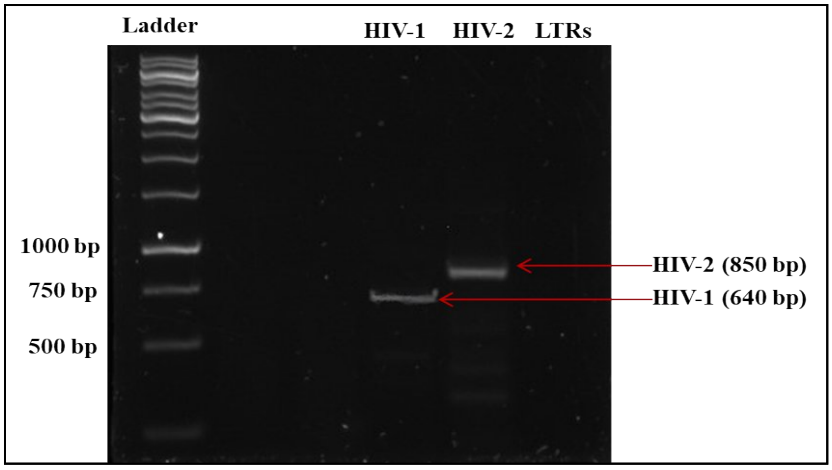

Figure 31: Gel electrophoresis image after PCR amplification of HIV-1 and HIV-2 LTRs from transduced Jurkat cells. The LTRs sizes were estimated at 850 and 640 base pairs for HIV-2 and HIV-1 respectively. Results are obtained from a single representative experiment.

6.5 Integration sites analysis

Following transduction of Jurkat cells with pseudoviruses, we compared HIV-1 and HIV-2 integration sites after genomic DNA sequencing. From our results, a higher proportion of integration occurred in the introns and intergenic regions in the case of both HIV-1 and HIV-2. However, HIV-1 showed a higher frequency of integration within the exons compared to HIV-2 **(Figure 32A).** Chromosomal distribution analysis showed that both viruses integrated broadly across all 23 human chromosomes but exhibited distinct preferences. HIV-1 favoured integration in chromosomes 15, 14, 6, and 12, while HIV-2 preferred chromosomes 13, 20, chromosome Y and 17 with an average distribution of approximately 70% across these favoured chromosomes **(Figure 32B)**.

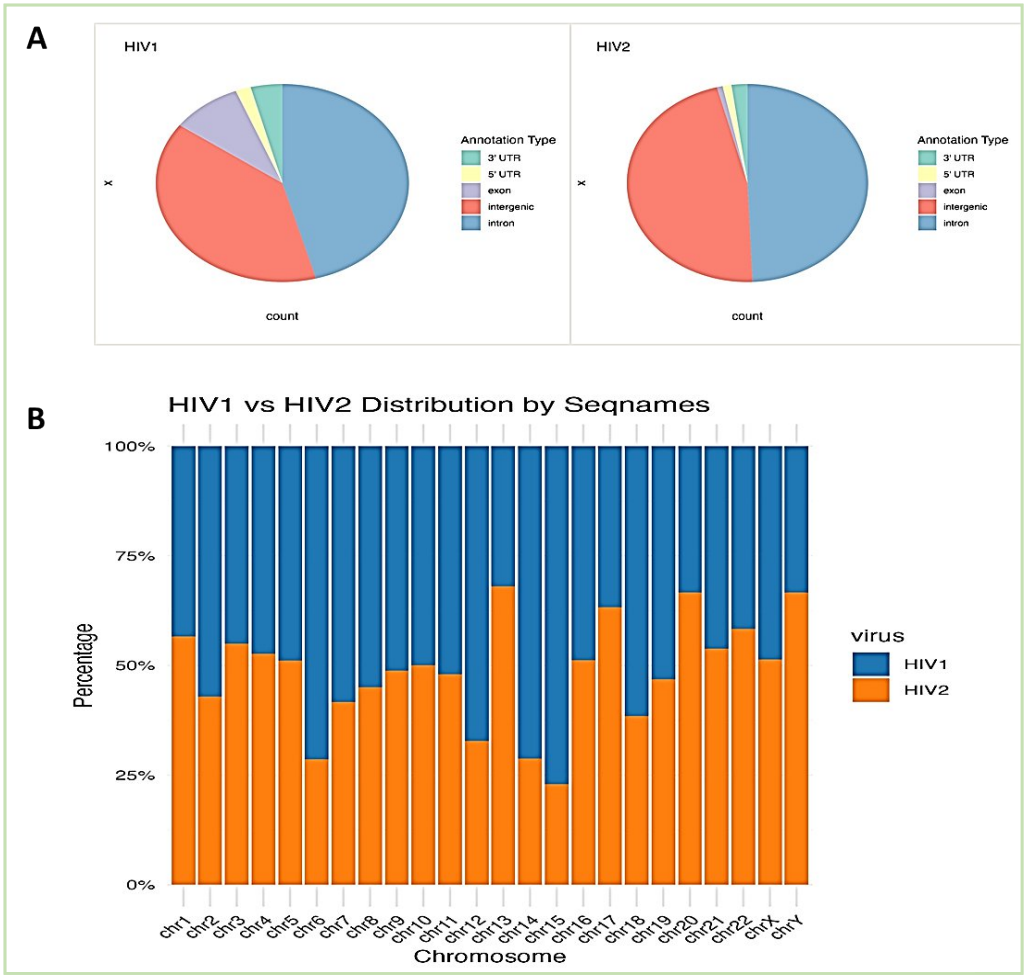

Figure 32: Distribution of HIV-1 and HIV-2 integration sites in Jurkat cells transduced with HIV-2 pseudoviruses at a MOI of 1. Results are representative of a single measurement.
A: Distribution of integration sites within genomic features (intronic, intergenic, exonic regions)
B: Percentage distribution of integration sites per chromosome with HIV-1 represented in blue and HIV-2 in orange.

To investigate the relationship between viral integration and chromatin accessibility, ATAC-seq signal intensity was mapped relative to the integration sites of HIV-1 and HIV-2. Comparative analysis revealed marked differences in both signal intensity and distribution patterns between the two viruses. For HIV-1, the average ATAC-seq signal showed a sharp peak at the integration start site correlating with a high intensity signal on the heat map with values reaching up to a maximum scale of 250. A strong signal depicted in white and red hues, was observed immediately at the insertion start point of the target regions **(Figure 33, left panel).**

In contrast, HIV-2 integration sites showed a different chromatin landscape. The heat map showed a weaker, more diffuse ATAC-seq signal dominated by blue and light blue shades. The

peak signal intensity reached only up to a maximum value of 40. The average plot for HIV-2 was relatively undefined and lacked a pronounced peak demonstrating less accessible chromatin or integration in more random regions**(Figure 33, right panel).**.

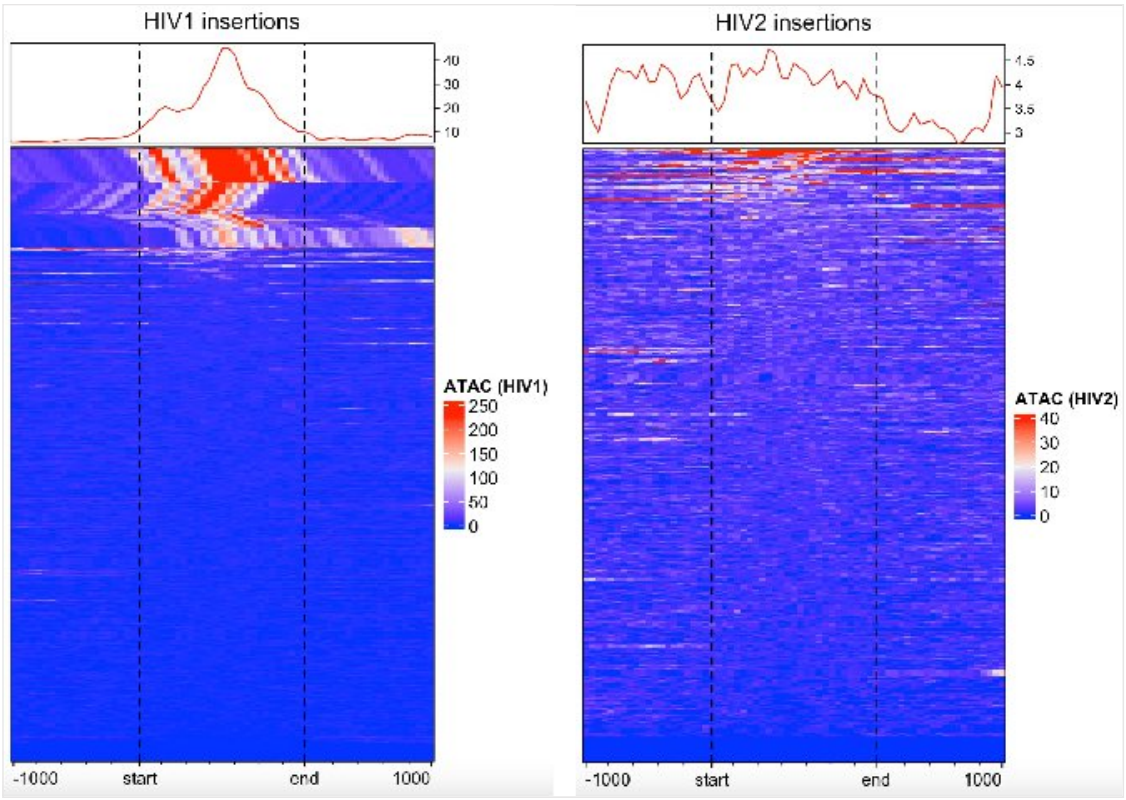

Figure 33: ATAC-seq profiles of HIV-1 and HIV-2 integration sites relative to chromatin accessibility. (Top): Line graph showing average ATAC-seq signal at the insertion sites. (Bottom): Heat map showing ATAC-seq signal intensity across individual insertion sites. Color scale represents chromatin accessibility with red/white showing high accessibility and blue indicating low accessibility. x-axis shows distance in base pairs from the insertion sites, y-axis shows the scale representing maximum and minimum signal intensity based on the number of insertion sites

7. DISCUSSION

7.1 Inhibition profiling of INSTIs and lenacapavir against HIV-2

To study the efficacy of INSTIs *in vitro,* we expressed the HIV-2 integrase in *Escherichia coli* bacteria and purified the enzyme by affinity chromatograph. We quantitatively measured the activity of the enzyme in the presence of serial dilutions of the inhibitors utilizing non-radioactive synthetic oligonucleotides substrates. The inhibitors were not effective against HIV-2 integrase enzyme even at high concentrations of 10 μM despite showing efficacy against HIV-1 under identical conditions. This observation suggested that probably HIV-2 integrase possess structural or conformational features that reduced inhibitor binding

efficiency in a purified system. Additionally, we hypothesized that the substrate (designed for HIV-1 integrase) did not meet the maximum threshold required for the activity of HIV-2 integrase, and further troubleshooting was hindered by the lack of research resources designed specifically for HIV-2. Nevertheless, HIV-2 integrase showed a good catalytic activity in control reactions confirming the functionality of the enzyme preparation, although the activity was lower compared to that of HIV-1 integrase. Studies have shown that the purified integrase is less soluble in solution; it's very hydrophobic and prone to precipitation reducing the activity of the enzyme (Oh & Shin, 1996). In addition, activity is influenced by both substrate and target oligonucleotide sequences affecting the 3' processing and strand transfer activity of integrase (Ad et al., 1992), which could affect the outcome.

In contrast to the *in vitro* findings, all the tested INSTIs exhibited potent antiviral activity against the HIV-2 ROD strain in cellular assays, achieving low nanomolar IC_{50} values. INSTIs are favourable key components of the first-line treatment of HIV-1 because of their efficacy and tolerability. They have shown excellent efficacy in treatment-naive patients as documented in clinical studies, however, their success rate with ART-experienced patients varies (Engelman, 2019).

With an IC_{50} value of 2.1 (±0.1) nM, raltegravir inhibited HIV-2 in our investigation, which was comparable to a prior study on HIV-2 ROD clinical isolates (Cook et al., 2020). Four clinical isolates were inhibited by raltegravir with an IC_{50} of 2.4 nM in a phenotypic study of INSTIs naive patients (Indu et al., 2020). Raltegravir was demonstrated in clinical trials to be effective in lowering the viral load in patients infected with HIV-2; however, the resistance mutations N155H and Q148R rapidly surfaced (Hicks & Gulick, 2009). Elvitegravir demonstrated efficacy as well, with an IC_{50} of 2.1 (±0.1) nM that was similar to earlier studies performed using clinical isolates. Elvitegravir's effectiveness was reported by Roquebert et al. at 0.7 nM. Elvitegravir demonstrated efficacy in vitro when combined with the NRTIs emtricitabine and tenofovir, with an EC_{50} of 1.6 nM (Roquebert et al., 2009).

Nine clinical isolates from integrase-naive patients showed an EC_{50} of 0.8 nM, which is comparable to our IC_{50} of 0.9 (±0.4) nM for dolutegravir; a well-established integrase inhibitor in treatment-naive patients. Dolutegravir's IC_{50} range in a single cycle cell assay was 1.3–2.6 nM (Kandel & Walmsley, 2015). The efficacy of more recent inhibitors, including bictegravir and cabotegravir, against HIV-2 is not well described. In comparison to other INSTIs,

bictegravir was shown to have a low rate of resistance to the development of mutations, and was effective against HIV-1. In a single spreading cycle assay in cell culture, bictegravir had an EC_{50} ranging from 1.4 to 5.6 nM against 15 clinical isolates (Tsiang et al., 2016) comparable to our study with an IC_{50} of 1.8 (±0.08) nM. Cabotegravir has also shown efficacy in inhibiting HIV-2 *in vitro* with a low EC_{50} of 1.8–2.6 nM (Whitfield et al., 2016). It demonstrated efficacy against HIV-2 ROD-based pseudovirions in our investigation, with an IC_{50} of 2 (±0.1) nM.

As far as we are aware, no prior research has systematically assessed the effectiveness of all currently available INSTIs against HIV-2 integrase. The strength of our study lies in its consistent approach—evaluating the inhibitors using the same ROD-based integrase sequence within a standardized cell culture system, thereby minimizing variability and eliminating potential interference from other compounds.

Furthermore, we assessed the efficacy of INSTIs raltegravir, dolutegravir, and cabotegravir against the activity of SARS-CoV-2, and found that the inhibitors were unable to significantly inhibit the three variants; wuhan-1(GHB), B.1.1.7 or omicron BA.2. An urgent search for effective treatments was prompted by the global crisis caused by the SARS-CoV-2 pandemic in 2019. With differing results, several studies have investigated the repurposing of HIV antiretroviral medications such as protease inhibitors and INSTIs to fight different SARS-CoV-2 variants (Dittmar et al., 2021).

In one *in vitro* and *in silico* study, Vero E6 cells infected with the D614G variant from a Colombian isolate were treated with six antiretroviral medications, including raltegravir. Raltegravir exhibited the highest binding energies in the *in silico* analysis and showed inhibitory effects at concentrations between 6.3 and 25 μM (Zapata-Cardona et al., 2023). However, INSTIs and tenofovir did not significantly affect the acquisition or outcomes of SARS-CoV-2 infection, according to an *in vivo* study conducted on a Dutch cohort of people living with HIV (Dittmar et al., 2021). Drugs like dolutegravir, raltegravir, and bictegravir demonstrated moderate antiviral effects *in vitro* using cell lines like Vero E6, HEK293T, and Calu-3, with dose-dependent inhibition of viral replication. However, due to potential differences in the replication mechanisms of SARS-CoV-2 and HIV, these medications were not strong enough to completely stop viral replication (Sang et al., 2020).

The capsid inhibitor lenacapavir also demonstrated potent activity against HIV-2, achieving picomolar IC_{50} values of 206.2 (±0.2) that were superior to those observed against HIV-1 at

399.3 (±0.2). Earlier studies have demonstrated EC_{50} values ranging from 50–314 pM in HIV-1 infected cell cultures (Bester et al., 2020), with specific activities of 105 pM in MT-4 cells, 56 pM in macrophages and 32 pM in primary $CD4^+$ T cells. In primary human peripheral blood mononuclear cells, lenacapavir maintained activity across clinical HIV-1 isolates with EC_{50} values between 20–160 pM. Notably, only one study indicated its activity against two HIV-2 isolates (Link et al., 2020). Mechanistically, lenacapavir disrupts capsid-capsid interactions by binding at the interface of adjacent hexamers, resulting in the generation of structurally defective virions (Di Perri et al., 2019). Our functional assay experiment indicated that while the reverse transcriptase activity of the pseudovirions remained unaffected by lenacapavir treatment during virus production, transduction efficiency was significantly impaired.

Molecular docking simulations supported the experimental findings by demonstrating favourable binding of bictegravir, cabotegravir, and dolutegravir within the HIV-2 integrase active site, providing insights into their binding interactions with the enzyme. Structural evaluations of our model showed that Mg2+ ions binding to the active site was nearly covalent as described (Buffone et al., 2018) and consistent with effective strand transfer inhibition. Furthermore, lenacapavir exhibited favorable docking to the HIV-2 capsid model (p26), displaying similar binding characteristics to those observed in the HIV-1 capsid crystal structure.

7.2 Transcriptomic changes induced by Vpx

To examine Vpx's broader impact, we analysed proteo-transcriptomic changes induced by Vpx in THP-1 cells transfected with GFP-tagged wild-type and functionally restricted Vpx, followed by next-generation sequencing. Our data showed that vpx altered the expression of hundreds of genes coding for zinc finger proteins, helicases, transcription factors, chaperons, and DNA methylation proteins. The genes significantly upregulated by the wild-type Vpx included the protocadherin gamma subfamily C4 (PCDHGC4), caspase 3 (CASP3), NOP58 ribonucleoprotein (NOP58), and sorting nexin 14 (SNX14) while down regulating expression of SKI family transcriptional co-repressor 2 (SKOR2), CORO7-PAM16 readthrough (CORO7-PAM16) and U2 small nuclear RNA auxiliary factor 1 (U2AF1). In HIV replication, several host genes play distinct roles by either facilitating or dampening viral processes in response to infections.

PCDHGC4, a member of the protocadherin gamma family, is a cell adhesion molecule involved in maintaining cellular integrity and signalling. While studies specifically addressing PCDHGC4 in HIV replication are limited, the protocadherin family has been linked to cell-cell interactions that may aid viral spread by allowing HIV to traverse cellular junctions and establish infection (Pancho

et al., 2020). Protocadherins are associated with pathways such as PYK2 and FAK tyrosine kinases, as well as mTOR signalling, which could impact viral propagation (Shan et al., 2016).

CASP3, a central player in apoptosis, significantly affects HIV replication and pathogenesis by triggering programmed cell death in infected CD4+ T cells, hastening immune deterioration (Garden et al., 2002). HIV accessory proteins Vpr and Vpu are known to interact with CASP3, with Vpr halting cells at various stages of the cell cycle and Vpu enhancing CASP3 expression and activation, which also contributes to the inhibition of NF-κB (Vermeire et al., 2016). There was an upregulation of CASP3 in Vpx-transfected cells in our study after 16 hrs of incubation; however, qPCR validation experiment for CASP3 gave conflicting results whereby CASP3 was significantly down regulated after 48 hrs incubation following transduction with HIV-2 isolate 1654 in comparison to HIV-1. When we further measured the activity of CASP3 in Vpx-transfected cell lysate using a colorimetric substrate, it was significantly upregulated. From literature, variations observed between qPCR and transcriptomic results may arise due to both technical and biological differences specific to each approach. RNA-seq and similar transcriptomic techniques are highly sensitive and capable of detecting widespread gene expression changes, including subtle decreases in expression. In contrast, qPCR has more limited sensitivity and may fail to detect minor changes, particularly for genes with low baseline expression(Eskandari & Eaves, 2022). We hypothesized that the CASP3 down regulation detected by qPCR after two days could have been a delayed cellular compensatory response for the earlier upregulation.

SKOR2, a transcriptional repressor within the SKI family, plays a role in gene regulation and cellular differentiation by interacting with other regulatory proteins to inhibit gene expression (Tecalco-Cruz et al., 2018). Although the impact of SKOR2 on HIV replication is not yet fully understood, its reduced expression may alter cellular transcriptional responses to HIV. In particular, SKOR2 acts as a significant inhibitor in the TGF-β1/Smad signalling pathway, a regulatory axis whose disturbance can affect TGF-β1 levels, influencing cell function and disease progression. Research has connected this pathway to HIV-1 infection, showing increased TGF-β expression in HIV-infected monocytes (Chinnapaiyan et al., 2019). Additionally, in SIV-infected rhesus macaques, the TGF-β pathway influences SMAD2 and SMAD3 activation while down regulating SMAD7 (Boby et al., 2021).

In this study, we posited that Vpx-induced down regulation of SKOR2 may activate TGF-β signalling by facilitating SMAD2/3 and SMAD4 interactions. The degradation of SKOR2 and

related proteins has been shown to increase TGF-β1 expression and increasing levels of TGF-β cytokine (Wang et al., 2001). There was an upregulation of TGF-β signalling factors, including SMAD4 and TGF-βR1 in our differential gene expression analysis. TGF-β1 overexpression is linked to enhanced HIV pathogenesis, latency, apoptosis induction, and suppression of innate immunity (Yim et al., 2023). TGF-β1 may further drive apoptosis through upregulation of apoptosis-related proteins like CASP3 (Akari et al., 2001). Indeed, our cytokine analysis showed elevated TGF-β in the medium of Vpx-transfected cells compared to controls, supporting our hypothesis.

Vpx increased the levels of pro-inflammatory cytokines IL-6, IL-1, and TNF-α in the medium of transfected cells, additionally, elevated levels of TGF-β1 was observed, which parallels findings in SIV and HIV-2 infections and supports Vpx's role in modulating the immune response (Appay & Sauce, 2008). Inflammatory cytokines have been linked to tissue damage in people living with HIV. Although HIV-2 Vpr, is known to enhance type I IFN signalling in human dendritic cells, we found no evidence of Vpx affecting type I IFN secretion in our experimental model (Fujita et al., 2010). Moreover, in our quantitative PCR analysis, the expression of SKOR2 gene in cells transfected with Vpx or transduced with HIV-2 did not show significant alteration compared to the control.

U2AF1, a vital component in pre-mRNA splicing, is crucial for recognizing 3' splice sites and supporting spliceosome assembly. Efficient splicing of HIV RNA is necessary for producing the array of viral proteins required for replication and infection (Sertznig et al., 2018). Reduced U2AF1 expression may hinder splicing efficiency, potentially lowering functional HIV protein levels. This reduction could decelerate viral replication, as HIV depends on precise and diverse splicing to create the transcripts essential for its life cycle (Dlamini & Hull, 2017).

During replication, alternative splicing by HIV produces early regulatory proteins like Tat and Rev from fully spliced transcripts. Binding of U2AF factors to the 3'A3 splice site, where Tat is generated, stabilizes splicing of HIV's weak polypyrimidine tract (Yukl et al., 2018). Enhanced mutations in this region were shown to drastically reduce Tat mRNA and, subsequently, dampening viral replication in infected cells (Ponti et al., 2008). Additionally, complex splicing is involved in HIV-1 latency and transcriptional regulation in infected CD4+ T cells, with latency often linked to limited levels of transcription factors (Sertznig et al., 2018).

In our analysis of differential gene expression, we observed Vpx-induced down regulation of U2AF1. We hypothesized that reduced U2AF1 levels might impact Tat protein expression. Indeed, Western blot analysis in HEK-293T cells indicated lower Tat expression in the presence of Vpx. Further real-time qPCR validation confirmed the down regulation of U2AF1 in Vpx-transfected and transduced cells, aligning with our hypothesis linking U2AF1 to the down regulation of HIV-1 tat.

Alteration of essential cellular transcription factors, like NF-κB, and insufficient levels of Tat protein have been linked to the latency of HIV (Fink et al., 2022). Additionally, in our study, Vpx downregulated MYD88; an adaptor protein in innate immune signalling that activates NF-κB (Deguine & Barton, 2014). This down-regulation could potentially reduce proviral transcription, encouraging latency, though further research is necessary to confirm this effect and elucidate the exact pathways involved.

7.3 Interaction between HIV-2 IN and LEDGF/p75, and preliminary analysis of integration sites preference

Integration site selection by HIV-1 is well known to be influenced by the host LEDGF/p75; however, its role in HIV-2 integration remains less clearly defined. To explore this, we utilized a duolink proximity ligation assay to investigate the potential interaction between LEDGF/p75 and HIV-2 integrase. Our findings revealed a specific and temporally regulated interaction between the two proteins, with the strongest PLA signal (indicating interaction) detected approximately six hours post-transduction. This was earlier than anticipated, given that reverse transcription is typically thought to initiate around five hours after viral entry (Murray et al., 2011). Interestingly, this early detection may support emerging evidence for intra-nuclear uncoating and reverse transcription of the HIV-1 genome (Burdick et al., 2020), a mechanism that could be conserved in HIV-2.

Silencing LEDGF/p75 via RNA interference 24 hours prior to infection resulted in a significant decrease in the PLA signal, indicating a diminished interaction between LEDGF/p75 and HIV-2 integrase. Notably, transduction efficiency remained unaffected by LEDGF/p75 silencing, suggesting that alternative host cofactors may compensate for its absence during integration. These findings highlight a possible divergence in host factor utilization between HIV-1 and HIV-2, warranting further investigation into the cellular determinants of HIV-2 integration. To further investigate the mechanistic role of LEDGF/p75 in HIV-2 integration, we are conducting follow-up

experiments in which cells are transduced after LEDGF/p75 silencing, followed by genome-wide integration site mapping using high-throughput sequencing.

To investigate the integration site preferences of HIV-1 and HIV-2, we transduced Jurkat cells with pseudoviruses of both strains and performed high-throughput genomic sequencing of the isolated DNA. Our results indicate that both HIV-1 and HIV-2 predominantly integrate into intronic regions of actively transcribed genes, consistent with their reliance on host factors such as LEDGF/p75. HIV-1 showed a slightly higher frequency of integration into exonic regions compared to HIV-2, though intronic integration remained dominant for both viruses.

The integration patterns of HIV-1 and HIV-2 showed some differences in their distribution across chromosomes. HIV-1 exhibited integration hotspots in gene-dense regions, including chromosomes 6, 12, 14, and 15, which harbor genes involved in immune regulation, cell signaling, and T-cell function. For example, chromosome 6 contains the Human Leukocyte Antigen (HLA) locus, which is critical for immune responses. HIV-2 integration sites were similarly biased toward active genes but showed less pronounced clustering in these chromosomes, preferentially integrating into chromosomes 13, 20 and the Y chromosome, suggesting potential differences in integration preferences that warrant further investigation.

Analysis of ATAC-seq profiles showed distinct patterns of chromatin accessibility at HIV-1 and HIV-2 integration sites. HIV-1 insertions were strongly associated with regions of high chromatin openness, as shown by a sharp peak in average ATAC-seq signal and concentrated high-intensity regions on the heat map. In contrast, HIV-2 insertions occurred in areas with lower chromatin accessibility, displaying a diffuse and flatter ATAC-seq signal distribution with no defined peak suggesting a broader and less selective integration pattern.

Further analysis is ongoing on the integration of HIV-1 and HIV-2 within the repetitive sequences such as the short interspersed elements (SINEs) with the prominent Alu repeats and the long-terminal interspersed elements (LINEs). From other studies, HIV-1 demonstrates a strong bias toward gene-dense, transcriptionally active regions, with a moderate enrichment in SINEs—particularly Alu elements—which are often located near promoters and regulatory regions of actively transcribed genes (Schröder et al., 2002). This preference is largely mediated by host factors such as LEDGF/p75 which guide the integration machinery toward euchromatic regions (Christ et al., 2012). Conversely, HIV-2 exhibits a broader and more

flexible integration profile, with comparatively reduced enrichment in Alu repeats and a slightly higher tolerance for integration into LINE elements (Delelis et al., 2010).

8. CONCLUSION

To our knowledge, no prior study has comprehensively investigated the efficacy of all currently available INSTIs against HIV-2 integrase. Our analysis presents a distinct advantage by testing these inhibitors against a consistent ROD-based integrase sequence, using a standardized cell culture methodology free from interference by host factors or other drugs. While limited data exist on the efficacy of cabotegravir and bictegravir against HIV-2, and given that lenacapavir has been tested against only two isolates, our study provides broader insights on the potency of these inhibitors against HIV-2. Further studies exploring the mechanistic basis for the in vitro resistance of HIV-2 integrase are warranted. Additionally, we confirmed experimentally that raltegravir, despite earlier in silico predictions, did not exhibit meaningful antiviral activity against SARS-CoV-2. These findings underscore the critical role of in vitro and cell culture-based assays in validating in silico results.

Our transcriptomic analysis of HIV-2 Vpx-transfected cells highlights the extensive impact of this accessory protein on multiple pathways. Analysis of GO terms revealed a wide range of cellular processes influenced by Vpx, including inhibition of viral processes, assembly of spliceosomal snRNPs, activation of type I interferon signalling, regulation of RNA polymerase II transcription elongation, suppression of innate immune responses, enhancement of interferon-beta production, and promotion of DNA-templated transcription elongation. Vpx was also shown to influence cytokine profiles by increasing key pro-inflammatory cytokines. Notably, HIV-2 Vpx appears to enhance the TGF-β1/SMAD signalling pathway, likely through the down regulation of SKOR2. Additionally, our findings suggest that Vpx down regulates HIV-1 Tat, a factor warranting further study due to its potential role in viral latency. Overall, we provide valuable insights into how HIV-2 Vpx manipulates the cellular environment to facilitate infection.

Our findings also show the distinct integration site preferences and chromatin accessibility profiles of HIV-1 and HIV-2 viruses, as well as the interaction of LEDGF/p75 with HIV-2 integrase suggesting its potential function in influencing integration site selection. These differences may be linked to the distinct replication dynamics of the two viruses and warrant further investigation in future studies.

9. SUMMARY

This PhD research investigated key aspects of HIV-2 biology, focusing on integration events, drug susceptibility, and the functional roles of the Vpx protein. The primary aims were to evaluate the susceptibility of HIV-2 to lenacapavir and integrase strand transfer inhibitors (INSTIs), explore the transcriptomic effects of Vpx, and characterize HIV-2 integration patterns and interaction with the LEDGF/p75 host factor.

The study utilized a multifaceted methodological approach. In vitro assays were conducted using purified HIV-2 integrase to assess inhibitor efficacy, while cell-based assays using pseudoviruses determined antiviral activity. Transcriptomic changes induced by wild-type and mutant Vpx were analysed through RNA sequencing and gene ontology analysis in THP-1 cells. Cytokine profiling and Western blotting were employed to investigate Vpx's effects on HIV-1 Tat expression and host immune responses. Integration site mapping was performed using next-generation sequencing of pseudovirus-transduced Jurkat cells, complemented by ATAC-seq analysis to assess chromatin accessibility. LEDGF/p75-IN interaction was evaluated via proximity ligation assay and silencing experiments.

Key findings include the observation that INSTIs exhibited potent antiviral effects against HIV-2 in cell culture despite a lack of inhibition in in vitro enzyme assays, suggesting a complex interaction influenced by host cell context. Lenacapavir also showed efficacy against HIV-2 in culture. Vpx was found to modulate host gene expression, enhance pro-inflammatory cytokine production, and suppress HIV-1 Tat expression, likely through down regulation of U2AF1. Integration analysis revealed that HIV-2 preferentially integrated into intronic and intergenic regions, with a broader chromosomal distribution and weaker association with open chromatin compared to HIV-1. The interaction between HIV-2 integrase and LEDGF/p75 was confirmed, implicating its role in HIV-2 integration targeting.

In conclusion, the study expands our understanding of HIV-2 integration and drug susceptibility. It highlights possible interactions between HIV-2 integrase and host factors, underscores the potential of lenacapavir and INSTIs in HIV-2 treatment, and unveils novel functions of Vpx in viral regulation and immune modulation. These findings contribute valuable insights for therapeutic strategies targeting HIV-2 and inform future research into viral latency and integration dynamics.

10. KEYWORDS

HIV-2, Inhibition profiling, INSTIs, lenacapavir, Vpx, transcriptomic changes, gene expression, integrase, integration, LEDGF/p75

11. REFERENCES

Ad, L., Rb, R., & He, V. (1992). Both substrate and target oligonucleotide sequences affect in vitro integration mediated by human immunodeficiency virus type 1 integrase protein produced in Saccharomyces cerevisiae. *Journal of Virology*, *66*(4). https://doi.org/10.1128/JVI.66.4.2359-2368.1992

Ahmed, S., Mahtarin, R., Ahmed, S. S., Akter, S., Islam, Md. S., Mamun, A. A., Islam, R., Hossain, M. N., Ali, M. A., Sultana, M. U. C., Parves, MD. R., Ullah, M. O., & Halim, M. A. (n.d.). Investigating the binding affinity, interaction, and structure-activity-relationship of 76 prescription antiviral drugs targeting RdRp and Mpro of SARS-CoV-2. *Journal of Biomolecular Structure & Dynamics*, 1–16. https://doi.org/10.1080/07391102.2020.1796804

Akari, H., Bour, S., Kao, S., Adachi, A., & Strebel, K. (2001). The Human Immunodeficiency Virus Type 1 Accessory Protein Vpu Induces Apoptosis by Suppressing the Nuclear Factor κB–dependent Expression of Antiapoptotic Factors. *The Journal of Experimental Medicine*, *194*(9), 1299–1312. https://doi.org/10.1084/jem.194.9.1299

Aknin, C., Smith, E. A., Marchand, C., Andreola, M.-L., Pommier, Y., & Metifiot, M. (2019). Discovery of Novel Integrase Inhibitors Acting outside the Active Site Through High-Throughput Screening. *Molecules*, *24*(20), Article 20. https://doi.org/10.3390/molecules24203675

Anstett, K., Brenner, B., Mesplede, T., & Wainberg, M. A. (2017). HIV drug resistance against strand transfer integrase inhibitors. *Retrovirology*, *14*(1), 36. https://doi.org/10.1186/s12977-017-0360-7

Appay, V., & Sauce, D. (2008). Immune activation and inflammation in HIV-1 infection: Causes and consequences. *The Journal of Pathology*, *214*(2), 231–241. https://doi.org/10.1002/path.2276

Arias, J. F., Heyer, L. N., von Bredow, B., Weisgrau, K. L., Moldt, B., Burton, D. R., Rakasz, E. G., & Evans, D. T. (2014). Tetherin antagonism by Vpu protects HIV-infected cells from antibody-dependent cell-mediated cytotoxicity. *Proceedings of the National*

Academy of Sciences of the United States of America, *111*(17), 6425–6430. https://doi.org/10.1073/pnas.1321507111

Arts, E. J., & Hazuda, D. J. (2012). HIV-1 Antiretroviral Drug Therapy. *Cold Spring Harbor Perspectives in Medicine*, *2*(4), a007161. https://doi.org/10.1101/cshperspect.a007161

Barin, F., Cazein, F., Lot, F., Pillonel, J., Brunet, S., Thierry, D., Damond, F., Brun-Vézinet, F., Desenclos, J.-C., & Semaille, C. (2007). Prevalence of HIV-2 and HIV-1 group O infections among new HIV diagnoses in France: 2003–2006. *AIDS*, *21*(17), 2351. https://doi.org/10.1097/QAD.0b013e3282f15637

Bártolo, I., Moranguinho, I., Gonçalves, P., Diniz, A. R., Borrego, P., Martin, F., Figueiredo, I., Gomes, P., Gonçalves, F., Alves, A. J. S., Alves, N., Caixas, U., Pinto, I. V., Barahona, I., Pinho e Melo, T. M. V. D., & Taveira, N. (2022). High Instantaneous Inhibitory Potential of Bictegravir and the New Spiro-β-Lactam BSS-730A for HIV-2 Isolates from RAL-Naïve and RAL-Failing Patients. *International Journal of Molecular Sciences*, *23*(22), 14300. https://doi.org/10.3390/ijms232214300

Belshan, M., & Ratner, L. (2003). Identification of the nuclear localization signal of human immunodeficiency virus type 2 Vpx. *Virology*, *311*(1), 7–15. https://doi.org/10.1016/S0042-6822(03)00093-X

Berger, A., Münk, C., Schweizer, M., Cichutek, K., Schüle, S., & Flory, E. (2010). Interaction of Vpx and Apolipoprotein B mRNA-editing Catalytic Polypeptide 3 Family Member A (APOBEC3A) Correlates with Efficient Lentivirus Infection of Monocytes. *The Journal of Biological Chemistry*, *285*(16), 12248–12254. https://doi.org/10.1074/jbc.M109.090977

Bester, S., Wei, G., Zhao, H., Adu-Ampratwum, D., Iqbal, N., Courouble, V. V., Francis, A. C., Annamalai, A. S., Singh, P. K., Shkriabai, N., Van Blerkom, P., Morrison, J., Poeschla, E. M., Engelman, A. N., Melikyan, G. B., Griffin, P. R., Fuchs, J. R., Asturias, F., & Kvaratskhelia, M. (2020). Structural and mechanistic bases for a potent HIV-1 capsid inhibitor. *Science (New York, N.Y.)*, *370*(6514), 360–364. https://doi.org/10.1126/science.abb4808

Blair, W. S., Pickford, C., Irving, S. L., Brown, D. G., Anderson, M., Bazin, R., Cao, J., Ciaramella, G., Isaacson, J., Jackson, L., Hunt, R., Kjerrstrom, A., Nieman, J. A., Patick, A. K., Perros, M., Scott, A. D., Whitby, K., Wu, H., & Butler, S. L. (2010). HIV capsid is a tractable target for small molecule therapeutic intervention. *PLoS Pathogens*, *6*(12), e1001220. https://doi.org/10.1371/journal.ppat.1001220

Blissenbach, M., Grewe, B., Hoffmann, B., Brandt, S., & Uberla, K. (2010). Nuclear RNA export and packaging functions of HIV-1 Rev revisited. *Journal of Virology*, *84*(13), 6598–6604. https://doi.org/10.1128/JVI.02264-09

Boby, N., Ransom, A., Pace, B. T., Williams, K. M., Mabee, C., Das, A., Srivastav, S. K., Porter, E., & Pahar, B. (2021). Enhanced Intestinal TGF-β/SMAD-Dependent Signaling in Simian Immunodeficiency Virus Infected Rhesus Macaques. *Cells*, *10*(4), 806. https://doi.org/10.3390/cells10040806

Bock, P. J., & Markovitz, D. M. (2001). Infection with HIV-2. *AIDS (London, England)*, *15 Suppl 5*, S35-45. https://doi.org/10.1097/00002030-200100005-00006

Bolger, A. M., Lohse, M., & Usadel, B. (2014). Trimmomatic: A flexible trimmer for Illumina sequence data. *Bioinformatics (Oxford, England)*, *30*(15), 2114–2120. https://doi.org/10.1093/bioinformatics/btu170

Bose, D. (2017). *Tat-independent lentivirus genomes for vaccination and host/pathogen interaction studies* [Phdthesis, Université Grenoble Alpes]. https://theses.hal.science/tel-01938074

Buffone, C., Martinez-Lopez, A., Fricke, T., Opp, S., Severgnini, M., Cifola, I., Petiti, L., Frabetti, S., Skorupka, K., Zadrozny, K. K., Ganser-Pornillos, B. K., Pornillos, O., Di Nunzio, F., & Diaz-Griffero, F. (2018). Nup153 Unlocks the Nuclear Pore Complex for HIV-1 Nuclear Translocation in Nondividing Cells. *Journal of Virology*, *92*(19), e00648-18. https://doi.org/10.1128/JVI.00648-18

Burdick, R. C., Li, C., Munshi, M., Rawson, J. M. O., Nagashima, K., Hu, W.-S., & Pathak, V. K. (2020). HIV-1 uncoats in the nucleus near sites of integration. *Proceedings of the National Academy of Sciences of the United States of America*, *117*(10), 5486–5493. https://doi.org/10.1073/pnas.1920631117

Campbell, E. M., & Hope, T. J. (2015a). HIV-1 Capsid: The Multifaceted Key Player in HIV-1 infection. *Nature Reviews. Microbiology*, *13*(8), Article 8. https://doi.org/10.1038/nrmicro3503

Campbell, E. M., & Hope, T. J. (2015b). HIV-1 Capsid: The Multifaceted Key Player in HIV-1 infection. *Nature Reviews. Microbiology*, *13*(8), 471–483. https://doi.org/10.1038/nrmicro3503

Campbell-Yesufu, O. T., & Gandhi, R. T. (2011). Update on Human Immunodeficiency Virus (HIV)-2 Infection. *Clinical Infectious Diseases*, *52*(6), 780–787. https://doi.org/10.1093/cid/ciq248

Cardoso, M., Vasconcelos, J., Baptista, T., Diogo, I., Gonçalves, F., Mansinho, K., & Gomes, P. (2021). Management of HIV-2 resistance to antiretroviral therapy in a HIV-1/HIV-2/HBV co-infected patient. *AIDS Research and Therapy*, *18*(1), 69. https://doi.org/10.1186/s12981-021-00394-4

Carvalho, A. C., Valadas, E., França, L., Carvalho, C., Aleixo, M. J., Mendez, J., Marques, R., Sarmento, A., Doroana, M., Antunes, F., Branco, T., Aguas, M., Sarmento E Castro, R., Lazarus, J. V., & Barros, H. (2012). Population mobility and the changing epidemics of HIV-2 in Portugal. *HIV Medicine*, *13*(4), 219–225. https://doi.org/10.1111/j.1468-1293.2011.00963.x

Ceccarelli, G., Giovanetti, M., Sagnelli, C., Ciccozzi, A., d'Ettorre, G., Angeletti, S., Borsetti, A., & Ciccozzi, M. (2021). Human Immunodeficiency Virus Type 2: The Neglected Threat. *Pathogens*, *10*(11), 1377. https://doi.org/10.3390/pathogens10111377

Chen, D., & Zhou, Q. (1999). Tat activates human immunodeficiency virus type 1 transcriptional elongation independent of TFIIH kinase. *Molecular and Cellular Biology*, *19*(4), 2863–2871. https://doi.org/10.1128/MCB.19.4.2863

Chinnapaiyan, S., Dutta, R. K., Nair, M., Chand, H. S., Rahman, I., & Unwalla, H. J. (2019). TGF-β1 increases viral burden and promotes HIV-1 latency in primary differentiated human bronchial epithelial cells. *Scientific Reports*, *9*(1), 12552. https://doi.org/10.1038/s41598-019-49056-6

Choi, E., Mallareddy, J. R., Lu, D., & Kolluru, S. (2018). Recent advances in the discovery of small-molecule inhibitors of HIV-1 integrase. *Future Science OA*, *4*(9), FSO338. https://doi.org/10.4155/fsoa-2018-0060

Chopra, P., Gupta, S., Dastidar, S. G., & Ray, A. (2009). Development of cell death-based method for the selectivity screening of caspase-1 inhibitors. *Cytotechnology*, *60*(1–3), 77. https://doi.org/10.1007/s10616-009-9217-9

Chougui, G., Munir-Matloob, S., Matkovic, R., Martin, M. M., Morel, M., Lahouassa, H., Leduc, M., Ramirez, B. C., Etienne, L., & Margottin-Goguet, F. (2018). HIV-2/SIV viral protein X counteracts HUSH repressor complex. *Nature Microbiology*, *3*(8), 891–897. https://doi.org/10.1038/s41564-018-0179-6

Christ, F., & Debyser, Z. (2013). The LEDGF/p75 integrase interaction, a novel target for anti-HIV therapy. *Virology*, *435*(1), 102–109. https://doi.org/10.1016/j.virol.2012.09.033

Christ, F., Shaw, S., Demeulemeester, J., Desimmie, B. A., Marchand, A., Butler, S., Smets, W., Chaltin, P., Westby, M., Debyser, Z., & Pickford, C. (2012). Small-Molecule

Inhibitors of the LEDGF/p75 Binding Site of Integrase Block HIV Replication and Modulate Integrase Multimerization. *Antimicrobial Agents and Chemotherapy*, *56*(8), 4365–4374. https://doi.org/10.1128/AAC.00717-12

Ciuffi, A., Llano, M., Poeschla, E., Hoffmann, C., Leipzig, J., Shinn, P., Ecker, J. R., & Bushman, F. (2005). A role for LEDGF/p75 in targeting HIV DNA integration. *Nature Medicine*, *11*(12), 1287–1289. https://doi.org/10.1038/nm1329

Clavel, F., Guyader, M., Guétard, D., Sallé, M., Montagnier, L., & Alizon, M. (1986). Molecular cloning and polymorphism of the human immune deficiency virus type 2. *Nature*, *324*(6098), 691–695. https://doi.org/10.1038/324691a0

Coffin, J. M., Hughes, S. H., & Varmus, H. E. (Eds.). (1997). *Retroviruses*. Cold Spring Harbor Laboratory Press. http://www.ncbi.nlm.nih.gov/books/NBK19376/

Cook, N. J., Li, W., Berta, D., Badaoui, M., Ballandras-Colas, A., Nans, A., Kotecha, A., Rosta, E., Engelman, A. N., & Cherepanov, P. (2020). Structural basis of second-generation HIV integrase inhibitor action and viral resistance. *Science*, *367*(6479), 806–810. https://doi.org/10.1126/science.aay4919

Craigie, R. (2012). The molecular biology of HIV integrase. *Future Virology*, *7*(7), 679–686. https://doi.org/10.2217/FVL.12.56

Das, K., Martinez, S. E., & Arnold, E. (2017). Structural Insights into HIV Reverse Transcriptase Mutations Q151M and Q151M Complex That Confer Multinucleoside Drug Resistance. *Antimicrobial Agents and Chemotherapy*, *61*(6), e00224-17. https://doi.org/10.1128/AAC.00224-17

De Clercq, E. (2009). A new drug combination therapy for treatment-naive patients with HIV-1 infection, consisting of raltegravir, emtricitabine and tenofovir disoproxil fumarate. *Expert Opinion on Pharmacotherapy*, *10*(17), 2935–2937. https://doi.org/10.1517/14656560903418467

de Mendoza, C., Cabezas, T., Caballero, E., Requena, S., Amengual, M. J., Peñaranda, M., Sáez, A., Tellez, R., Lozano, A. B., Treviño, A., Ramos, J. M., Pérez, J. L., Barreiro, P., Soriano, V., & Spanish HIV-2 Network. (2017). HIV type 2 epidemic in Spain: Challenges and missing opportunities. *AIDS (London, England)*, *31*(10), 1353–1364. https://doi.org/10.1097/QAD.0000000000001485

Deguine, J., & Barton, G. M. (2014). MyD88: A central player in innate immune signaling. *F1000Prime Reports*, *6*. https://doi.org/10.12703/P6-97

Delelis, O., Carayon, K., Saïb, A., Deprez, E., & Mouscadet, J.-F. (2008). Integrase and integration: Biochemical activities of HIV-1 integrase. *Retrovirology*, *5*, 114. https://doi.org/10.1186/1742-4690-5-114

Delelis, O., Zamborlini, A., Thierry, S., & Saïb, A. (2010). Chromosomal tethering and proviral integration. *Biochimica et Biophysica Acta (BBA) - Gene Regulatory Mechanisms*, *1799*(3), 207–216. https://doi.org/10.1016/j.bbagrm.2009.08.005

Desbois, D., Roquebert, B., Peytavin, G., Damond, F., Collin, G., Bénard, A., Campa, P., Matheron, S., Chêne, G., Brun-Vézinet, F., & Descamps, D. (2008). In Vitro Phenotypic Susceptibility of Human Immunodeficiency Virus Type 2 Clinical Isolates to Protease Inhibitors. *Antimicrobial Agents and Chemotherapy*, *52*(4), 1545–1548. https://doi.org/10.1128/AAC.01284-07

Desfarges, S., & Ciuffi, A. (2010). Retroviral Integration Site Selection. *Viruses*, *2*(1), 111–130. https://doi.org/10.3390/v2010111

Di Perri, G., Calcagno, A., Trentalange, A., & Bonora, S. (2019). The clinical pharmacology of integrase inhibitors. *Expert Review of Clinical Pharmacology*, *12*(1), 31–44. https://doi.org/10.1080/17512433.2019.1553615

Dittmar, M., Lee, J. S., Whig, K., Segrist, E., Li, M., Kamalia, B., Castellana, L., Ayyanathan, K., Cardenas-Diaz, F. L., Morrisey, E. E., Truitt, R., Yang, W., Jurado, K., Samby, K., Ramage, H., Schultz, D. C., & Cherry, S. (2021). Drug repurposing screens reveal cell-type-specific entry pathways and FDA-approved drugs active against SARS-Cov-2. *Cell Reports*, *35*(1), 108959. https://doi.org/10.1016/j.celrep.2021.108959

Dlamini, Z., & Hull, R. (2017). Can the HIV-1 splicing machinery be targeted for drug discovery? *HIV/AIDS - Research and Palliative Care*, *Volume 9*, 63–75. https://doi.org/10.2147/HIV.S120576

Dolan, J., Chen, A., Weber, I. T., Harrison, R. W., & Leis, J. (2009). Defining the DNA Substrate Binding Sites on HIV-1 Integrase. *Journal of Molecular Biology*, *385*(2), 568–579. https://doi.org/10.1016/j.jmb.2008.10.083

Dzinamarira, T., Almehmadi, M., Alsaiari, A. A., Allahyani, M., Aljuaid, A., Alsharif, A., Khan, A., Kamal, M., Rabaan, A. A., Alfaraj, A. H., AlShehail, B. M., Alotaibi, N., AlShehail, S. M., & Imran, M. (2023). Highlights on the Development, Related Patents, and Prospects of Lenacapavir: The First-in-Class HIV-1 Capsid Inhibitor for the Treatment of Multi-Drug-Resistant HIV-1 Infection. *Medicina*, *59*(6), Article 6. https://doi.org/10.3390/medicina59061041

Engelman, A., & Cherepanov, P. (2012). The structural biology of HIV-1: Mechanistic and therapeutic insights. *Nature Reviews. Microbiology*, *10*(4), 279–290. https://doi.org/10.1038/nrmicro2747

Engelman, A. N. (2019). Multifaceted HIV integrase functionalities and therapeutic strategies for their inhibition. *Journal of Biological Chemistry*, *294*(41), 15137–15157. https://doi.org/10.1074/jbc.REV119.006901

Engelman, A. N., & Cherepanov, P. (2021). Close-up: HIV/SIV intasome structures shed new light on integrase inhibitor binding and viral escape mechanisms. *The FEBS Journal*, *288*(2), 427–433. https://doi.org/10.1111/febs.15438

Eskandari, E., & Eaves, C. J. (2022). Paradoxical roles of caspase-3 in regulating cell survival, proliferation, and tumorigenesis. *Journal of Cell Biology*, *221*(6), e202201159. https://doi.org/10.1083/jcb.202201159

Esposito, F., & Tramontano, E. (2014). Past and Future. Current Drugs Targeting HIV-1 Integrase and Reverse Transcriptase-Associated Ribonuclease H Activity: Single and Dual Active Site Inhibitors. *Antiviral Chemistry and Chemotherapy*, *23*(4), 129–144. https://doi.org/10.3851/IMP2690

Faria, N. R., Hodges-Mameletzis, I., Silva, J. C., Rodés, B., Erasmus, S., Paolucci, S., Ruelle, J., Pieniazek, D., Taveira, N., Treviño, A., Gonçalves, M. F., Jallow, S., Xu, L., Camacho, R. J., Soriano, V., Goubau, P., de Sousa, J. D., Vandamme, A.-M., Suchard, M. A., & Lemey, P. (2012). Phylogeographical footprint of colonial history in the global dispersal of human immunodeficiency virus type 2 group A. *The Journal of General Virology*, *93*(Pt 4), 889–899. https://doi.org/10.1099/vir.0.038638-0

Fauci, A. S. (1988). The human immunodeficiency virus: Infectivity and mechanisms of pathogenesis. *Science (New York, N.Y.)*, *239*(4840), 617–622. https://doi.org/10.1126/science.3277274

Faysal, K. R., Walsh, J. C., Renner, N., Márquez, C. L., Shah, V. B., Tuckwell, A. J., Christie, M. P., Parker, M. W., Turville, S. G., Towers, G. J., James, L. C., Jacques, D. A., & Böcking, T. (n.d.). Pharmacologic hyperstabilisation of the HIV-1 capsid lattice induces capsid failure. *eLife*, *13*, e83605. https://doi.org/10.7554/eLife.83605

Fernandez, C., & van Halsema, C. L. (2019). Evaluating cabotegravir/rilpivirine long-acting, injectable in the treatment of HIV infection: Emerging data and therapeutic potential. *HIV/AIDS (Auckland, N.Z.)*, *11*, 179–192. https://doi.org/10.2147/HIV.S184642

Fink, D. L., Cai, J., Whelan, M. V. X., Monit, C., Maluquer De Motes, C., Towers, G. J., & Sumner, R. P. (2022). HIV-2/SIV Vpx antagonises NF-κB activation by targeting p65. *Retrovirology*, *19*(1), 2. https://doi.org/10.1186/s12977-021-00586-w

Fujita, M., Otsuka, M., Nomaguchi, M., & Adachi, A. (2010). Multifaceted activity of HIV Vpr/Vpx proteins: The current view of their virological functions. *Reviews in Medical Virology*, *20*(2), 68–76. https://doi.org/10.1002/rmv.636

Gallo, R. C., Sarin, P. S., Gelmann, E. P., Robert-Guroff, M., Richardson, E., Kalyanaraman, V. S., Mann, D., Sidhu, G. D., Stahl, R. E., Zolla-Pazner, S., Leibowitch, J., & Popovic, M. (1983). Isolation of human T-cell leukemia virus in acquired immune deficiency syndrome (AIDS). *Science (New York, N.Y.)*, *220*(4599), 865–867. https://doi.org/10.1126/science.6601823

Gandhi, R. T., Landovitz, R. J., Sax, P. E., Smith, D. M., Springer, S. A., Günthard, H. F., Thompson, M. A., Bedimo, R. J., Benson, C. A., Buchbinder, S. P., Crabtree-Ramirez, B. E., Del Rio, C., Eaton, E. F., Eron, J. J., Hoy, J. F., Lehmann, C., Molina, J.-M., Jacobsen, D. M., & Saag, M. S. (2025). Antiretroviral Drugs for Treatment and Prevention of HIV in Adults: 2024 Recommendations of the International Antiviral Society-USA Panel. *JAMA*, *333*(7), 609–628. https://doi.org/10.1001/jama.2024.24543

Gao, F., Yue, L., White, A. T., Pappas, P. G., Barchue, J., Hanson, A. P., Greene, B. M., Sharp, P. M., Shaw, G. M., & Hahn, B. H. (1992). Human infection by genetically diverse SIVSM-related HIV-2 in west Africa. *Nature*, *358*(6386), 495–499. https://doi.org/10.1038/358495a0

Garden, G. A., Budd, S. L., Tsai, E., Hanson, L., Kaul, M., D'Emilia, D. M., Friedlander, R. M., Yuan, J., Masliah, E., & Lipton, S. A. (2002). Caspase Cascades in Human Immunodeficiency Virus-Associated Neurodegeneration. *The Journal of Neuroscience*, *22*(10), 4015–4024. https://doi.org/10.1523/JNEUROSCI.22-10-04015.2002

Gil, H., Delgado, E., Benito, S., Moreno-Lorenzo, M., & Thomson, M. M. (2022). Factors associated with HIV-1 resistance to integrase strand transfer inhibitors in Spain: Implications for dolutegravir-containing regimens. *Frontiers in Microbiology*, *13*, 1051096. https://doi.org/10.3389/fmicb.2022.1051096

Goldstone, D. C., Ennis-Adeniran, V., Hedden, J. J., Groom, H. C. T., Rice, G. I., Christodoulou, E., Walker, P. A., Kelly, G., Haire, L. F., Yap, M. W., de Carvalho, L. P. S., Stoye, J. P., Crow, Y. J., Taylor, I. A., & Webb, M. (2011). HIV-1 restriction

factor SAMHD1 is a deoxynucleoside triphosphate triphosphohydrolase. *Nature*, *480*(7377), 379–382. https://doi.org/10.1038/nature10623

Görlich, D., Prehn, S., Laskey, R. A., & Hartmann, E. (1994). Isolation of a protein that is essential for the first step of nuclear protein import. *Cell*, *79*(5), 767–778. https://doi.org/10.1016/0092-8674(94)90067-1

Gottlieb, G. S., Raugi, D. N., & Smith, R. A. (2018). 90-90-90 for HIV-2? Ending the HIV-2 epidemic by enhancing care and clinical management of patients infected with HIV-2. *The Lancet. HIV*, *5*(7), e390–e399. https://doi.org/10.1016/S2352-3018(18)30094-8

Guyader, M., Emerman, M., Sonigo, P., Clavel, F., Montagnier, L., & Alizon, M. (1987). Genome organization and transactivation of the human immunodeficiency virus type 2. *Nature*, *326*(6114), 662–669. https://doi.org/10.1038/326662a0

Hamel, D. J., Sankalé, J.-L., Eisen, G., Meloni, S. T., Mullins, C., Gueye-Ndiaye, A., Mboup, S., & Kanki, P. J. (2007). Twenty Years of Prospective Molecular Epidemiology in Senegal: Changes in HIV Diversity. *AIDS Research and Human Retroviruses*, *23*(10), 1189–1196. https://doi.org/10.1089/aid.2007.0037

Hansen, M. S., & Bushman, F. D. (1997). Human immunodeficiency virus type 2 preintegration complexes: Activities in vitro and response to inhibitors. *Journal of Virology*, *71*(4), 3351–3356. https://doi.org/10.1128/JVI.71.4.3351-3356.1997

Hare, S., Maertens, G. N., & Cherepanov, P. (2012). 3′-Processing and strand transfer catalysed by retroviral integrase in crystallo. *The EMBO Journal*, *31*(13), 3020–3028. https://doi.org/10.1038/emboj.2012.118

Hare, S., Smith, S. J., Métifiot, M., Jaxa-Chamiec, A., Pommier, Y., Hughes, S. H., & Cherepanov, P. (2011). Structural and Functional Analyses of the Second-Generation Integrase Strand Transfer Inhibitor Dolutegravir (S/GSK1349572). *Molecular Pharmacology*, *80*(4), 565–572. https://doi.org/10.1124/mol.111.073189

Heitzinger, K., Sow, P. S., Dia Badiane, N. M., Gottlieb, G. S., N'Doye, I., Toure, M., Kiviat, N. B., & Hawes, S. E. (2012). Trends of HIV-1, HIV-2 and dual infection in women attending outpatient clinics in Senegal, 1990–2009. *International Journal of STD & AIDS*, *23*(10), 710–716. https://doi.org/10.1258/ijsa.2012.011219

Hernandez-Vargas, E. A., & Middleton, R. H. (2013). Modeling the three stages in HIV infection. *Journal of Theoretical Biology*, *320*, 33–40. https://doi.org/10.1016/j.jtbi.2012.11.028

Hicks, C., & Gulick, R. M. (2009). Raltegravir: The First HIV Type 1 Integrase Inhibitor. *Clinical Infectious Diseases*, *48*(7), 931–939. https://doi.org/10.1086/597290

Hurley, J. H., & Cada, A. K. (2018). Inside Job: How the ESCRTs release HIV-1 from infected cells. *Biochemical Society Transactions*, *46*(5), 1029–1036. https://doi.org/10.1042/BST20180019

Indu, P., Rameshkumar, M. R., Arunagirinathan, N., Al-Dhabi, N. A., Valan Arasu, M., & Ignacimuthu, S. (2020). Raltegravir, Indinavir, Tipranavir, Dolutegravir, and Etravirine against main protease and RNA-dependent RNA polymerase of SARS-CoV-2: A molecular docking and drug repurposing approach. *Journal of Infection and Public Health*, *13*(12), 1856–1861. https://doi.org/10.1016/j.jiph.2020.10.015

Isaacs, D., Mikasi, S. G., Obasa, A. E., Ikomey, G. M., Shityakov, S., Cloete, R., & Jacobs, G. B. (2020). Structural Comparison of Diverse HIV-1 Subtypes using Molecular Modelling and Docking Analyses of Integrase Inhibitors. *Viruses*, *12*(9), 936. https://doi.org/10.3390/v12090936

Jaskolski, M., Alexandratos, J. N., Bujacz, G., & Wlodawer, A. (2009). Piecing together the structure of retroviral integrase, an important target in AIDS therapy. *The FEBS Journal*, *276*(11), 2926–2946. https://doi.org/10.1111/j.1742-4658.2009.07009.x

Jeeninga, R. E., Hoogenkamp, M., Armand-Ugon, M., de Baar, M., Verhoef, K., & Berkhout, B. (2000). Functional Differences between the Long Terminal Repeat Transcriptional Promoters of Human Immunodeficiency Virus Type 1 Subtypes A through G. *Journal of Virology*, *74*(8), 3740–3751.

Jochmans, D., Leyssen, P., & Neyts, J. (2012). A novel method for high-throughput screening to quantify antiviral activity against viruses that induce limited CPE. *Journal of Virological Methods*, *183*(2), 176–179. https://doi.org/10.1016/j.jviromet.2012.04.011

Jóźwik, I. K., Passos, D. O., & Lyumkis, D. (2020). Structural Biology of HIV Integrase Strand Transfer Inhibitors. *Trends in Pharmacological Sciences*, *41*(9), 611–626. https://doi.org/10.1016/j.tips.2020.06.003

Kandel, C. E., & Walmsley, S. L. (2015). Dolutegravir – a review of the pharmacology, efficacy, and safety in the treatment of HIV. *Drug Design, Development and Therapy*, *9*, 3547–3555. https://doi.org/10.2147/DDDT.S84850

Klotman, M. E., & Chang, T. L. (2006). Defensins in innate antiviral immunity. *Nature Reviews. Immunology*, *6*(6), 447–456. https://doi.org/10.1038/nri1860

Kurnaeva, M. A., Zalevsky, A. O., Arifulin, E. A., Lisitsyna, O. M., Tvorogova, A. V., Shubina, M. Y., Bourenkov, G. P., Musinova, Y. R., Golovin, A. V., Vassetzky, Y. S., & Sheval, E. V. (2021). *Mechanisms and evolutionary implications of integration of*

different functions within HIV-1 Tat (p. 2021.04.20.440437). bioRxiv. https://doi.org/10.1101/2021.04.20.440437

Laakso, M. M., Lee, F.-H., Haggarty, B., Agrawal, C., Nolan, K. M., Biscone, M., Romano, J., Jordan, A. P. O., Leslie, G. J., Meissner, E. G., Su, L., Hoxie, J. A., & Doms, R. W. (2007). V3 Loop Truncations in HIV-1 Envelope Impart Resistance to Coreceptor Inhibitors and Enhanced Sensitivity to Neutralizing Antibodies. *PLoS Pathogens*, *3*(8), e117. https://doi.org/10.1371/journal.ppat.0030117

Laguette, N., Sobhian, B., Casartelli, N., Ringeard, M., Chable-Bessia, C., Ségéral, E., Yatim, A., Emiliani, S., Schwartz, O., & Benkirane, M. (2011). SAMHD1 is the dendritic- and myeloid-cell-specific HIV-1 restriction factor counteracted by Vpx. *Nature*, *474*(7353), 654–657. https://doi.org/10.1038/nature10117

Lamorte, L., Titolo, S., Lemke, C. T., Goudreau, N., Mercier, J.-F., Wardrop, E., Shah, V. B., von Schwedler, U. K., Langelier, C., Banik, S. S. R., Aiken, C., Sundquist, W. I., & Mason, S. W. (2013). Discovery of novel small-molecule HIV-1 replication inhibitors that stabilize capsid complexes. *Antimicrobial Agents and Chemotherapy*, *57*(10), 4622–4631. https://doi.org/10.1128/AAC.00985-13

Lampi, Y., Van Looveren, D., Vranckx, L. S., Thiry, I., Bornschein, S., Debyser, Z., & Gijsbers, R. (2019). Targeted editing of the PSIP1 gene encoding LEDGF/p75 protects cells against HIV infection. *Scientific Reports*, *9*(1), 2389. https://doi.org/10.1038/s41598-019-38718-0

Le Hingrat, Q., Collin, G., Lê, M., Peytavin, G., Visseaux, B., Bertine, M., Tubiana, R., Karmochkine, M., Valin, N., Collin, F., Lemaignen, A., Bernard, L., Damond, F., Matheron, S., Descamps, D., Charpentier, C., & French National Agency for Research on AIDS and Viral Hepatitis (ANRS) CO5 HIV-2 Cohort. (2019). A New Mechanism of Resistance of Human Immunodeficiency Virus Type 2 to Integrase Inhibitors: A 5-Amino-Acid Insertion in the Integrase C-Terminal Domain. *Clinical Infectious Diseases: An Official Publication of the Infectious Diseases Society of America*, *69*(4), 657–667. https://doi.org/10.1093/cid/ciy940

Le Hingrat, Q., Visseaux, B., Bertine, M., Chauveau, L., Schwartz, O., Collin, F., Damond, F., Matheron, S., Descamps, D., & Charpentier, C. (2020). Genetic Variability of Long Terminal Repeat Region between HIV-2 Groups Impacts Transcriptional Activity. *Journal of Virology*, *94*(7), e01504-19. https://doi.org/10.1128/JVI.01504-19

Lever, A. M. L. (2021). Molecular Biology of HIV-2. In T. J. Hope, M. Stevenson, & D. Richman (Eds.), *Encyclopedia of AIDS* (pp. 1–11). Springer. https://doi.org/10.1007/978-1-4614-9610-6_43-1

Link, J. O., Rhee, M. S., Tse, W. C., Zheng, J., Somoza, J. R., Rowe, W., Begley, R., Chiu, A., Mulato, A., Hansen, D., Singer, E., Tsai, L. K., Bam, R. A., Chou, C.-H., Canales, E., Brizgys, G., Zhang, J. R., Li, J., Graupe, M., … Cihlar, T. (2020). Clinical targeting of HIV capsid protein with a long-acting small molecule. *Nature*, *584*(7822), 614–618. https://doi.org/10.1038/s41586-020-2443-1

MacNeil, A., Sankalé, J.-L., Meloni, S. T., Sarr, A. D., Mboup, S., & Kanki, P. (2006). Genomic Sites of Human Immunodeficiency Virus Type 2 (HIV-2) Integration: Similarities to HIV-1 In Vitro and Possible Differences In Vivo. *Journal of Virology*, *80*(15), 7316–7321. https://doi.org/10.1128/jvi.00604-06

Maertens, G., Cherepanov, P., Pluymers, W., Busschots, K., Clercq, E. D., Debyser, Z., & Engelborghs, Y. (2003). LEDGF/p75 Is Essential for Nuclear and Chromosomal Targeting of HIV-1 Integrase in Human Cells *. *Journal of Biological Chemistry*, *278*(35), 33528–33539. https://doi.org/10.1074/jbc.M303594200

Mahdi, M., Szojka, Z., Mótyán, J. A., & Tőzsér, J. (2015). Inhibition Profiling of Retroviral Protease Inhibitors Using an HIV-2 Modular System. *Viruses*, *7*(12), 6152–6162. https://doi.org/10.3390/v7122931

Mahdi, M., Szojka, Z., Mótyán, J. A., & Tőzsér, J. (2018). Inhibitory Effects of HIV-2 Vpx on Replication of HIV-1. *Journal of Virology*, *92*(14), e00554-18. https://doi.org/10.1128/JVI.00554-18

Marcelin, A.-G., Charpentier, C., Jary, A., Perrier, M., Margot, N., Callebaut, C., Calvez, V., & Descamps, D. (2020). Frequency of capsid substitutions associated with GS-6207 in vitro resistance in HIV-1 from antiretroviral-naive and -experienced patients. *The Journal of Antimicrobial Chemotherapy*, *75*(6), 1588–1590. https://doi.org/10.1093/jac/dkaa060

Marchant, D., Neil, S. J. D., & McKnight, Á. (2006). Human immunodeficiency virus types 1 and 2 have different replication kinetics in human primary macrophage culture. *The Journal of General Virology*, *87*(Pt 2), 411–418. https://doi.org/10.1099/vir.0.81391-0

Marlink, R., Kanki, P., Thior, I., Travers, K., Eisen, G., Siby, T., Traore, I., Hsieh, C. C., Dia, M. C., & Gueye, E. H. (1994). Reduced rate of disease development after HIV-2 infection as compared to HIV-1. *Science (New York, N.Y.)*, *265*(5178), 1587–1590. https://doi.org/10.1126/science.7915856

Marquart, K. H., Müller, H. A., & Brede, H. D. (1988). HIV-2 in West Germany. *AIDS (London, England)*, *2*(2), 141.

Mbisa, J. L., Ledesma, J., Kirwan, P., Bibby, D. F., Manso, C., Skingsley, A., Murphy, G., Brown, A., Dunn, D. T., Delpech, V., & Geretti, A. M. (2020). Surveillance of HIV-1 transmitted integrase strand transfer inhibitor resistance in the UK. *Journal of Antimicrobial Chemotherapy*, *75*(11), 3311–3318. https://doi.org/10.1093/jac/dkaa309

McAllery, S. A., Ahlenstiel, C. L., Suzuki, K., Symonds, G. P., Kelleher, A. D., & Turville, S. G. (2016). The feasibility of incorporating Vpx into lentiviral gene therapy vectors. *Molecular Therapy Methods & Clinical Development*, *3*. https://doi.org/10.1038/mtm.2016.66

McGraw, A., Hillmer, G., Medehincu, S. M., Hikichi, Y., Gagliardi, S., Narayan, K., Tibebe, H., Marquez, D., Mei Bose, L., Keating, A., Izumi, C., Peese, K., Joshi, S., Krystal, M., DeCicco-Skinner, K. L., Freed, E. O., Sardo, L., & Izumi, T. (2024). Exploring HIV-1 Maturation: A New Frontier in Antiviral Development. *Viruses*, *16*(9), 1423. https://doi.org/10.3390/v16091423

Messiaen, P., Wensing, A. M. J., Fun, A., Nijhuis, M., Brusselaers, N., & Vandekerckhove, L. (2013). Clinical Use of HIV Integrase Inhibitors: A Systematic Review and Meta-Analysis. *PLOS ONE*, *8*(1), e52562. https://doi.org/10.1371/journal.pone.0052562

Mohamed, E. A. R., Abdel-Rahman, I. M., Zaki, M. E. A., Al-Khdhairawi, A., Abdelhamid, M. M., Alqaisi, A. M., Rahim, L. binti A., Abu-Hussein, B., El-Sheikh, A. A. K., Abdelwahab, S. F., & Hassan, H. A. (2023). In silico prediction of potential inhibitors for SARS-CoV-2 Omicron variant using molecular docking and dynamics simulation-based drug repurposing. *Journal of Molecular Modeling*, *29*(3), 70. https://doi.org/10.1007/s00894-023-05457-z

Montagnier, L., Chermann, J. C., Barré-Sinoussi, F., Klatzmann, D., Wain-Hobson, S., Alizon, M., Clavel, F., Brun-Vezinet, F., Vilmer, E., & Rouzioux, C. (1984). Lymphadenopathy associated virus and its etiological role in AIDS. *Princess Takamatsu Symposia*, *15*, 319–331.

Mörner, A., Björndal, A., Albert, J., Kewalramani, V. N., Littman, D. R., Inoue, R., Thorstensson, R., Fenyö, E. M., & Björling, E. (1999). Primary human immunodeficiency virus type 2 (HIV-2) isolates, like HIV-1 isolates, frequently use CCR5 but show promiscuity in coreceptor usage. *Journal of Virology*, *73*(3), 2343–2349. https://doi.org/10.1128/JVI.73.3.2343-2349.1999

Motomura, K., Chen, J., & Hu, W.-S. (2008). Genetic Recombination between Human Immunodeficiency Virus Type 1 (HIV-1) and HIV-2, Two Distinct Human Lentiviruses. *Journal of Virology*, *82*(4), 1923–1933. https://doi.org/10.1128/jvi.01937-07

Munis, A. M. (2020). Gene Therapy Applications of Non-Human Lentiviral Vectors. *Viruses*, *12*(10), 1106. https://doi.org/10.3390/v12101106

Murray, J. M., Kelleher, A. D., & Cooper, D. A. (2011). Timing of the Components of the HIV Life Cycle in Productively Infected CD4+ T Cells in a Population of HIV-Infected Individuals ▿. *Journal of Virology*, *85*(20), 10798–10805. https://doi.org/10.1128/JVI.05095-11

Nachega, J. B., Scarsi, K. K., Gandhi, M., Scott, R. K., Mofenson, L. M., Archary, M., Nachman, S., Decloedt, E., Geng, E. H., Wilson, L., Rawat, A., & Mellors, J. W. (2023). Long-acting antiretrovirals and HIV treatment adherence. *The Lancet. HIV*, *10*(5), e332–e342. https://doi.org/10.1016/S2352-3018(23)00051-6

Oh, J.-W., & Shin, C.-G. (1996). Purification and Characterization of the Human Immunodeficiency Virus Type 1 Integrase Expressed in *Escherichia coli*. *Molecules and Cells*, *6*(1), 96–100. https://doi.org/10.1016/S1016-8478(23)10976-9

Ortiz-Hernandez, G. L., Sanchez-Hernandez, E. S., Ochoa, P. T., & Casiano, C. A. (2024). The Emerging Roles of the Stress Epigenetic Reader LEDGF/p75 in Cancer Biology and Therapy Resistance: Mechanisms and Targeting Opportunities. *Cancers*, *16*(23), 3957. https://doi.org/10.3390/cancers16233957

Pancho, A., Aerts, T., Mitsogiannis, M. D., & Seuntjens, E. (2020). Protocadherins at the Crossroad of Signaling Pathways. *Frontiers in Molecular Neuroscience*, *13*, 117. https://doi.org/10.3389/fnmol.2020.00117

Pancio, H. A., & Ratner, L. (1998). Human immunodeficiency virus type 2 Vpx-Gag interaction. *Journal of Virology*, *72*(6), 5271–5275. https://doi.org/10.1128/JVI.72.6.5271-5275.1998

Pau, A. K., & George, J. M. (2014). Antiretroviral therapy: Current drugs. *Infectious Disease Clinics of North America*, *28*(3), 371–402. https://doi.org/10.1016/j.idc.2014.06.001

Payne, S. (2017). Chapter 37—Replication and Pathogenesis of Human Immunodeficiency Virus. In S. Payne (Ed.), *Viruses* (pp. 303–320). Academic Press. https://doi.org/10.1016/B978-0-12-803109-4.00037-4

Peeters, M., Courgnaud, V., Abela, B., Auzel, P., Pourrut, X., Bibollet-Ruche, F., Loul, S., Liegeois, F., Butel, C., Koulagna, D., Mpoudi-Ngole, E., Shaw, G. M., Hahn, B. H., &

Delaporte, E. (2002). Risk to Human Health from a Plethora of Simian Immunodeficiency Viruses in Primate Bushmeat. *Emerging Infectious Diseases*, *8*(5), 451–457. https://doi.org/10.3201/eid0805.01-0522

Pena, M. J., Chueca, N., D'Avolio, A., Zarzalejos, J. M., & Garcia, F. (2018). Virological Failure in HIV to Triple Therapy With Dolutegravir-Based Firstline Treatment: Rare but Possible. *Open Forum Infectious Diseases*, *6*(1), ofy332. https://doi.org/10.1093/ofid/ofy332

Perazzolo, S., Stephen, Z. R., Eguchi, M., Xu, X., Delle Fratte, R., Collier, A. C., Melvin, A. J., & Ho, R. J. Y. (2023). A novel formulation enabled transformation of 3-HIV drugs tenofovir-lamivudine-dolutegravir from short-acting to long-acting all-in-one injectable. *AIDS (London, England)*, *37*(14), 2131–2136. https://doi.org/10.1097/QAD.0000000000003706

Perrier, M., Bertine, M., Le Hingrat, Q., Joly, V., Visseaux, B., Collin, G., Landman, R., Yazdanpanah, Y., Descamps, D., & Charpentier, C. (2017). Prevalence of gag mutations associated with in vitro resistance to capsid inhibitor GS-CA1 in HIV-1 antiretroviral-naive patients. *The Journal of Antimicrobial Chemotherapy*, *72*(10), 2954–2955. https://doi.org/10.1093/jac/dkx208

Pettersen, E. F., Goddard, T. D., Huang, C. C., Couch, G. S., Greenblatt, D. M., Meng, E. C., & Ferrin, T. E. (2004). UCSF Chimera—A visualization system for exploratory research and analysis. *Journal of Computational Chemistry*, *25*(13), 1605–1612. https://doi.org/10.1002/jcc.20084

Pinto, R. M., Hall, E., & Tomlin, R. (2023). Injectable Long-Acting Cabotegravir–Rilpivirine Therapy for People Living With HIV/AIDS: Addressing Implementation Barriers From the Start. *The Journal of the Association of Nurses in AIDS Care*, *34*(2), 216–220. https://doi.org/10.1097/JNC.0000000000000386

Poeschla, E. M. (2008a). Integrase, LEDGF/p75 and HIV replication. *Cellular and Molecular Life Sciences: CMLS*, *65*(9), 1403–1424. https://doi.org/10.1007/s00018-008-7540-5

Poeschla, E. M. (2008b). Integrase, LEDGF/p75 and HIV replication. *Cellular and Molecular Life Sciences: CMLS*, *65*(9), 1403–1424. https://doi.org/10.1007/s00018-008-7540-5

Ponti, D., Troiano, M., Bellenchi, G. C., Battaglia, P. A., & Gigliani, F. (2008). The HIV Tat protein affects processing of ribosomal RNA precursor. *BMC Cell Biology*, *9*, 32. https://doi.org/10.1186/1471-2121-9-32

Prather, C., Lee, A., & Yen, C. (2023). Lenacapavir: A first-in-class capsid inhibitor for the treatment of highly treatment-resistant HIV. *American Journal of Health-System*

Pharmacy: AJHP: Official Journal of the American Society of Health-System Pharmacists, *80*(24), 1774–1780. https://doi.org/10.1093/ajhp/zxad223

Quashie, P. K., Mesplède, T., Han, Y.-S., Oliveira, M., Singhroy, D. N., Fujiwara, T., Underwood, M. R., & Wainberg, M. A. (2012). Characterization of the R263K mutation in HIV-1 integrase that confers low-level resistance to the second-generation integrase strand transfer inhibitor dolutegravir. *Journal of Virology*, *86*(5), 2696–2705. https://doi.org/10.1128/JVI.06591-11

Rabe, A. J., Tan, Y. Y., Larue, R. C., & Yoder, K. E. (2021). Prototype Foamy Virus Integrase Displays Unique Biochemical Activities among Retroviral Integrases. *Biomolecules*, *11*(12), 1910. https://doi.org/10.3390/biom11121910

Reeves, I., Cromarty, B., Deayton, J., Dhairyawan, R., Kidd, M., Taylor, C., Thornhill, J., Tickell-Painter, M., & Van Halsema, C. (2021). British HIV Association guidelines for the management of HIV-2 2021. *HIV Medicine*, *22*(S4), 1–29. https://doi.org/10.1111/hiv.13204

Reeves, J. D., & Doms, R. W. (2002). Human immunodeficiency virus type 2. *The Journal of General Virology*, *83*(Pt 6), 1253–1265. https://doi.org/10.1099/0022-1317-83-6-1253

Reviriego, C. (2014). Elvitegravir for the treatment of HIV infection. *Drugs of Today (Barcelona, Spain: 1998)*, *50*(3), 209–217. https://doi.org/10.1358/dot.2014.50.3.2122120

Richetta, C., Tu, N. Q., & Delelis, O. (2022). Different Pathways Conferring Integrase Strand-Transfer Inhibitors Resistance. *Viruses*, *14*(12), 2591. https://doi.org/10.3390/v14122591

Robertson, D. L., Sharp, P. M., McCutchan, F. E., & Hahn, B. H. (1995). Recombination in HIV-1. *Nature*, *374*(6518), 124–126. https://doi.org/10.1038/374124b0

Roquebert, B., Damond, F., Brun-Vézinet, F., & Descamps, D. (2009). [HIV genetic diversity and its consequences]. *Pathologie-biologie*, *57*(2), 142–148. https://doi.org/10.1016/j.patbio.2008.04.004

Rossi, E., Meuser, M. E., Cunanan, C. J., & Cocklin, S. (2021). Structure, Function, and Interactions of the HIV-1 Capsid Protein. *Life*, *11*(2), Article 2. https://doi.org/10.3390/life11020100

Sang, P., Tian, S.-H., Meng, Z.-H., & Yang, L.-Q. (2020). Anti-HIV drug repurposing against SARS-CoV-2. *RSC Advances*, *10*(27), 15775–15783. https://doi.org/10.1039/D0RA01899F

Savarino, A. (2007). In-Silico docking of HIV-1 integrase inhibitors reveals a novel drug type acting on an enzyme/DNA reaction intermediate. *Retrovirology*, *4*, 21. https://doi.org/10.1186/1742-4690-4-21

Sayyed, S. K., Quraishi, M., Jobby, R., Rameshkumar, N., Kayalvizhi, N., Krishnan, M., & Sonawane, T. (2023). A computational overview of integrase strand transfer inhibitors (INSTIs) against emerging and evolving drug-resistant HIV-1 integrase mutants. *Archives of Microbiology*, *205*(4), 142. https://doi.org/10.1007/s00203-023-03461-8

Schrijvers, R., & Debyser, Z. (2018). Role of LEDGF/p75 in Cell Biology and Disease Pathogenesis. In T. J. Hope, D. D. Richman, & M. Stevenson (Eds.), *Encyclopedia of AIDS* (pp. 1830–1844). Springer. https://doi.org/10.1007/978-1-4939-7101-5_72

Schröder, A. R. W., Shinn, P., Chen, H., Berry, C., Ecker, J. R., & Bushman, F. (2002). HIV-1 integration in the human genome favors active genes and local hotspots. *Cell*, *110*(4), 521–529. https://doi.org/10.1016/s0092-8674(02)00864-4

Segal-Maurer, S., DeJesus, E., Stellbrink, H.-J., Castagna, A., Richmond, G. J., Sinclair, G. I., Siripassorn, K., Ruane, P. J., Berhe, M., Wang, H., Margot, N. A., Dvory-Sobol, H., Hyland, R. H., Brainard, D. M., Rhee, M. S., Baeten, J. M., & Molina, J.-M. (2022). Capsid Inhibition with Lenacapavir in Multidrug-Resistant HIV-1 Infection. *New England Journal of Medicine*, *386*(19), 1793–1803. https://doi.org/10.1056/NEJMoa2115542

Senavirathne, G., London, J., Gardner, A., Fishel, R., & Yoder, K. E. (2023). DNA strand breaks and gaps target retroviral intasome binding and integration. *Nature Communications*, *14*(1), 7072. https://doi.org/10.1038/s41467-023-42641-4

Sertznig, H., Hillebrand, F., Erkelenz, S., Schaal, H., & Widera, M. (2018). Behind the scenes of HIV-1 replication: Alternative splicing as the dependency factor on the quiet. *Virology*, *516*, 176–188. https://doi.org/10.1016/j.virol.2018.01.011

Shan, M., Su, Y., Kang, W., Gao, R., Li, X., & Zhang, G. (2016). Aberrant expression and functions of protocadherins in human malignant tumors. *Tumor Biology*, *37*(10), 12969–12981. https://doi.org/10.1007/s13277-016-5169-9

Sharp, P. M., & Hahn, B. H. (2011). Origins of HIV and the AIDS Pandemic. *Cold Spring Harbor Perspectives in Medicine:*, *1*(1), a006841. https://doi.org/10.1101/cshperspect.a006841

Shimura, K., & Kodama, E. N. (2009). Elvitegravir: A New HIV Integrase Inhibitor. *Antiviral Chemistry and Chemotherapy*, *20*(2), 79–85. https://doi.org/10.3851/IMP1397

Shun, M.-C., Raghavendra, N. K., Vandegraaff, N., Daigle, J. E., Hughes, S., Kellam, P., Cherepanov, P., & Engelman, A. (2007). LEDGF/p75 functions downstream from preintegration complex formation to effect gene-specific HIV-1 integration. *Genes & Development*, *21*(14), 1767–1778. https://doi.org/10.1101/gad.1565107

Singhal, P. K., Kumar, P. R., Rao, M. R. K. S., Kyasani, M., & Mahalingam, S. (2006). Simian Immunodeficiency Virus Vpx Is Imported into the Nucleus via Importin Alpha-Dependent and -Independent Pathways. *Journal of Virology*, *80*(1), 526–536. https://doi.org/10.1128/JVI.80.1.526-536.2006

Smith, R. A., Anderson, D. J., Pyrak, C. L., Preston, B. D., & Gottlieb, G. S. (2009). Antiretroviral Drug Resistance in HIV-2: Three Amino Acid Changes Are Sufficient for Classwide Nucleoside Analogue Resistance. *The Journal of Infectious Diseases*, *199*(9), 1323–1326. https://doi.org/10.1086/597802

Smith, S. J., Zhao, X. Z., Burke, T. R., & Hughes, S. H. (2018). Efficacies of Cabotegravir and Bictegravir against drug-resistant HIV-1 integrase mutants. *Retrovirology*, *15*(1), 37. https://doi.org/10.1186/s12977-018-0420-7

Soriano, V., Gomes, P., Heneine, W., Holguín, A., Doruana, M., Antunes, R., Mansinho, K., Switzer, W. M., Araujo, C., Shanmugam, V., Lourenço, H., González-Lahoz, J., & Antunes, F. (2000). Human immunodeficiency virus type 2 (HIV-2) in Portugal: Clinical spectrum, circulating subtypes, virus isolation, and plasma viral load. *Journal of Medical Virology*, *61*(1), 111–116.

Spagnuolo, V., Castagna, A., & Lazzarin, A. (2018). Bictegravir. *Current Opinion in HIV and AIDS*, *13*(4), 326–333. https://doi.org/10.1097/COH.0000000000000468

Strebel, K. (2013). HIV Accessory Proteins versus Host Restriction Factors. *Current Opinion in Virology*, *3*(6), 10.1016/j.coviro.2013.08.004. https://doi.org/10.1016/j.coviro.2013.08.004

Summary of Changes from v12.0 to v12.1. (n.d.). EACS Guidelines. Retrieved August 3, 2025, from https://eacs.sanfordguide.com/contents/changes-v11-0-to-v11-1

Sunshine, S., Kirchner, R., Amr, S. S., Mansur, L., Shakhbatyan, R., Kim, M., Bosque, A., Siliciano, R. F., Planelles, V., Hofmann, O., Ho Sui, S., & Li, J. Z. (2016). HIV Integration Site Analysis of Cellular Models of HIV Latency with a Probe-Enriched Next-Generation Sequencing Assay. *Journal of Virology*, *90*(9), 4511–4519. https://doi.org/10.1128/JVI.01617-15

Talledge, N., Yang, H., Shi, K., Coray, R., Yu, G., Arndt, W. G., Meng, S., Baxter, G. C., Mendonça, L. M., Castaño-Díez, D., Aihara, H., Mansky, L. M., & Zhang, W. (2023).

HIV-2 Immature Particle Morphology Provides Insights into Gag Lattice Stability and Virus Maturation. *Journal of Molecular Biology*, *435*(15), 168143. https://doi.org/10.1016/j.jmb.2023.168143

Tam, L. W. Y., Chui, C. K. S., Brumme, C. J., Bangsberg, D. R., Montaner, J. S. G., Hogg, R. S., & Harrigan, P. R. (2008). The Relationship Between Resistance and Adherence in Drug-Naive Individuals Initiating HAART Is Specific to Individual Drug Classes. *Journal of Acquired Immune Deficiency Syndromes (1999)*, *49*(3), 266–271. https://doi.org/10.1097/QAI.0b013e318189a753

Tang, C., Loeliger, E., Kinde, I., Kyere, S., Mayo, K., Barklis, E., Sun, Y., Huang, M., & Summers, M. F. (2003). Antiviral inhibition of the HIV-1 capsid protein. *Journal of Molecular Biology*, *327*(5), 1013–1020. https://doi.org/10.1016/s0022-2836(03)00289-4

Tang, M. W., & Shafer, R. W. (2012). HIV-1 Antiretroviral Resistance. *Drugs*, *72*(9), e1–e25. https://doi.org/10.2165/11633630-000000000-00000

Tang, R., Yu, Z., Ma, Y., Wu, Y., Phoebe Chen, Y.-P., Wong, L., & Li, J. (2021). Genetic source completeness of HIV-1 circulating recombinant forms (CRFs) predicted by multi-label learning. *Bioinformatics*, *37*(6), 750–758. https://doi.org/10.1093/bioinformatics/btaa887

Taramasso, L., Andreoni, M., Antinori, A., Bandera, A., Bonfanti, P., Bonora, S., Borderi, M., Castagna, A., Cattelan, A. M., Celesia, B. M., Cicalini, S., Cingolani, A., Cossarizza, A., D'Arminio Monforte, A., D'Ettorre, G., Di Biagio, A., Di Giambenedetto, S., Di Perri, G., Esposito, V., … Maggiolo, F. (2023). Pillars of long-term antiretroviral therapy success. *Pharmacological Research*, *196*, 106898. https://doi.org/10.1016/j.phrs.2023.106898

Tecalco-Cruz, A. C., Ríos-López, D. G., Vázquez-Victorio, G., Rosales-Alvarez, R. E., & Macías-Silva, M. (2018). Transcriptional cofactors Ski and SnoN are major regulators of the TGF-β/Smad signaling pathway in health and disease. *Signal Transduction and Targeted Therapy*, *3*(1), 1–15. https://doi.org/10.1038/s41392-018-0015-8

Tong, S., & Revill, P. (2016). Overview of viral replication and genetic variability. *Journal of Hepatology*, *64*(1 Suppl), S4–S16. https://doi.org/10.1016/j.jhep.2016.01.027

Triki, D., Cano Contreras, M. E., Flatters, D., Visseaux, B., Descamps, D., Camproux, A.-C., & Regad, L. (2018). Analysis of the HIV-2 protease's adaptation to various ligands: Characterization of backbone asymmetry using a structural alphabet. *Scientific Reports*, *8*(1), 710. https://doi.org/10.1038/s41598-017-18941-3

Trivedi, J., Mahajan, D., Jaffe, R. J., Acharya, A., Mitra, D., & Byrareddy, S. N. (2020). Recent Advances in the Development of Integrase Inhibitors for HIV Treatment. *Current HIV/AIDS Reports*, *17*(1), 63–75. https://doi.org/10.1007/s11904-019-00480-3

Tsiang, M., Jones, G. S., Goldsmith, J., Mulato, A., Hansen, D., Kan, E., Tsai, L., Bam, R. A., Stepan, G., Stray, K. M., Niedziela-Majka, A., Yant, S. R., Yu, H., Kukolj, G., Cihlar, T., Lazerwith, S. E., White, K. L., & Jin, H. (2016). Antiviral Activity of Bictegravir (GS-9883), a Novel Potent HIV-1 Integrase Strand Transfer Inhibitor with an Improved Resistance Profile. *Antimicrobial Agents and Chemotherapy*, *60*(12), 7086–7097. https://doi.org/10.1128/AAC.01474-16

Vermeire, J., Roesch, F., Sauter, D., Rua, R., Hotter, D., Van Nuffel, A., Vanderstraeten, H., Naessens, E., Iannucci, V., Landi, A., Witkowski, W., Baeyens, A., Kirchhoff, F., & Verhasselt, B. (2016). HIV Triggers a cGAS-Dependent, Vpu- and Vpr-Regulated Type I Interferon Response in CD4 + T Cells. *Cell Reports*, *17*(2), 413–424. https://doi.org/10.1016/j.celrep.2016.09.023

Walmsley, S. L., Antela, A., Clumeck, N., Duiculescu, D., Eberhard, A., Gutiérrez, F., Hocqueloux, L., Maggiolo, F., Sandkovsky, U., Granier, C., Pappa, K., Wynne, B., Min, S., Nichols, G., & SINGLE Investigators. (2013). Dolutegravir plus abacavir-lamivudine for the treatment of HIV-1 infection. *The New England Journal of Medicine*, *369*(19), 1807–1818. https://doi.org/10.1056/NEJMoa1215541

Wang, J., Guan, E., Roderiquez, G., & Norcross, M. A. (2001). Synergistic Induction of Apoptosis in Primary CD4+ T Cells by Macrophage-Tropic HIV-1 and TGF-β1. *The Journal of Immunology*, *167*(6), 3360–3366. https://doi.org/10.4049/jimmunol.167.6.3360

Wang, Y., Gu, S.-X., He, Q.-Q., & Fan, R. (2021). Advances in the development of HIV integrase strand transfer inhibitors. *European Journal of Medicinal Chemistry*, *225*, 113787. https://doi.org/10.1016/j.ejmech.2021.113787

Waterhouse, A., Bertoni, M., Bienert, S., Studer, G., Tauriello, G., Gumienny, R., Heer, F. T., de Beer, T. A. P., Rempfer, C., Bordoli, L., Lepore, R., & Schwede, T. (2018). SWISS-MODEL: Homology modelling of protein structures and complexes. *Nucleic Acids Research*, *46*(W1), W296–W303. https://doi.org/10.1093/nar/gky427

Weiss, R. A. (1993). How does HIV cause AIDS? *Science (New York, N.Y.)*, *260*(5112), 1273–1279. https://doi.org/10.1126/science.8493571

Whitcomb, J. M., & Hughes, S. H. (1991). The sequence of human immunodeficiency virus type 2 circle junction suggests that integration protein cleaves the ends of linear DNA asymmetrically. *Journal of Virology*, *65*(7), 3906–3910. https://doi.org/10.1128/JVI.65.7.3906-3910.1991

Whitfield, T., Torkington, A., & van Halsema, C. (2016). Profile of cabotegravir and its potential in the treatment and prevention of HIV-1 infection: Evidence to date. *HIV/AIDS (Auckland, N.Z.)*, *8*, 157–164. https://doi.org/10.2147/HIV.S97920

Witvrouw, M., Pannecouque, C., Van Laethem, K., Desmyter, J., De Clercq, E., & Vandamme, A. M. (1999). Activity of non-nucleoside reverse transcriptase inhibitors against HIV-2 and SIV. *AIDS (London, England)*, *13*(12), 1477–1483. https://doi.org/10.1097/00002030-199908200-00006

Woldegeorgis, B. Z., Asgedom, Y. S., Habte, A., Kassie, G. A., & Badacho, A. S. (2024). Highly active antiretroviral therapy is necessary but not sufficient. A systematic review and meta-analysis of mortality incidence rates and predictors among HIV-infected adults receiving treatment in Ethiopia, a surrogate study for resource-poor settings. *BMC Public Health*, *24*(1), 1735. https://doi.org/10.1186/s12889-024-19268-1

Yeni, P. (2006). Update on HAART in HIV. *Journal of Hepatology*, *44*(1 Suppl), S100-103. https://doi.org/10.1016/j.jhep.2005.11.021

Yim, L. Y., Lam, K. S., Luk, T.-Y., Mo, Y., Lu, X., Wang, J., Cheung, K.-W., Lui, G. C. Y., Chan, D. P. C., Wong, B. C. K., Lau, T. T.-K., Ngan, C. B., Zhou, D., Wong, Y. C., Tan, Z., Liu, L., Wu, H., Zhang, T., Lee, S. S., & Chen, Z. (2023). Transforming Growth Factor β Signaling Promotes HIV-1 Infection in Activated and Resting Memory $CD4^+$ T Cells. *Journal of Virology*, *97*(5), e00270-23. https://doi.org/10.1128/jvi.00270-23

Yoder, K. E. (2019). Absence of LEDGF/p75 Expression in Astrocytes May Affect HIV-1 Integration Efficiency. *Molecular Genetics, Microbiology and Virology: Molekulyarnaya Genetika, Mikrobiologiya I Virusologiya*, *34*(2), 81–83. https://doi.org/10.3103/s0891416819020113

Yukl, S. A., Kaiser, P., Kim, P., Telwatte, S., Joshi, S. K., Vu, M., Lampiris, H., & Wong, J. K. (2018). HIV latency in isolated patient $CD4^+$ T cells may be due to blocks in HIV transcriptional elongation, completion, and splicing. *Science Translational Medicine*, *10*(430), eaap9927. https://doi.org/10.1126/scitranslmed.aap9927

Zapata-Cardona, M. I., Florez-Alvarez, L., Guerra-Sandoval, A. L., Chvatal-Medina, M., Guerra-Almonacid, C. M., Hincapie-Garcia, J., Hernandez, J. C., Rugeles, M. T., & Zapata-Builes, W. (2023). In vitro and in silico evaluation of antiretrovirals against SARS-CoV-2: A drug repurposing approach. *AIMS Microbiology*, *9*(1), 20–40. https://doi.org/10.3934/microbiol.2023002

Zhao, A. V., Crutchley, R. D., Guduru, R. C., Ton, K., Lam, T., & Min, A. C. (2022). A clinical review of HIV integrase strand transfer inhibitors (INSTIs) for the prevention and treatment of HIV-1 infection. *Retrovirology*, *19*, 22. https://doi.org/10.1186/s12977-022-00608-1

Zheng, J., Yant, S., Ahmadyar, S., Chan, T., Chiu, A., Cihlar, T., Link, J., Lu, B., Mwangi, J., Rowe, W., Schroeder, S., Stepan, G., Wang, K., Subramanian, R., & Tse, W. (2018). *GS-6207: A Novel, Potent and Selective First-In-Class Inhibitor of HIV-1 Capsid Function Displays Nonclinical Pharmacokinetics Supporting Long-Acting Potential in Humans*.

12. LIST OF PUBLICATIONS PREPARED BY KENÉZY LIFE SCIENCE LIBRARY

UNIVERSITY of DEBRECEN

UNIVERSITY AND NATIONAL LIBRARY
UNIVERSITY OF DEBRECEN
H-4002 Egyetem tér 1, Debrecen
Phone: +3652/410-443, email: publikaciok@lib.unideb.hu

Registry number: DEENK/273/2025.PL
Subject: PhD Publication List

Candidate: Irene Wanjiru Kiarie
Doctoral School: Doctoral School of Molecular Cellular and Immune Biology

List of publications related to the dissertation

1. Szojka, Z., Kunkli, B., **Kiarie, I. W.**, Linkner, T. R., Al-Muffti, A. S., Ahmad, H., Benkő, S., Jansson, M., Tőzsér, J., Mahdi, M.: Transcriptomic Analysis Reveals Key Pathways Influenced by HIV-2 Vpx.
   Int. J. Mol. Sci. 26 (8), 1-21, 2025.
   DOI: http://dx.doi.org/10.3390/ijms26083460
   IF: 4.9 (2023)
2. **Kiarie, I. W.**, Hoffka, G., Laporte, M., Leyssen, P., Neyts, J., Tőzsér, J., Mahdi, M.: Efficacy of Integrase Strand Transfer Inhibitors and the Capsid Inhibitor Lenacapavir against HIV-2, and Exploring the Effect of Raltegravir on the Activity of SARS-CoV-2.
   Viruses-Basel. 16 (10), 1-15, 2024.
   DOI: http://dx.doi.org/10.3390/v16101607
   IF: 3.8 (2023)

List of other publications

3. Mahdi, M., **Kiarie, I. W.**, Mótyán, J. A., Hoffka, G., Al-Muffti, A. S., Tóth, A., Tőzsér, J.: Receptor Binding for the Entry Mechanisms of SARS-CoV-2: Insights from the Original Strain and Emerging Variants.
   Viruses-Basel. 17 (5), 1-25, 2025.
   DOI: http://dx.doi.org/10.3390/v17050691
   IF: 3.8 (2023)

DEBRECENI EGYETEM * Egyetemi és Nemzeti Könyvtár *

Total IF of journals (all publications): 12,5
Total IF of journals (publications related to the dissertation): 8,7

The Candidate's publication data submitted to the Tudóstér have been validated by DEENK on the basis of the Journal Citation Report (Impact Factor) database.

21 May, 2025

13. ACKNOWLEDGMENTS

I am deeply grateful to Dr. Mohamed Mahdi, my supervisor, for his guidance, patience & support in the course of my study. His expertise and mentorship were invaluable.

I am thankful to Prof. József Tőzsér for giving me the opportunity to join his research group and for his valuable insights on the projects.

I wish to express my sincere gratitudes to the dissertation committee members for their helpful criticism, insightful questions, and viewpoints on my work.

I'm grateful to Tamás Richárd Linkner for training me on relevant laboratory techniques. His time, sacrifice and dedication played a vital role in my experimental work.

I wish to thank my co-workers at the University of Debrecen's Retroviral Biochemistry laboratory; Dr. Mária Golda, Dr. Krisztina Matuz, Dr. András Szabó, Dr. János András Mótyán, Aya Shamal Almuffti, Samara Mhana and Dr. Márió Miczi, for their friendship and support during the study. Special thanks to our dedicated laboratory assistant, Szilvia Janics-Pető, for her help and assistance in the laboratory.

I am grateful to Gyula Hoffka, Balázs Kunkli and Noemi Cabarello Sanchez for their contributions to the bioinformatics analysis that supported my research findings.

Special thanks to Stipendium Hungaricum for the funding and financial support without which my studies in Hungary would have been impossible. Finally, sincere thanks to my dear friends and family for their patience, support, and encouragement throughout my study.

14. DEDICATION

To my spouse Martin, and to my children - Patrick, Sharon and Peter - for being my greatest source of strength and motivation.